AD-A117 844 FLOW ANALYSIS ASSOCIATES ITHACA NY F/G 13/2
A THEORETICAL APPRAISAL OF THE JOINT EFFECTS OF TURBULENCE AND --ETC(U)
SEP 81 S LEIBOVICH, J L LUMLEY DTCG23-80-C-20019
UNCLASSIFIED FAA-8101 USCG-D-26-82 NL

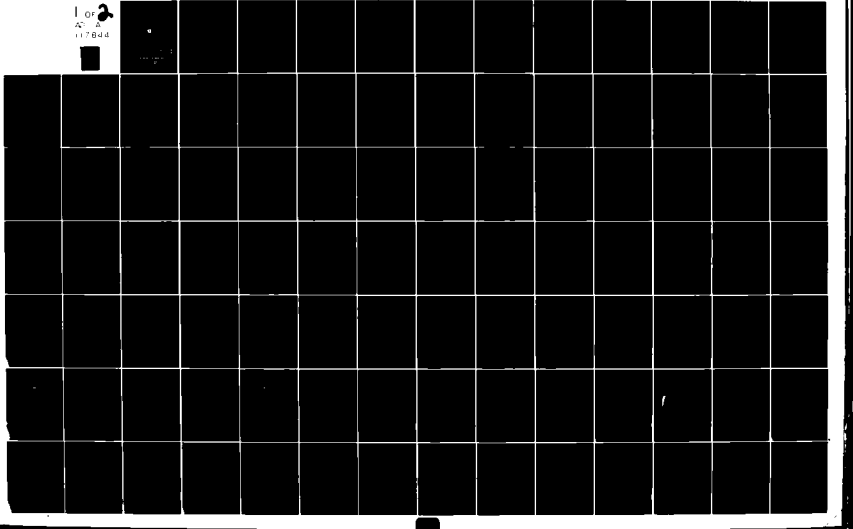

(13)

REPORT NO. CG-D-26-82

A THEORETICAL APPRAISAL OF THE JOINT EFFECTS OF TURBULENCE AND OF LANGMUIR CIRCULATIONS ON THE DISPERSION OF OIL SPILLED IN THE SEA

S. Leibovich and J. L. Lumley

Flow Analysis Associates
999 Cayuga Heights Road
Ithaca, New York 14850

SEPTEMBER 1981

FINAL REPORT

PREPARED FOR

U.S. DEPARTMENT OF TRANSPORTATION
UNITED STATES COAST GUARD
OFFICE OF RESEARCH AND DEVELOPMENT
WASHINGTON, D.C. 20590

Technical Report Documentation Page

1. Report No	2. Government Accession No.	3. Recipient's Catalog No.
CG-D-26-82	AD-A117 814	

4. Title and Subtitle
A THEORETICAL APPRAISAL OF THE JOINT EFFECTS OF TURBULENCE AND OF LANGMUIR CIRCULATIONS ON THE DISPERSION OF OIL SPILLED IN THE SEA

5. Report Date
September, 1981

6. Performing Organization Code

7. Author(s)
S. Leibovich and J. L. Lumley

8. Performing Organization Report No
FAA Report No. 8101

9. Performing Organization Name and Address
Flow Analysis Associates
999 Cayuga Heights Road
Ithaca, New York 14850

10. Work Unit No (TRAIS)

11. Contract or Grant No.
DTCG23-80-C-20019

12. Sponsoring Agency Name and Address
Office of Research and Development
United States Coast Guard
Washington, D.C. 20590

13. Type of Report and Period Covered
Final Report
August, 1980 to
September, 1981

14. Sponsoring Agency Code
USCG

15. Supplementary Notes

16. Abstract

The extent to which oil spilled at sea can be dispersed by the action of oceanic turbulence and of Langmuir circulations is investigated theoretically. The bulk of the study concerns the mixing of oil, in the form of small noninteracting particles, into the water column. Computer simulations using physically derived models of turbulent dispersion and of Langmuir circulations indicate that bouyant oil particles can be suspended to depths of tens of meters under moderate environmental conditions. This is thought to explain the deep oil observed under oil slicks from the IXTOC-I incident in the Gulf of Mexico. In addition, a simple model is devised to estimate the thickness and total volume of oil collected into windrows on the water surface.

17. Key Words	18. Distribution Statement
Oil spills, dispersion, turbulence, Langmuir circulations, windrows, oil concentration, oil dispersion, sea states	Document is available to the U.S. public through the National Technical Information Service, Springfield, Virginia 22161

19. Security Classif. (of this report)	20. Security Classif. (of this page)	21. No. of Pages	22. Price
Unclassified	Unclassified	120	

Form DOT F 1700.7 (8-72) Reproduction of completed page authorized

TABLE OF CONTENTS

1. INTRODUCTION

This report describes theoretical work aimed at estimating the dispersion of oil engendered by the joint effects of turbulence and the large scale, wind-generated convective motions in the ocean known as Langmuir circulations.

The physical problems of interest in oil spills concern the location of spilled oil as a function of time. Oil, almost always being lighter than water, tends to float on the surface. The natural action of water turbulence, particularly that generated by breaking waves, is known to be capable of disintegrating floating oil layers into small droplets, which can then be entrained into the water column. This process is dramatically accelerated by the addition of chemical dispersants (McCarthy et al, 1978), and is the basis for a method of oil spill cleanup.

Although most attempts to model the distribution and disposition of oil in the sea have dealt only with surface oil, vertical dispersion of oil also occurs and is important to understand. Since mechanical methods of oil spill cleanup rely upon oil being on or very close to the water surface, the ability to estimate the fraction of oil driven down into the water column as a function of sea state may be a key question for oil spill clean-up operations. Furthermore, oil dispersed by chemical means continues to be buoyant (Canevari 1978) and will rise to the surface in quiescent water. Thus, the problem of vertical dispersion allows one to estimate the success expected when dispersants are employed. One of the advantages of vertical dispersion, whether by natural processes or promoted by chemical means, is the division of oil into volumes more accessible to biodegradation (Canevari 1978); the vertical extent of the dispersion may play a role in determining which, if any, biological forms are able to attack the oil.

The problem of the vertical dispersion of oil has not been extensively studied. The first published work seems to be that by Leibovich (1975), followed by Raj (1978) and by Milgram et al (1978). At the time those attempts were written, there was little observational evidence of vertical dispersion of oil except under circumstances (Forrester, 1971; Hess, 1978) in which the spill occurred rather near the shore. (In the

latter cases, onshore currents and surf may result in a sediment and oil agglomeration with a composite density greater than seawater.) The blow-out of the Ixtoc I oil well in the Gulf of Mexico, beginning in June, 1979 and continuing for more than four months, allowed prolonged observation of an oil spill clearly away from surf zones and hundreds of miles from its source. Visual observations (made by divers) of subsurface oil, though few in number, were remarkable (Williams (1979), Robinson, Galt (1980), Hooper (1981)). Apparently oil, in the form of flakes the size of corn flakes and thought to be the fragmented semisolid skin of large oil "pancakes", was mixed to a depth of 40 feet. The explanation for the existence of buoyant particles in substantial numbers, originating at the surface and mixed to depths such as these, defies all self-consistent models of turbulent transport previously known to us. It seems almost certain that the explanation must reside in the existence of a mixing mechanism of large scale.

The likely mixing mechanism is related to a phenomenon known to the scientific world for more than a century (see the discussion of observations by James Thomson and his brother William, Lord Kelvin (1862)); these are windrows, long bands of flotsam, or compressed organic film or foam from breaking waves, that are approximately parallel to the wind direction. Windrows are now known to be the visible surface manifestations of large scale subsurface vortical motions discovered by Langmuir (1938), and known as Langmuir circulations. The rows mark lines of surface convergence, below which water sinks at speeds orders of magnitude larger than turbulent fluctuations and comparable to the surface wind induced water drift. Since oil provides an ideal visual marker, windrows marked by long bands of collected oil, often in the form of ropy water-in-oil emulsion referred to as "chocolate mousse", are much more clearly visible when oil is spilled than under natural circumstances. They have, consequently, often figured in accounts of oil spills - the earliest one we know of is one reproduced in N.K. Adams (1936) report to the Royal Society of London on oil-spill problems. More recent accounts of oil bands in windrows include Battelle's (1969) review of the Santa Barbara blowout and Galt (1978) in his discussion of the Amoco Cadiz and Hawaiian Patriot spills.

Accounts of the windrows in the Ixtoc-I spill indicate that they were a dominant feature, and are carefully described by Atwood et al (1980).

The simultaneous appearances of a banded surface structure and the appearance of oil at surprisingly great depths are quite likely related; the working hypothesis of the investigation reported here is that both features result from motions in Langmuir circulations. If so, when oil in windrows is evident, and when the oil present can be broken into small particles, then it is likely that oil particles will be carried down into the water column by this mechanism. Our object here is to try to estimate the amount of oil held in suspension in this way, given the availability of standard environmental parameters such as wind speed and sea state, and perhaps visual observations of surface windrows.

The complicated processes by which a floating oil mass can be broken into small droplets or fragments is considered at length by Milgram et al (1978), and we do not address the question here.

While the deep penetration of oil is attributed to persistent large scale motions, the possibility of any oil being dispersed into the water column is due to turbulence. As in most problems in fluid dynamics, the treatment of the turbulence is the most difficult and uncertain part of the problem. A purely theoretical approach may be disasterous; for example, reasonable people can easily arrive at estimates for the dissipation rate of turbulent energy (a key figure) that differ by ten orders of magnitude. To approach the question of dispersion in a rational way, we must introduce the best available information about turbulence in the surface layers of the sea. Although experimental information is accumulating at an accelerating rate, data on oceanic turbulence is not plentiful and much of the existing data is of dubious quality. Fortunately, pertinent new turbulence measurements below surface waves in the ocean have been made in the last two years, and even more recently in Lake Ontario, which provide important guidelines for our investigations.

Assuming that turbulence data are available, it remains to determine their effect on the transport of oil. The question posed in the present work is the determination of the dispersion of oil due to mean motions generated by Langmuir circulations, which are calculated using a theory

due to Craik and Leibovich (1976) (see Leibovich 1980 for a summary), and superimposed turbulent fluctuations. A model for the motion of the oil incorporating turbulent fluctuations is based on the work of Lumley (1978) and of Csanady (1963) and is not straightforward; and a considerable amount of attention is devoted to it in this report.

We have explored the joint effects of Langmuir circulations and turbulence by computing the distribution of oil in 27 cases illustrating a range of surface wind speeds, and sea states and for several oil droplet terminal velocities. The results of our study may be summarized:

1) Under typical sea states and wind conditions, Langmuir circulations gather oil into windrows in volumes that can be estimated by the method of §8.

2) Oil may be trapped below the surface in extensive zones, which we call "Stommel retention zones" (or "SRZ") in recognition of earlier work by Stommel (1949) on a related problem. Each of these zones lies beneath a windrow and its size and placement is determined by the oil terminal velocity and the Langmuir circulation speeds. Oil particles can be found, with equal probability, anywhere within the zone. The size of these zones of trapped oil easily accounts for the deep penetration observed in the Ixtoc-I spill. For example, for one illustrative case evaluated here (oil particle terminal velocity = 0.5 cm/sec., wind speed = 15 m/s, significant wave height = 70.4 cm), the SRZ penetrates to a depth of 24 meters.

3) A Stommel retention zone is fed by oil transferred from the windrow lying above it. The fraction of oil trapped in a SRZ can be calculated by the method of §6. The fraction of oil in an SRZ depends upon the efficiency of transfer from the windrow, and this depends strongly upon the distance between the windrow and the top of the SRZ. This distance, in turn, depends upon the speed and length scales in the Langmuir circulations, and upon the terminal velocity of the oil particle. In the cases we have computed, the fractions of oil trapped exceeds 90% for terminal velocities as large as 1 cm for wind speeds of 15 m s^{-1} results are discussed in §7.

2. LANGMUIR CIRCULATIONS AND TURBULENT DISPERSION OF OIL DROPLETS. BACKGROUND.

It is generally agreed that the visible windrows that occur on the surface of oceans and lakes most frequently result from subsurface convective motions known as Langmuir circulations. These motions, which were first described in detail by I. Langmuir (1938), consist of a series of parallel counter-rotating vortices that are aligned with the wind direction. The vortices produce downwelling and upwelling regions that lie, respectively, below lines of surface water convergence and divergence. Naturally occuring surface tracer material, such as seaweed, foam, or slicks of organic film, are swept into the convergence zones, creating a visible surface pattern of bands or slicks parallel to the wind direction. The associated surface streaks are readily detectable at the surface when the wind speed exceeds 3m/sec.

In this section, a summary of field observations of Langmuir circulations will be given, followed by laboratory experiments and a description of the physics. Following this, the physics of dispersion of particles in a turbulent fluid will be described.

2.1 Field Observations

A sketch illustrating the general features of Langmuir circulations (which we will abbreviate by LC) is shown in Figure 2.1. The surface streaks are often very regularly spaced; at other times, they are somewhat less regular but they are always aligned close to the wind direction. Since windrows lie above convergence zones, the spacing between two neighboring rows describes the horizontal width of a pair of counter-rotating cells. Reported cell spacings (Langmuir (1938), Scott el al (1969)) range from 2-25 meters in lakes, and from 2m up to hundreds of meters (at least 300m) in the ocean (Langmuir (1938),Katz et al (1965), Ichiye (1967), Gordon (1970), Assaf et al (1971)). The largest scales are most easily detectable by aerial observation. Large scale LC's are associated with smaller cells that are somewhat less well-defined; thus, when large scales appear, they often exist as members of a heirachy of different cell sizes, Langmuir (1938), Williams (1965).

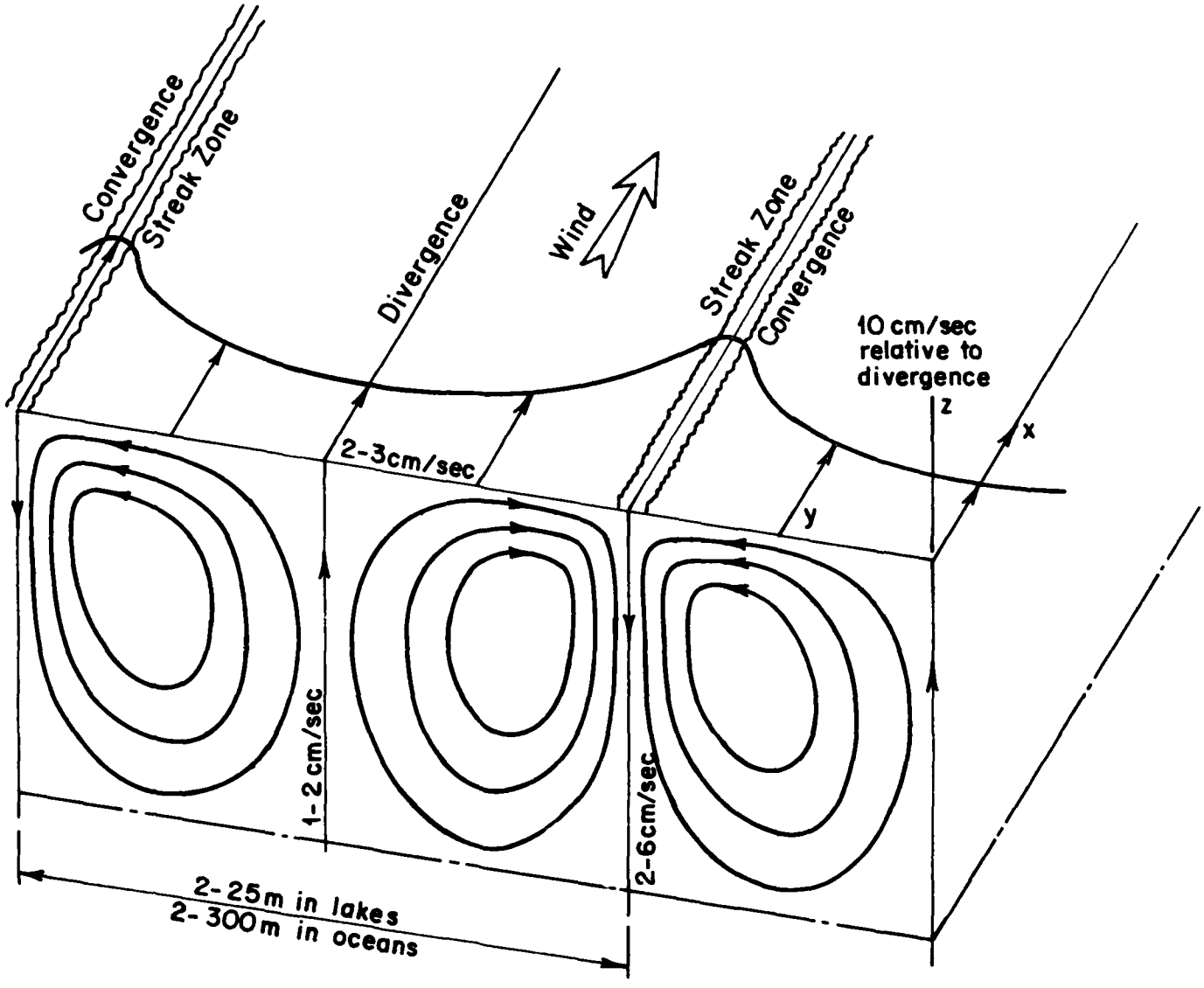

Figure 2-1. Sketch of Langmuir circulations showing the nature and scales of the motion.

Conflicting information has been given concerning factors that determine cell width. A correlation, roughly $L=4V_a$ seconds, between cell width L and wind speed V_a has been reported by some observers (Katz et al (1965), Maratos (1971), Faller & Woodcock (1964), for LC in the ocean. Others (Scott et al (1969), Myer (1969)) report work on Lake George that suggests only a slight correlation with wind speed. Observations on Lake George by Langmuir (1938), Scott et al (1969) and Myer (1969)), and combined aerial and surface measurements in the ocean by Assaf et al (1971) suggest a correlation of row spacing with the depth of the seasonal thermocline.

It is more difficult to determine the depth of penetration of the cells. The common expectation is that the cell penetration is comparable to the distance between windrows. Some data exist (Langmuir (1938), Scott et al (1969), Myer (1969), Assaf et al (1971)) that tend to confirm Langmuir's conclusion that the cells can extend to depths just above the seasonal thermocline.

Observational information on current speeds consists of disconnected parts. Both the cross-wind (or sweeping) component towards convergence lines, the windward component, and the downwelling component, have been measured, but not simultaneously. From the data reported, however, one can estimate that the average sweeping speed is comparable to the downwelling speeds. Data on downwelling speeds W_d from several sources have been collected by Scott et al (1969), and found to be well-correlated by $0.0085\ V_a$. A very recent report by Filatov et al (1981) on measurements made in Lake Ladoga in the Soviet Union also provides correlation of the vertical velocity near (the specific depth is not reported) the water surface in convergence (downwelling) zones. Analysis of 160 measurements with wind speeds in the range 3-14 ms^{-1}, yields $W_d = c_1 V_a^{c2}$ where V_a is the average wind speed 10m above the surface, and c_1 and c_2 apparently depend upon the density stratification of the airflow just above the surface. For neutral airflow conditions, they cite the values $c_1=3.6\times10^{-2}$, $c_2=0.7$ (c_1 has dimensions $(cm/s)^{c2-1}$), for unstable airflow (density decreasing upwards) $c_1=3.7\times10^{-2}$, $c_2=0.7$, and for stable airflow $c_1=6\times10^{-2}$, $c_2=0.6$. Thus, all available data indicate

that W_d increases with V_a although the rate is not agreed upon. Since the average surface wind drift speed is usually estimated to be around $0.03V_a$ to $0.035V_a$, and since this is a good measure of the maximum mass transport speed in the ocean that can be traced to the wind, the downwelling speeds in LC are surprisingly large. Upwelling velocities, centered under lines of surface divergence, are always reported to be smaller than downwelling speeds (implying an asymmetry of the cells); Langmuir (1938) estimated upwelling to be about half as strong as downwelling motion. Surface windward speeds are larger near lines of surface convergence and the effect is sufficiently large to be noted by all observers.

LC are readily observable for wind speeds exceeding 3m s^{-1}, but this is not a critical condition and observations have been made at speeds lower than 0.7 m/s (Stommel, 1951). As Faller (1981) has pointed out, the commonly cited figure of 3m s^{-1} is open to doubt since the observation of streakiness is subjective; the variable amount of material available on the surface as tracer, and other factors, may play a role in making identification of existing streaks less likely at lower winds. It is in fact likely, as theory indicates (supported by laboratory experiments described in the next subsection), that exceptional circumstances can occur in which LC appear in the absence of wind.

The time required to form LC after the wind begins to blow, or to reorient the cells following a shift in wind direction, is on the order of minutes. For example, Langmuir (1938) reported that a large scale system (spacing of hundreds of meters) of LC in the North Atlantic reformed and realigned with the wind 20 minutes after a shift in the wind direction.

2.2 Laboratory Experiments

Laboratory experiments on Langmuir circulations have been carried out in wind-wave tanks. The experiments demonstrated that the phenomenon can be produced in the laboratory provided surface waves and a sheared current, as an applied wind stress necessarily produces, are simultaneously present. A wind stress itself is not necessary, but the current shear is essential; the existence of a current without waves, or waves without current, is insufficient for the production of LC's.

The experiments of Faller (1978) were specifically designed to test one of the two mechanisms (called CL I by Faller and Caponi (1978)) by which the Craik Leibovich (Craik and Leibovich, 1976, Leibovich 1977a, Leibovich and Radhakrishnan, 1977) theory produces Langmuir circulations. The experiments of Faller and Caponi (1978), like those of Faller (1978), carried out in a relatively small wind-wave tank at the University of Maryland, also had as one primary purpose the testing of the CL I mechanism.

As will be explained further in the next subsection, the CL I mechanism produces LC by direct wave forcing that can be exerted by a coherent short-crested sea. The CL I theory shows that when the wind stress is applied in the directions of wave propagation LC form with surface convergence lines at nodal lines of the wave field, and divergence lines midway between; the direction of circulation in the LC is predicted to reverse when the wind stress is applied in the direction opposite to that of wave propagation. Regular short-crested wave fields were produced in these experiments by specifically designed wave-makers, and a wind stress was also supplied; in all cases, the experiments confirmed the predictions of the CL I mechanism. The prediction of reversal of cell circulation was confirmed in Faller's (1978) experiments.

All of these experiments were carried out before the CL II mechanism, which produces LC's by an instability, (which can arise from a completely random wave field in the presence of current shear created by an applied stress, to be discussed in the next section) had been fully described. Nevertheless, earlier experiments by Faller (1969) showed that LC could be produced in the laboratory by random wind-waves. Furthermore, the scalings of both CL I and CL II theories are the same, and, as it turns out (Leibovich and Paolucci (1980)), the structure and strengths of the motions in LC cells produced by the two mechanisms are very similar.

2.3. Physics of Langmuir Circulations

Although a variety of ideas has been suggested to explain Langmuir circulations (see Scott et al, 1969, for example, for a discussion of most

of these early specifications), it is now generally agreed that all of these processes, except those involving interactions between waves and currents, are either irrelevant (cannot account for LC) or not necessary but may modify the phenomenon (i.e. thermal convection can strenghten LC, but since LC are observed in thermally stable conditions, thermal instability is not an underlying causal mechanism for LC). Furthermore, it now seems clear (Leibovich, 1980) that all aspects of wave and current interactions relevant to LC (for example, Garrett's (1976) theory), may be incorporated in the CL (Craik-Leibovich) theory, which will now be described.

If attention is focussed on phenomena occuring on a time scale larger than a typical period of a surface gravity wave, it is appropriate to filter out the wave-generated "hash" by considering only quantities averaged over several wave periods. The averaged momentum equations contain the rectified effects of the surface waves only through a modification of the pressure, and through an apparent force term which represents a direct interaction between the waves and current. The first effect is of not particular consequence since it only alters the mean pressure by a small amount. The second effect, however, is crucial. Wave-current interactions arise as a vortex force, (Leibovich, 1977b) which may be represented as

$$\mathbf{F}_{vl} = \mathbf{u} \times \text{curl } \mathbf{u}_s \qquad (2\text{-}1)$$

where $\mathbf{u}_s$ is the particle drift velocity vector (Stokes drift, see §4) caused by progressive water waves and $\mathbf{u} = (u,v,w)$ is the mean water velocity vector measured at the point x, y, z at time t. (Thus, the momentum of the waves is carried by the Stokes drift.)

Suppose we consider, for simplicity of explanation, a case where u and u_s are both in the same direction (say the x-direction) and both decrease with depth (where z is measured vertically upwards from the mean free surface) but do not vary horizontally. This situation is the simplest intuitive model of a wind-generated sea; the average motion is in the wind direction and varies only with depth, while the wave field (statistically) does not vary in the horizontal (thus leading to a Stokes drift varying only with depth. Then $\mathbf{F_v}$ has a component only in the z-direction, (upwards, acting like a buoyant force), and therefore has an effect analogous to density stratification. Provided the symmetry of a perfectly layered configuration is attained, the motion can continue to maintain its layered structure. If, however, there is a slight deviation e.g., if any horizontal variations in either u or u_s develop, the vortex force causes accelerations perpendicular to the current direction and Langmuir circulations must develop. This we show below, assuming for simplicity that there are no variations in the direction of the wind.

This is most easily seen when the Stokes drift varies horizontally; in that event LC are created by direct wave forcing: this is the CL I mechanism referred to earlier. For short time intervals at least, the structure of wind waves is typically short-crested, with the waves appearing to be due to two coherent wavetrains propagating at equal but opposite angles to the wind direction. This, if maintained for a time long enough to obtain meaningful averages, leads to a spanwise periodic Stokes drift, (see Figure 2.2), so that $\partial u_s/\partial y \neq 0$. This leads to an acceleration in the spanwise (y) direction perpendicular to the current of amount

$$-(\partial u_s/\partial y)(\partial u/\partial z)$$

Since $\partial u_s/\partial y$ alternates in sign the water moves, from both sides,

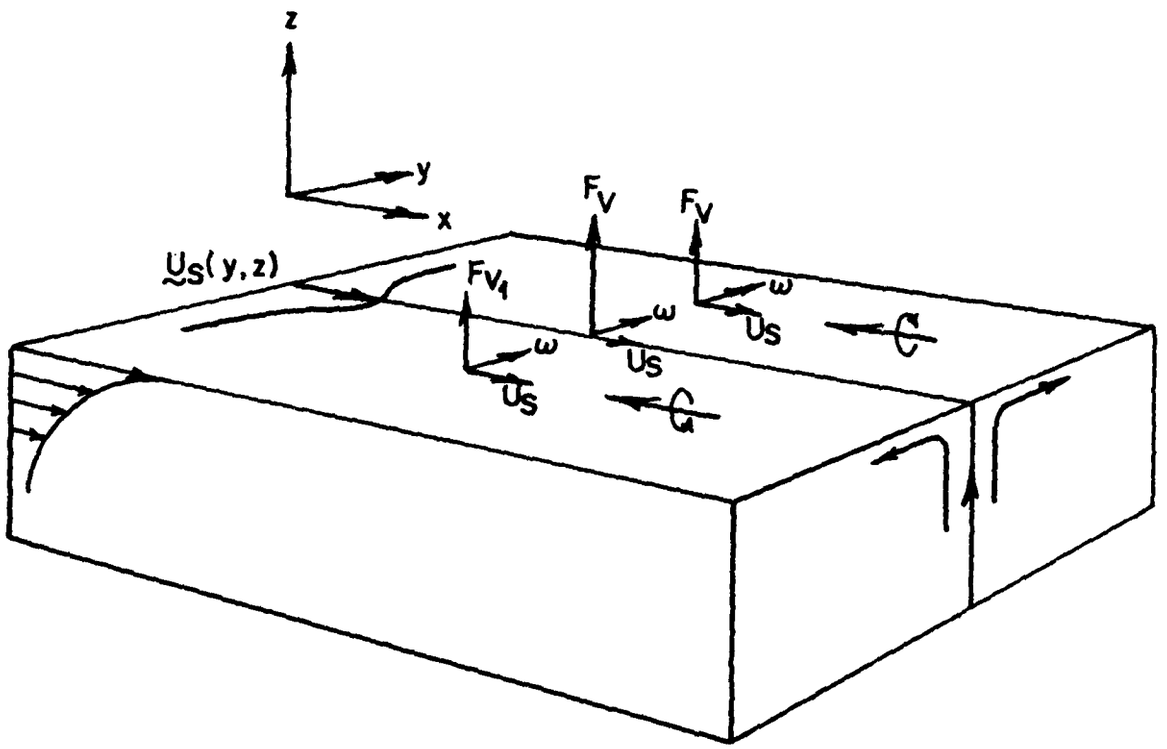

Figure 2-2. Sketch illustrating the generation of Langmuir circulations by spanwise variations of the Stokes drift.

towards those planes where u_s is a minimum. There, by continuity, water must sink.

The CL I mechanism requires that the wave structure remain coherent for time scales comparable with the lifetime of a Langmuir cell. While this may in fact be the case under certain circumstances, it is not likely to be common. The second, or CL II, (Craik, 1977, Leibovich 1977a and Paolucci 1980a, 1980b, 1981), mechanism is an instability and, by contrast, is <u>always</u> a possibility. Suppose u_s is horizontally uniform (consistent with statistically homogeneous waves), but that a small spanwise irregularity is present in an otherwise horizontally uniform current. Such irregularities, of course, are unavoidable and everywhere present in nature. In such a case $\partial u/\partial y \neq 0$, and the vortex force F_v causes an acceleration towards the planes of <u>maximum</u> u, where by continuity the fluid must sink (Figure 2-3).

It is essential to know whether the initial irregularity grows. If not, then there is no reason for the horizontal motions to grow, and all that we conclude is that these small irregularities in the wind directed velocity component are accompanied by comparably small irregularities in the other two velocity components. If a feedback mechanism exists permitting this system to grow, then coherent and measureable convection patterns can develop. Conservation of x-momentum for a vanishingly thin slab of fluid surrounding the convergence plane shows that as the fluid sinks the x-velocity must increase, assuming, that $\partial u/\partial z > 0$ (as one expects in an oceanic current). Thus, provided this increase of x-speed is not eliminated by frictional effects, the slight acceleration of fluid leading to the initial current irregularity will force side motions due to vortex force and this will in turn amplify the irregularity. We therefore have an instability of the system which has the potential to develop into LC. The analysis in the literature (in particular, Leibovich and Paolucci 1981), shows that in typical wind-generated seas, frictional forces almost never are strong enough to overcome this feedback process.

In chapter 4, we will present the theory in mathematical form. The CL I and CL II mechanisms are based upon the same scaling assumption and therefore the general features of the convective cells resulting from both

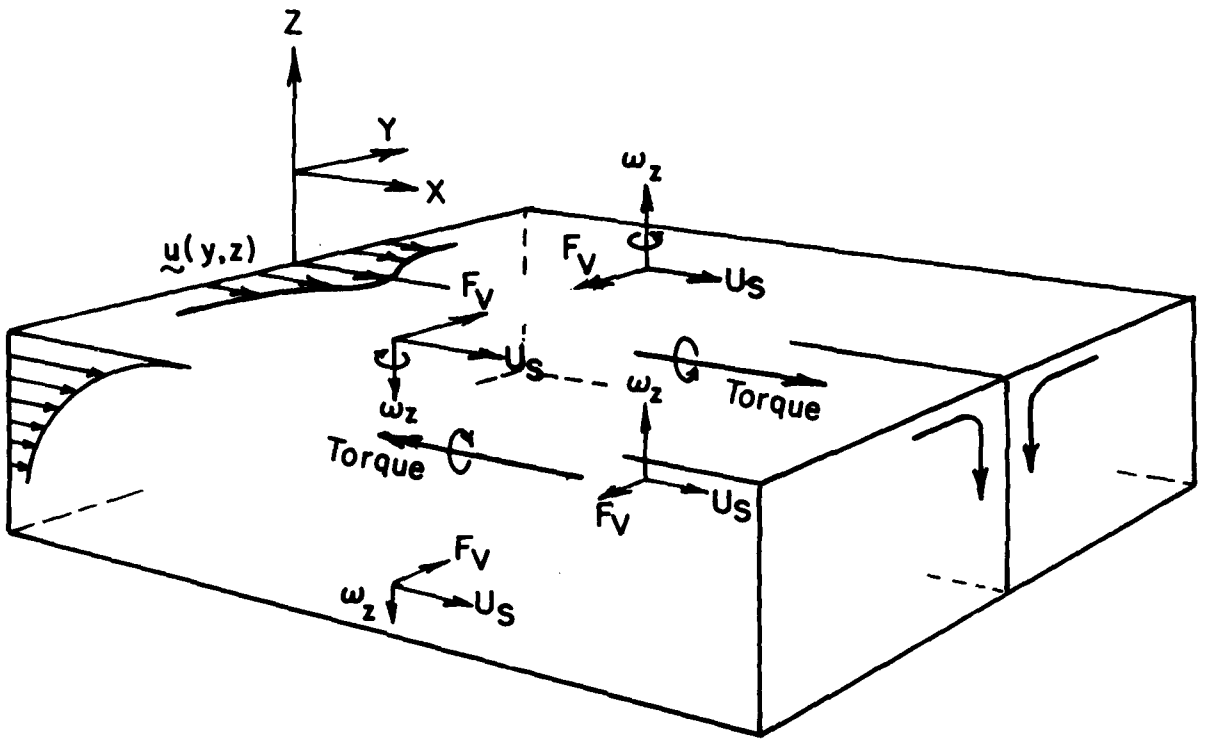

Figure 2-3. Sketch illustrating the generation of Langmuir circulations by the instability mechanism. The Stokes drift need not vary in the spanwise direction.

the direct and the instability mechanisms are similiar (Leibovich and Radhakrishnan, 1977; Craik, 1977; Leibovich and Paolucci, 1980a). Since the instability mechanism does not depend upon any special surface wave organization, it would seem to be the more attractive possibility for Langmuir circulations and this is the mechanism utilized in the present work. It should be noted, however, that the direct forcing mechanism always acts, but may be able to exert a coherent effect only for short periods of time. While this short-time duration limits its ability to produce a long-lived Langmuir cell structure, the direct forcing can be expected to lead to initial perturbations that can be subsequently amplified into long-lived Langmuir circulations by the instability mechanism.

2.4 Description of the Physics of Turbulent Dispersion of Oil Droplets.

When there is relative motion between an oil droplet and the surrounding sea water, a drag is produced. This drag may be steady, unsteady, or quasi-steady (which we will explain in a moment), depending on the circumstances. The drag, of course, results from the fact that the sea water cannot slip where it meets the surface of the oil droplet; if there are impurities on the interface between the seawater and the oil, the droplet skin may act like a rigid surface to a greater or lesser extent. Otherwise, there may be a circulation within the oil droplet so that there is an effective slip at the surface, although the velocity of circulation within the droplet will be relatively small in any event, since the oil is so much more viscous than the sea water. The droplet may deform, depending on the size, velocity and surface tension, combined in a dimensionless group called the Weber number. Under more extreme conditions it may be torn apart. It may interact with other droplets, depending on the concentration. Depending on the Reynolds number of the relative flow around the droplet, the drag may be a non-linear function of the relative velocity, and other non-linear effects may become important, such as lateral forces resulting from spin (the Magnus effect), or even from the unsteadiness of the wake, which may result in the drag not being in the instantaneous direction of the relative motion. If the oil has lost its fluidity, and forms into non-spherical oil particles rather than

droplets, slow rotation of the particles will result in unsteady lateral forces, as the particle deflects the oncoming flow now to one side, now to the other. At higher values of the relative Reynolds number unsteady separation may occur, leading to unsteady lateral forces. A material point (of water) in a turbulent flow will slowly wander from its original neighborhood; that is, in a turbulent flow under waves, the original neighborhood will follow an orbit described by the potential motion driven by the surface waves. A material point will begin by tracing one of these orbits, but will gradually wander away from it. An oil droplet will do a similar thing, but will also wander away from the material point, since there is a relative motion between it and the sea water. Hence, the diffusion of the oil droplet will be different from the diffusion of the material point. In addition, the mean density of the oil droplet is different from that of the sea water. As a result, the droplet will rise (in general) through the water. In rising, it leaves the parcel of sea water with which it started, and hence the velocity history following the wandering droplet will in general lose correlation faster than that of a wandering material point. Finally, if we include a mean flow (such as the Langmuir circulation), we envision a droplet with a basic motion consisting of a superposition of a very small steady rise, a relatively rapid orbital motion, the Langmuir circulation (stronger than the steady rise), and superposed on this an unsteady wandering resulting from both the unsteady turbulent velocity and the other possible sources of unsteadiness inherent in the droplet's own wake, and in the interactions with other droplets.

This is clearly an extremely complicated situation. No approach exists which is capable of handling all these phenomena simultaneously. Fortunately, it is possible to sort realistic scenarios into groups in which one or more of the complicating factors are not present, and obtain a solution. Scenarios which cannot be handled in this way represent relatively rare occurrences.

The first difficulty to be eliminated is interaction. There is no method for dealing with interacting droplets. For spherical or non-spherical droplets, interaction is negligible for volume fractions (of circum-

scribed spheres) below 0.003 (Lumley, 1978). To get a physical feel for this number, for oil droplets one millimeter in diameter, this volume fraction corresponds to six droplets per cubic centimeter. While it is clear that many situations of interest may have volume fractions higher than this, it is also clear that many situations of interest, in particular the transport and dispersion of droplets by turbulence in Langmuir cells, are likely to satisfy this limitation. We will probably violate this limitation only near the windrow area, where we expect the droplets to coalesce in any event, so that a droplet description is no longer valid. In everything that follows, we will assume negligible interaction. This does not mean that there is no interaction; only that the interactions are sufficiently infrequent for the presence of the droplets to make a less than one percent contribution to the viscosity of the suspension. Hence, it would be legitimate to use a non-interactingmodel to compute the rate of coalescence of droplets at low concentrations, for example.

The next difficulty is that of the unsteady wakes. There is no known method for treating vortex shedding, unsteady separation, Magnus effects, and the like. Fortunately, these are all Reynolds-number effects, and extensive information exists on the relative Reynolds number at which the wake becomes unsteady (see Van Dyke, 1975). This appears to be approximately 60. Hence, as long as we consider only particles for which the Relative Reynolds number is less than 60, we can eliminate most of the unsteady effects. The only exception is the fluctuating sideways force resulting from the Magnus effect, which we will discuss in a moment. In section 5. we will discuss in detail the implications of this limiting relative Reynolds number for droplet size; the relative Reynolds number is due, of course, to both droplet inertia and to the terminal velocity resulting from buoyancy. Different density/diameter combinations result in different situations. In section 5 we will conclude that droplets of roughly 1.5 mm in diameter can be considered without exceeding the Reynolds number limitation. Droplets of this size certainly include many of those of interest.

So far as the Magnus effect is concerned, a droplet in a shear will try to spin with the local vorticity. To the extent that the flow field

around the droplet is non-linear (and it certainly will be if the relative Reynolds number is not small compared to unity), if there is a relative velocity there will be developed a force normal to the direction of the relative velocity. We may estimate the order of magnitude of this force as

$$\rho_w \Delta U \Gamma d \tag{2-3}$$

where ρ_w is the density of the water, ΔU is the relative velocity, and Γ is the circulation about the droplet. This is the standard expression used for the lift on wings and other bodies which induce a circulation. We may estimate Γ as $\pi d^2 u/\lambda$, where u is the rms fluctuating velocity of the turbulence, and λ is the Taylor microscale. This assumes that the droplet will rotate with the local shear. Equivalently, we may use the expression $3.87\ell/R_\ell^{1/2}$ for λ where ℓ is the length of the energy-containing eddies, and Re is the Reynolds number based upon u and ℓ. If we take the ratio of the lift force (say, F_L) to the drag force (say, F_D) we obtain

$$F_L/F_D = 3(\rho_w/\rho_0)(ua/\lambda)/[1 + (3/16)R] \tag{2-4}$$

where R is the relative Reynolds number, a is the droplet time scale, and ρ_0 is the density of the oil droplet. The substantive part of expression (2-4) is the ratio of the droplet time scale to the time scale of the dissipative eddies. This is the same time scale ratio that will be estimated later in another context, and it is a small number. We will find that a is no larger than 3×10^{-3} sec, that a reasonable estimate for u is 1×10^{-2} m/s, and that ℓ is roughly 1 m, while R_ℓ is about 1×10^{-4}, giving $\lambda/u \approx 3.87$ sec. Hence, we may conclude that the fluctuating lift forces generated by the spin are a very small fraction of the drag forces, and hence that the dispersion produced by these forces is a similar fraction of the dispersion produced by the drag forces.

One final source of unsteadiness and lateral forces cannot be completely eliminated. If the oil particle is non-spherical (we cannot now say droplet), a situation that may arise depending on the age and condition of the oil, the drag will not be steady and will not be instantaneously in the direction of the relative motion. Even in the absence of

turbulence, the oil particle will slowly rotate as it rises, and as it rotates the direction and magnitude of the drag will fluctuate as the oil particle presents different aspects to the oncoming flow. The lateral force resulting from this effect is of the same form as that due to spin, discussed above, but here the circulation is caused by the lateral deflection of the flow by the orientation of the oil particle. We may guess that the maximum velocity difference across the oil particle that can be induced in this manner will be no larger than the oncoming relative velocity. With this assumption, the lateral-to-drag force ratio has the same form as in equation (2-2), but the important part is now ($\Delta Ua/d$). The maximum relative velocity will be estimated as no more than roughly 1×10^{-2} m/s, with $d = 1\times10^{-3}$ m, so that the ratio is about 3×10^{-2}; hence, the lateral forces resulting from lateral turbulent gusts are much larger than the lateral forces resulting from asymmetrical orientation of non-spherical oil particles. In what follows, we will refer generally to droplets, implying sphericity, but in fact what we say will be applicable to non-spherical oil particles. The appropriate terminal velocity, of course, cannot be determined from the expressions for spherical droplets, but must in general be determined experimentally.

The next problem that we must eliminate has to do with unsteady effects in the drag (other than those discussed above). That is, our problem will be made much easier if the drag may be assumed to be a quasi-steady function of the relative velocity. Unsteady effects of this type result from the time necessary to establish a viscous region around the particle in equilibrium with the oncoming flow. The thicker the viscous region, generally speaking, the longer it takes to establish it when there is a change in the oncoming relative velocity. Hence, for droplets in the Stokes regime (relative Reynolds numbers small compared to unity) this can be a problem, and for density ratios close to unity the additional forces resulting from this effect can be non-negligible. This type of force is referred to as a Basset force, from the investigator who first discussed the form of this term in the equation. Fortunately, the vast majority of the oil droplets in which we are interested, the larger ones which carry most of the oil volume, have a relative Reynolds number well above the Stokes range. For these droplets, the viscous region is relatively thin, and consequently the time required to establish it after a change in the

relative velocity is negligibly short. In Lumley (1978) estimates are made of the relative time scales; we do not reproduce them here, but simply state that for all the droplets of interest to us, we may consider that the drag is a quasi-steady function of the relative velocity, so that the drag force may always be taken to be in equilibrium with the relative velocity.

The next complication is that of non-linear drag. If the relative Reynolds number is as large as sixty, it is clear that the drag force is not linear in the relative velocity. This could be a very complicating factor; if the droplet rise were opposed by a turbulent gust, the downward force would be greater than the corresponding upward force if a similar gust were to aid the rise. Hence, the terminal velocity would be reduced in a turbulent field, and would be a function of the turbulence parameters, as well as the droplet inertia. In general, the droplet dispersion would be dominated by the more intense turbulent velocity fluctuations, and prediction of the dispersion would become very difficult. However, if we could linearize around the rise at the terminal velocity, all these problems would be eliminated. This would automatically eliminate the change in the terminal velocity due to the turbulence, and would produce a fluctuating drag force which was a linear function of the turbulent fluctuations, making the prediction of the dispersion relatively simple. Fortunately, the conditions for this linearization are simple to obtain, and they result in a fairly loose restriction on the fluctuating relative Reynolds number. We find that as long as the fluctuating relative Reynolds number is less than 12.5, the first nonlinear term neglected is no more than 20% of the linear term; hence, in the worst case we will make no more than a 20% error in the dispersion. Considering the other uncertainties in this analysis, a 20% error is certainly acceptable. This error, in fact, will in general be much smaller.

The prediction of the fluctuating relative Reynolds number is difficult, because the seawater velocity at the droplet location depends on the droplet motion. This is a classical problem which has not been completely resolved. However, two limiting cases are relatively simple to understand: the case in which the droplet essentially follows the motion of the sea water perfectly, called the Lagrangian case, and the case in which the droplet nearly ignores the motion of the sea water, rising through it rap-

idly (relatively). Of course, both cases are approximations, and the truth lies somewhere between; however, consideration of the two cases allows bracketing estimates to be made of the fluctuating relative Reynolds number. Proceeding in this way, we will find that the majority of the droplets in which we are interested are much closer to the Eulerian limit than they are to the Lagrangian limit. We easily obtain in this way a limitation on droplet diameter to assure the appropriate limitation on the fluctuating relative Reynolds number, and find that we can consider droplets up to approximate 1.5 millimeters in diameter.

Finally, we must consider the fact that the wandering droplet rises out of the turbulent eddy with which it begins, and the fluctuating droplet velocity loses correlation faster than the fluctuating velocity of a material point which began with it. This is called the crossing-trajectories effect, and has been much studied by Csanady and Yudine (for references, see Lumley, 1978). Essentially, the matter is resolved in an approximate manner by noting that in the two limiting cases discussed above the dispersion takes on a relatively simple form. Essentially, an interpolation form between these two limiting cases is constructed, assuming only that the velocity correlations at all intermediate values of the parameters are similar in form, and that iso-correlation contours are elliptical. The resulting forms are particularly simple, and depend only on the ratio of the terminal velocity to the turbulent fluctuating velocity. The net result is a reduction of the dispersion of the droplet relative to the dispersion of a material point, and a difference of the dispersion in the vertical direction relative to that in the horizontal direction.

Finally, we must consider the dispersion as a function of time. As a droplet begins to be dispersed by the turbulent fluctuations, the dispersion changes as a function of time, growing at first parabolically, and later linearly in time. The exact form of the growth depends on the form of the correlation functions that is assumed; it is possible to make simple assumptions that are more than adequate for this prediction. However, if this transient period is a relatively small part of the total time over which the droplets are dispersed by the turbulence, the transient period may be ignored, and the asymptotic value of the diffusivity

used; the error introduced in this way is negligible. In our case, fortunately, this is the case, since the circulation in the Langmuir cells is relatively slow, and the transient period of the dispersion corresponds to a small fraction of the cell turnover time.

In this way we have finally reduced the droplet dispersion problem to the dispersion of spherical, non-interacting droplets with constant diffusivities, different in different directions, and under different conditions. Such a situation may be described by a diffusion equation in which the diffusivities are functions of position and direction.

3. PLAN OF WORK

The primary purpose of this work is the determination of subsurface oil dispersion created by Langmuir circulations and smaller scale turbulence. In this section, the major assumptions adopted in the work are recorded, the sequence of steps followed is outlined, and specific choices are made for the Langmuir circulations to be computed.

Dispersion results from the random displacement of material caused by the fluid turbulence. A description requires information about the turbulence as well as mean fluid motions and both turbulence and the large scale convective motions are extremely complicated. According to the theory of Langmuir circulations that we employ here, convective activity arises as an instability whose detailed evolution depends upon the wind stress, fetch, ambient currents, sea state, water density stratification, water depth, turbulent momentum transport, initial perturbations, time of observation, and the rotation of the earth. Some of these effects have been studied, but many have not. Even if all contributing factors were well understood, a sample of Langmuir circulation observations taken under identical conditions of the principal environmental observables (wind speed and sea state) is expected to yield random results and only statistical measures of the observations will be reproducible. This is because the theory is an instability theory, because the flow details depend upon prior history, and because many factors other than the principal observables influence the motion. This situation is characteristic of all geophysical fluid dynamics problems. One has a reasonable right to expect from a theory the significant trends; it is not reasonable to expect an accurate prediction of a real geophysical event when, as is invariably the case, only part of the data required to specify the event is known.

In the present work, we assume that the ocean is infinitely deep, and we ignore density stratification and the earth's rotation. The motion is assumed to start from rest under the action of an applied stress, and therefore it is assumed that there are no ambient currents, or if such currents are present, the associated vorticity may be ignored. Although we use a semi-empirical model to relate the sea state to the wind speed

and fetch, we do not take into account the time required for the surface wave field to develop.

We believe that Coriolis accelerations have a major effect on Langmuir circulations when the wind blows for a time exceeding a quarter of a pendulum day. Although density stratification strongly modifies the rate of penetration of Langmuir circulations in deep water, it is the Coriolis acceleration which probably determines the maximum depth of penetration. Unfortunately, this effect is not yet understood. Without a Coriolis force, the motion in infinitely deep water has no steady limit, and some criterion must be used to describe when to terminate a calculation. We use arbitrary specified (maximum) penetration depths to help organize our calculations.

The first step in our analysis is the calculation of several Langmuir circulation flow patterns thought to be representative of a range of environmental conditions of practical interest; the specific parameter choices are described in §3.1. Turbulence is represented in the Langmuir circulations by a constant eddy viscosity, and the choices made are also described in §3.1. Calculation of all three velocity components requires the solution of a fully nonlinear problem. This is carried out by a numerical scheme to be described in §4, and the results are stored on magnetic tape for further use.

It is assumed that the presence of oil has no dynamical consequences, and that the Langmuir circulation fields are therefore not affected by the presence of oil. While this assumption is hard to dispute as far as subsurface oil, which typically has very low volume concentrations, is concerned, the presence of surface oil clearly has an effect on surface waves and perhaps therefore on LC. Nevertheless, the assumption is expected to be sound under most circumstances, since thin surface oil films primarily damp short (capillary) surface waves. Waves in the gravity wave regime are responsible for LC, and these are not expected to be substantially affected by surface oil. We have not, however, analyzed this question in detail, and it is a point that requires and deserves further study.

Each of the computed Langmuir circulation fields is regarded as a possible outcome of an actual observation. Furthermore, in order to make the dispersion calculation tractable, we assume that these Langmuir circulation fields are possible steady motions, even though they are stages in the time development of an inherently unsteady mathematical problem. Since the motions generated are believed to scale properly with the primary environmental parameters, we believe that dispersion calculations based upon these assumptions will be at least qualitatively meaningful. As we have already stated, this is all one can usually expect in geophysical problems.

After generating the water motions, we consider the trajectory of a single buoyant particle released at an arbitrary point in any of our Langmuir circulation fields. The key assumption made is that the velocity field into which the particle is placed is completely time independent (e.g., there are no turbulent fluctuations). This idealized problem, which follows a similiar study by Stommel (1949), reveals the presence of subsurface zones in which buoyant particles can be trapped. If a particle is placed within a closed boundary defining one of these zones, it will move in a closed orbit lying inside the boundary of the zone. The size (depth and volume) of these zones depends upon the buoyancy of the particle and upon the intensity and length scale of the LC motion, but for typical values expected in oil-spill situations, these regions are extensive. For each of the LC fields generated, these zones are mapped for three values of particle buoyant terminal velocity, and stored on computer tape.

The generation of LC fields and subsurface trapping zones (which we refer to as SRZ, or "Stommel retention zones") is described in §3.1 and in §4.

How does a particle get into a SRZ? In the idealized problem, a particle is either in or out; it cannot cross the closed SRZ boundary. Of course, if a particle can get in, it must also be possible to get out, and so the trapping is not complete. The idealized analysis omits velocity fluctuations, and crossing of the boundary is expected to be possible as a result of the turbulent fluctuations, inevitably present.

The investigation of the appropriate model for transport due to turbulence is the subject of §5. This model must allow the calculation of the distribution of oil particles resulting from the combined effects of Langmuir cell mean motions and superposed random velocity fluctuations. The model adopted as a consequence of the considerations of §5 is based upon eddy diffusivity, and describes the volume fraction of oil in terms of convection by the mean (LC) velocity field, buoyant rise, and diffusion due to turbulence. The principal matter to be determined in such a model is the relationship between eddy diffusivity and the turbulence characteristics. In the course of §5, influence of wave accelerations, and the influence of oil particle inertia terms upon the rate of approach of the turbulent diffusivity to its asymptotic values are evaluated. In addition, the influence of the crossing-trajectories effect, which causes vertical and horizontal diffusivities to be unequal, is taken into account. Throughout our analysis, the oil is assumed to be in the form of small, noninteracting particles: the important question of the process by which these particles are formed is not considered.

Section 6 is devoted to the construction of a suitable computational method to determine oil concentrations from the model devised in §5. Since the diffusivities are very small, the time required to achieve a steady distribution of oil is found to be too large and the spatial scales too small to allow a direct finite difference simulation to resolve the entire region. Instead, we resort to a combination of analytical and numerical methods. A byproduct of this method of solution is a much clearer picture of the injection and loss of oil to SRZ's.

Section 7 describes the results of our computations of subsurface oil dispersion.

In §8 an attempt is made to describe the effects of LC on a coherent layer of oil floating on the surface. It is a departure from the main theme of the work: subsurface motions are not considered, and the form that the oil takes is not that assumed in the rest of the work. A simple model is developed that predicts a collection of oil into windrows, and allows an estimate of the amount of oil present.

Finally, in §9, we discuss the conclusions that we arrive at, and we suggest ways that the information we have found may to be put to use.

3.1 Parameter Ranges for Langmuir Circulations Computations

The complete mathematical model for Langmuir circulations will be presented in §4; it requires as input the Stokes drift of the surface waves, or characteristic wave frequency, the wind stress applied at the ocean surface, and the eddy viscosity representing the effects of turbulence. In our model, we represent wind generated wave fields by a single representative wavetrain obtained by considering known properties of empirically determined ocean wave spectra. Since the spectra depend upon wind speed and upon the wind fetch and/or duration, these factors will be accounted for in the specification of the wave characteristics.

The wind stress will also be related to wind speed, and so the wind speed V_a, and the sea state will be the primary environmental inputs. Calculations are done here with wind speeds V_a of 5, 10, and 15ms^{-1}.

Three choices of "ocean mixed layer depth" which we denote by H (taken to be 5, 10, and 20 meters) are made to fix the maximum depth of penetration of LC to be considered. The actual mixed layer depth may exceed these values, and in fact the real mixed layer plays no role in the calculation except that we expect that the LC depth cannot exceed it. Thus, for each value of H and wind speed, we calculate three LC fields, one penetrating to depth H, and two others penetrating to intermediate depths. Altogether, twenty-seven LC fields are calculated in this way.

We now describe the rationale used to relate each of the input parameters to the wind speed.

Wind Stress

The water friction velocity, u_*, is a measure of the applied wind stress, τ_a, which is taken to be $\tau_a=\rho_w u_*^2$, where ρ_w is the water density. Using the standard estimates (such as that in Leibovich (1977, p. 740), we correlate u_* with wind speed through

$$u_* = V_a/660 \qquad (3\text{-}1)$$

where V_a is the wind speed a few meters (5 or more; the exact height is not critical) above the surface.

Correlations for a Fully-Developed Sea

The spectrum of wind generated waves is sharply peaked, and this spectral peak is near the frequency corresponding to the waves of "significant height" (i.e., the mean of the 1/3 highest waves). As time (wave duration T, in cases where the wind is switched on at a definite time) or distance (wave fetch F, in steady cases with wind blowing over a finite distance) increases, the spectral peak moves to lower and lower frequencies. An idealized asymptotic state (as duration T or fetch $F \to \infty$) in which no further wave growth occurs and known as a "fully-developed sea", has been found to be a useful hypothesis. In this state (the existence of which, as argued by Phillips (1977), is conjectural), the wave characteristics (height $H_{1/3}$, frequency σ, wavenumber κ, phase speed c) for deep water wind-driven waves may be related to the wind speed as follows:

$$H_{1/3} \simeq \alpha V_a^2/g \tag{3-2}$$

$$c \simeq \beta V_a \tag{3-3}$$

and we assume σ and κ are related to c through the linear deep water dispersion relation

$$c = \sigma/\kappa = g/\sigma \tag{3-4}$$

where g is the acceleration of gravity. The values for the dimensionless constants α and β given in the literature vary. Longuet-Higgins (1969) takes $\beta \simeq 1$, $\alpha \simeq 0.25$, Stewart (1967) and Neumann & Pierson (1966) also suggest $\beta \simeq 1$, but take $\alpha \simeq 0.2$, while Bretschneider (1966) takes $\beta \simeq 1.95$, $\alpha \simeq 0.283$.

A truly fully-developed sea may never be approached for high speed winds, since a fetch greater than the circumference of the earth may be required (Bretschneider (1966)), and this must be recognized when estimates using the above values for α and β are used. Real wind waves, with finite duration T and/or fetch F, can be related to a steady imposed wind field V_a via (3-3) and (3-4), provided α and β are taken to be functions of T and/or F. For a developing sea, α and β will both be less than their fully developed values.

In the LC model to be used, the natural length is κ^{-1}, which is $\lambda/2\pi$, where λ is the length of the dominant surface waves. A relation between κ and V_a is found from (3-3) and (3-4),

$$\kappa = \beta^{-2} g V_a^{-2} \tag{3-5}$$

Eddy Viscosity

The mathematical model of Langmuir circulations that we use represents the dynamical effects of turbulence on the coherent convective motions by use of an eddy viscosity, ν_T. This is the input parameter about which least is known, and it is, consequently, the most difficult to estimate. Semi-empirical estimates which correlate eddy-viscosity with surface wave characteristics (see, for example, Ichiye (1967)) relate ν_T to the significant height $H_{1/3}$ (average height of the highest-third of the waves in the spectrum) and frequency σ in the form

$$\nu_T = C_T H_{1/3}^2 \sigma \tag{3-6}$$

where C_T is a dimensionless constant. An estimate of this form is independently arrived at in Leibovich & Radhakrishnan (1977) (equation 2) by matching theoretical results on Langmuir circulation with observations. The constant C_T in that case is 0.7×10^{-3}. Two other estimates are found, also independently, in that paper; using correlations appropriate for a fully-developed sea, C_T is found to be 0.58×10^{-3} and 1.5×10^{-3} and the mean of the three values is approximately 0.9×10^{-3}.

There is (inevitably, due to the scarcity of data, and the intrinsic problems of using and of specifying an eddy viscosity for a turbulent flow) a considerable scatter in the value of C_T, although the order of magnitude is consistent in the estimates cited above, and is consistent with estimates of C_T given by other sources. We adopt the form (3-6), and in the section on "Langmuir number", we choose $C_T = 1.5\times10^{-3}$. It is argued there that the final results in the Langmuir circulation problem ought not to be overly sensitive to the precise value of C_T selected.

The Langmuir Number

In water of constant density, the LC problem can be reduced to a dimensionless form involving one dimensionless parameter, the Langmuir number, La. This parameter depends upon sea state, eddy viscosity, and friction velocity as follows:

$$La = 2(\sigma_0 \nu_T)^{3/2}/gH_{1/3}u_* \tag{3-7}$$

where deep water gravity waves have been assumed, and where the characteristic wave frequency and height are taken to be σ_0, the frequency of the spectral peak, and $H_{1/3}$.

Introducing the correlations (3-1) to (3-4),

$$La = 1.32\times10^{3} C_T^{3/2}\alpha^2\beta^{-3} \tag{3-8}$$

which is independent of wind speed. If we adopt, for purposes of estimation, $\alpha = 0.25$, $\beta = 1$ (following Longuet-Higgins (1969)), and $C_T = 1.5\times10^{-3}$ (representing the upper value of those discussed below (3-6), we find

$$La \simeq 0.005 \tag{3-9}$$

We believe that this is a reasonable value to take for La, despite the uncertainities in the parameters C_T, α, and β. Thus we adopt (3-9) in our calculations.

There is reason to believe that the particular form of the Langmuir cells may not be sensitive to the value for ν_T (hence C_T) in any event. Since reasonable estimates generally indicate that La is small, the dynamics are nearly inviscid. The eddy viscosity ν_T is likely to play a significant role only near the air-sea interface, where it serves as the mechanism for momentum transfer from wind to water. The rate of momentum transfer is fixed by u_* only, and does not involve ν_T. Below the thin surface boundary layer (the layer in which ν_T is dynamically significant), momentum transfer is accomplished mainly by convective motions, once Langmuir circulation is initiated. Thus, ν_T is expected to affect the onset to LC convection, but once convection is effectively initiated, ν_T should primarily determine the thickness of the surface boundary layer.

LC Length Scale Parameter

The inverse of surface wavenumber, or κ^{-1}, serves as the length scale in the LC model. Since we have denoted the maximum LC penetration depth by H, the maximum dimensionless depth allowed is κH . For a given wind speed and fetch, one may compute κ; together with H, this sets a minimum numerical value, κH, of the (dimensionless) computational domain. The depth of well-developed LC corresponds to κH on the order of unity. Very little qualitative change in the structure of LC is evident beyond $\kappa H = 3$ to 4 in the published simulations of LC. Thus we have arbitrarily set the maximum dimensionless value of the depth of the LC field calculations to be 5.6. This is large enough to capture all known Langmuir features.

We fix the wavelength of the surface waves under consideration by prescribing $\kappa H = 5$: in this way, the specification of H fixes κ for the purposes of our calculations . Given the wind speed, the wave field under consideration will correspond to a definite fetch. If one adopts the empirical spectral development model to be presented below, this fetch can be calculated. (This will be illustrated, but the information on fetch is not essential for the subsequent work.) More important is the fact that

the selection of κ also determines $H_{1/3}$, as shown below, and therefore the sea state.

Development of the Wind Wave Spectra and Stokes Drift

While a nearly fully developed sea may be established in light winds, the idealization is less realistic in moderate winds, and is unlikely ever to occur, as previously mentioned, in heavy winds. If we insist upon LC penetration depths of 5, 10 and 20 meters - the cases dealt with here - a developing sea is more appropriate than a fully-developed one, except at the lowest wind speed (5m s^{-1}) to be considered. Furthermore, there is some question about the applicability of a "fully-developed sea" at wind speeds as high as 15m s^{-1}. For example,for this wind speed, Bretschneider (1966) estimates that a minimum wind duration of 307 hours is required to raise a fully-developed sea. We note that even a very young sea will generally produce LC in a matter of a few tens of minutes. In addition, for the same wind speed and $\beta = 1$, (3-5)predicts $\kappa = 0.04$m, (length, λ, of surface equals 144 meters), so the length scale (κ^{-1}) of LC is 23m. A mixed layer with a depth of 5m is thin compared to the depth of LC generation, and, once LC activity is initiated, strong convective activity will reach to depths comparable to, Thus, for a high wind speed, a fully-developed sea predicts wave activity that is too vigorous and unlikely to represent sea states actually realized.

From the extensive data summarized by Phillips (1977, pp. 161-3), the frequency of the spectral peak, σ_0, is given in terms of the fetch F and the friction velocity u_{*a} of the airflow above the water by

$$\sigma_0 \approx 2.2(g/u^2_{*a})(gFu^2_{*a})^{-1/4} \qquad (3\text{-}11)$$

and the mean-square displacement of the water surface $\overline{\zeta^2}$ is

$$\overline{\zeta^2} \approx 1.6\times10^{-4}(u^2_{*a}F/g). \qquad (3\text{-}12)$$

If the development of the spectrum is limited by wind duration T rather than fetch F, it is reasonable to interpret (3-11) and (3-12) by replacing F by $c_g T$, where c_g is the group velocity of waves at the frequency σ_0, or $c_g = 1/2(g/\sigma_0)$.

The Stokes drift (see §4) for the ocean contains contributions from all the waves in the spectrum. Our model replaces these by a single representative wavetrain with frequency σ_0 and the amplitude of the "waves of significant height". This replacement can be justified by considering the effect of a spectral spread on the drift, following (for example) the work of Kenyon (1969).

The amplitudes (half height) of the waves of significant height, $a_{1/3}$, may be related to the rms amplitude (3-12) by (Longuet-Higgins, 1952)

$$a_{1/3} = 1.42\sqrt{\xi^2} = 1/2H_{1/3}. \tag{3-13}$$

The Stokes drift for the replacement wave is (Phillips, 1977)

$$u_s = a^2_{1/3}\kappa^2_0 c_0 \exp(2\kappa_0 z) \tag{3-14}$$

where $c_0 = \sigma_0/\kappa_0$ is the phase speed of a wave having frequency σ_0 and wavenumber κ_0, and z is a coordinate measured vertically upwards from the mean free water surface: $a_{1/3}\kappa_0$ is a measure of the slope of the replacement wave. Since κ_0 is constructed from σ_0 by the deepwater dispersion relation

$$\sigma_0^2 = g\kappa_0 \tag{3-15}$$

(3-10), (3-11), (3-12) imply a wave-slope

$$a_{1/3}\kappa_0 = 0.087 \tag{3-16}$$

which is <u>independent</u> of fetch or duration.

We now have enough information to assemble a table summarizing the set of LC fields generated. Given H and V_a, we determine κ_0 from (3-16) (in considerations of the effect of a spectral spread, we arrived at .088 for the slope parameter rather than 0.087, and it is the former value we actually have used), u_* from (3-1), and La from (3-9). From these values, the convective velocity scale, V, of the LC model (see §4) can be calculated. This is given by (see §4),

$$V = a_{1/3} u_* (\sigma/\nu_T)^{1/2},$$

Using (3-6), we see that V may be expressed as

$$V = u_*/2\sqrt{C_T} = 12.9 u_* \qquad (3\text{-}17)$$

if we use the value suggested for C_T. Thus the convective velocity varies linearly with wind stress if the parameterization (3-6) is adopted; Thus, using (3-1), we relate V to the wind speed V_a through

$$V = 1.96 \times 10^{-2} V_a. \qquad (3\text{-}18)$$

The values of V for the three wind speeds in our calculations are given in Table 3-1

Table 3-1 -Entries give the LC convection velocity scale, V, in cm/s.

	Wind Speed (in meters/second)		
	5 (Case A)	10 (Case B)	15 (Case C)
V	9.8	19.6	29.4

Cases 1, 2, and 3 correspond to depths H of 5, 10, and 20 meters. The length scaling factors (κ_0^{-1}) and wave heights $H_{1/3}$ (= $2a_{1/3}$) are the same for all wind speeds, and are given in Table 3-2.

Table 3-2. - LC length scaling factors κ_0^{-1} in meters, and the significant wave heights for cases computed.

Case	κ_0^{-1} (in meters)	$H_{1/3}$ (in m)
1	1	17.6
2	2	35.2
3	4	70.4

For each of the 9 combinations of wind speeds and maximum depths H of Table 3.1, we have computed three LC fields. As described in §4, the LC model predicts a continually deepening penetration of Langmuir circulations. For each of the nine input combinations, we select LC fields at three time stages in this continuing development; one corresponds to the time at which the LC have penetrated to depth H, and two others representing intermediate stages of development. So far as the dispersion calculation is concerned, we regard each of these fields as a possible steady realization of a LC field.

It is worth noting that the cases illustrated here for the highest wind speed and lowest H values correspond to very immature seas. For example, if interpreted in terms of wind duration, the case of V_a = 15m s^{-1} corresponds, according to the estimates presented earlier, to a duration of only 5.25 minutes. In such a case, our dispersion calculation will probably be of little value, since the seas will rapidly become much more vigorous than assumed; in turn this means that the LC fields can only be confined to the assumed small depth for a short time, and soon will penetrate to substantially greater depths. We could (although we do not here) interpret our dimensionless LC fields in a different way that avoids this loss of significance. We could fix κ_0 by relating it to fetch via (3-11) and (3-15) for example, or by arbitrarily fixing $H_{1/3}$ and working backwards to κ_0 using (3-16).

4. MATHEMATICAL MODELS FOR THE SIMULATION OF LANGMUIR CIRCULATION, STOMMEL RETENTION ZONES, AND OIL DISPERSION

The wave-current interaction theories of Langmuir circulations describe the water motions by the averaged Navier-Stokes equations. Averages are taken over times comparable to the period of surface waves, and so the motions described by the resulting set of equations have surface wave frequencies filtered out. The required averaging process, (which is not straightforward), is given in Craik and Leibovich (19[illegible]) and more systematically in Leibovich (1977a). The theory can also be derived from the generalized Langrangian mean formalism, an exact theory of wave-current mean flow interactions due to Andrews and McIntyre (1978): a derivation of the LC governing equations by this route is given by Leibovich (1980). In the theory, it is assumed that incoherent (turbulent) motions may be described by a constant eddy viscosity.

Following the presentation of the LC model a brief discussion of its numerical solution in sections 4.1 and 4.2, we turn to a description of Stommel retention zones in §4.3; the diffusion model to be used for the dispersion calculations is then is then presented in §4.4. The important question of the justification for the use of a diffusion model for the dispersion is given an entire section (5).

4.1 Governing Equations for Langmuir Circulations

The equations governing the formation of Langmuir circulations in water of constant density are, according to Leibovich (1977a),

$$v_{,t} + (\mathbf{v}\cdot\nabla) \mathbf{v} = - \nabla \pi + \mathbf{u}_s \times(\text{curl } \mathbf{v}) + \nu_T \nabla^2 \mathbf{v} \qquad (4\text{-}1)$$

$$\nabla\cdot\mathbf{v} = 0 \qquad (4\text{-}2)$$

where a comma denotes partial differentiation, v is the Eulerian mean velocity vector in the water, π is a scalar modified pressure, and u_s is the Stokes drift due to the water waves. In the absence of u_s, and if ν_T is interpreted not as an eddy viscosity (as we shall do) but as the molecular velocity, then (4-1,2) are the Navier-Stokes equations for the conservation of momentum and mass of an incompressible fluid. The

rectified effects of the surface waves appear only in the form of the "vortex force"

$$\mathbf{u}_s \times(\text{curl } \mathbf{v}\ ). \tag{4-3}$$

Here the Stokes drift of surface waves of small slope is given by (Phillips, 1977)

$$\mathbf{u}_s = \overline{\left(\int^t \mathbf{u}_w\, dt \cdot \nabla\right) \mathbf{u}_w} \tag{4-4}$$

where $\mathbf{u}_w$ is the wave velocity vector and the overbar represents a time average over intervals extending over several surface wave periods. In this work, we assume that $\mathbf{u}_s$ is in the direction of the wind stress, taken to be the x-direction, and that $\mathbf{u}_s$ varies only with depth z (measured vertically upwards from the mean free surface). The water depth is taken to be infinite, and so the ocean lies in $-\infty<z\leq 0$. The assumptions made about $\mathbf{u}_s$ are consistent with a random, wind-generated sea over restricted fetch intervals. We make the further assumption that we may replace $\mathbf{u}_s$ by the Stokes drift of a "replacement wave" (see §3), and take (3-14) for $|\ \mathbf{u}_s\ |$.

The ocean is assumed to be at rest initially, and to begin to move in response to an applied wind stress $\tau = \rho u_*^2$ and surface wave field imposed at time $t = 0$. If we take (u,v,w) to be the (x, y, z) velocity compoments, then the boundary and initial conditions on the velocity vector $\mathbf{v}(x,y,z,t)$ are

$$u_{,z} = u_*^2/\nu_T,\ u_{,z} = w = 0 \text{ on } z = 0 \tag{a}$$

$$(u,v,w) \to 0 \text{ as } z \to -\infty \tag{b}$$

$$(u,v,w) = 0 \text{ at } t = 0 \tag{c}$$

(4-5)

The problem is made dimensionless by the following scaling scheme:

length scale: κ_0^{-1} (a)

velocity scale in x direction = $U = u_*^2/\nu_T\kappa_0$ (b)

velocity scale in the y and z directions (convective scale)
$= V = a_{1/3}u_*(\sigma_0/\nu_T)^{1/2}$ (c)

time scale: $(\kappa_0 V)^{-1}$ (d) (4-6)

modified pressure: $u_*^2 a_{1/3}^2(\sigma_0/\nu_T)$ (e)

Stokes drift: $a_{1/3}^2\kappa_0\sigma_0$. (f)

When substituted into (4-1), (4-2) and (4-5), the dimensionless problem is (we use the same symbols for dimensionless variables and their dimensional counterparts since no confusion is likely)

$$\mathbf{v}_{,t} + (\mathbf{v}\cdot\nabla)\mathbf{v} = u_s \nabla u - \nabla\pi + La\,\nabla^2\mathbf{v} \quad (a)$$

$$\nabla\cdot\mathbf{v} = 0 \quad (b) \qquad (4\text{-}7)$$

and (4-5) remains the same except that $u_{,z}=u_*^2/\nu_T$ is replaced by $u_{,z} = 1$ in (4-5a). The parameter La is the Langmuir number defined by

$$La = \kappa_0\nu_T/V. \qquad (4\text{-}8)$$

The solution to the problem as posed is inherently time-dependent, since the force applied at the water surface is resisted only by the fluid inertia. A steady motion is obtainable only by taking into account effects, such as the Coriolis acceleration due to the Earth's rotation (important for problems where the motion persists for times larger than about one quarter pendulum day), a finite bottom (which, under most circumstances is probably irrelevant), or some less obvious sink for momentum. We accept the present problem, and calculate the evolving motion.

It is worth noting that a purely rectilinear solution is possible (Leibovich, 1977a) in which $v = w = 0$ and u varies only with z and t. This motion is unstable for La <0.66 (Leibovich and Paolucci (1981)),

however, and the expected form of the instability, according to the theoretical work of Leibovich and Palucci (1980b), is rolls (disturbances independent of x), consistent with the long windrow patterns actually observed in the ocean. To get such an instability numerically, one need only calculate the rectilinear solution out to some arbitrary time level, and then superimpose at that time a very small perturbation-such as a weak spanwise sinuosity-and continue the computation. If La <0.66, the convective rolls will grow with time to produce well formed simulated Langmuir circulations. The next section discribes the numerical method used.

4.2 Numerical Method

The solutions were carried out by the explicit finite difference algorithm developed by Radhakrishnan (1975) and modified by Paolucci (1979). A description of the method, which is applied to the x-independent version of (4-7) in vorticity-streamfunction form, is given by Leibovich and Paolucci (1980a), and will not be reproduced here.

It is necessary to choose a finite spanwise dimensionless width for the computational domain, and our computations were done for $0 \leq y \leq 4$. This is sufficiently large to encompass Langmuir circulations with a windrow-to-windrow dimensional distance of $8\kappa_0^{-1}$ or smaller. For the cases computed this allows the description of LC with windrow spacings up to 32 meters.

The spatial mesh used was $\Delta y = \Delta z = 0.1$, which implies a cell Reynolds number of around 10. The discussion of numerical diffusion given by Leibovich and Paolucci (1980) applies here as well.

By placing the problem in dimensionless form, we are able to reduce all cases to be run (see Table 3-1) to a single numerical problem. The initial value problem is calculated until the convective activity has penetrated to a dimensionless depth of 5.6 (see §3.1) and complete sets of the three velocity components are stored at numerous intermediate time levels. From this collection, three data sets are selected, the final one and two representative sets at intermediate times. Each of these is converted to nine dimensional velocity fields by use of the scaling

factors (4-6) and Tables 3-1 and 3-2. This produces 27 different velocity fields, each of which is regarded as a possible realization of a Langmuir circulation convective motion. The three basic dimensionless LC fields are shown in figures 4-1, 2, 3.

As an example of a dimensional realization, we note that for case C, with a windspeed 10m s^{-1}, figure 4-3 describes a case for which the distance between windrows is 16 meters. Each of these is stored on magnetic tape, and converted to a Stommel retention zone as described in the next subsection.

4.3 Calculation of Stommel Retention Zones

The vertical velocity in LC vanishes at the surface , and grows in magnitude with depth below convergence lines. If a buoyant particle is introduced at a point below the convergence line where downwelling speeds exceed the (positive) buoyant terminal velocity of rise, V_T, the particle will be carried down. On the other hand, the particle will eventually be swept laterally away from its initial position into a region where water downwelling is less than V_T, and the particle will tend to rise back towards the surface. A fascinating result of Stommel's (1949) (in a paper in which an artificial velocity field was used to show that LC can prevent heavy particles from sinking) is that a buoyant particle can be trapped forever in a zone some distance below the surface if it is injected into that zone and if turbulence is ignored. A subsurface zone in which particles can become trapped will be called a "Stommel retention zone" or SRZ here . These zones will play a major role in the oil dispersion calculation method introduced in §4.4.

We continue to use the same coordinate system of and suppose an LC field has developed. Then the horizontal and vertical velocity components, v and w may be given in terms of a streamfunction in ψ, or

$$v = \psi_{,z}, \quad w = -\psi_{,y}. \tag{4-8}$$

If we assume, as Stommel did, that the velocity of the oil relative to the surrounding water is always in the vertical direction with constant speed V_T, then the trajectory of an oil particle $y = Y(t)$, $z = Z(t)$ is given by

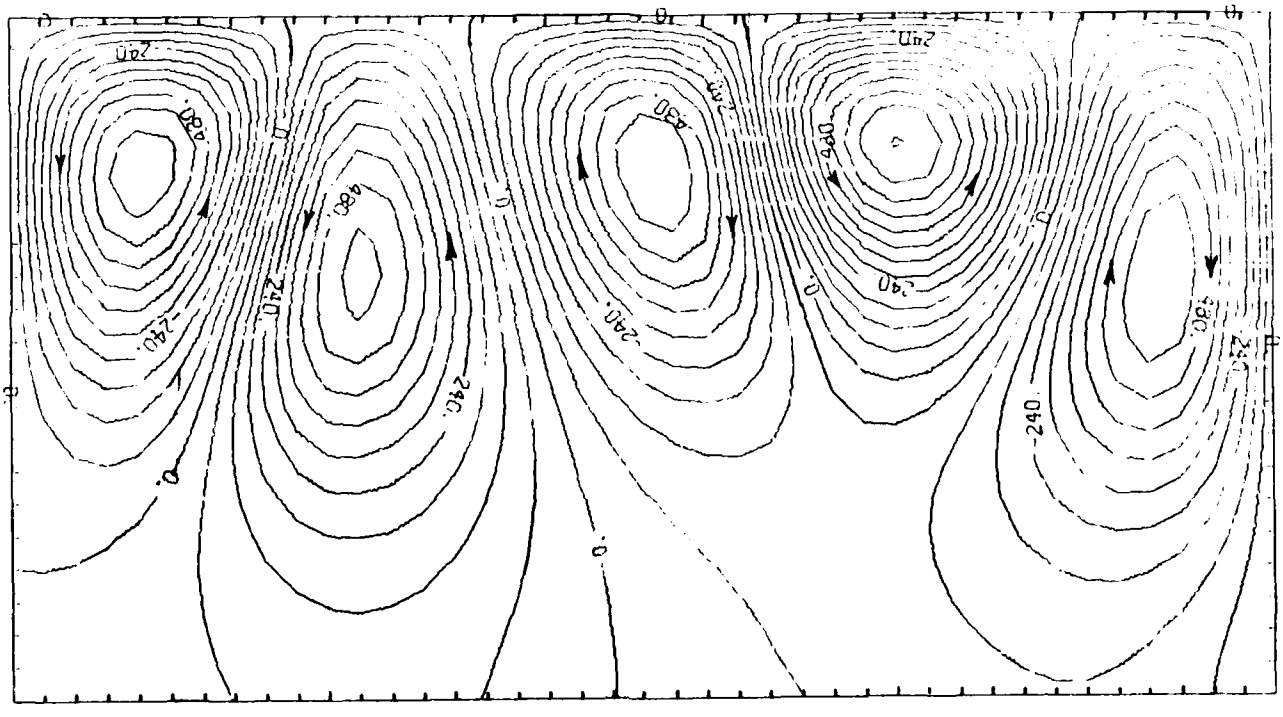

Figure 4-1. Streamfunction contours for the dimensionless Langmuir circulation field 35 dimensionless time units after onset of the motion.

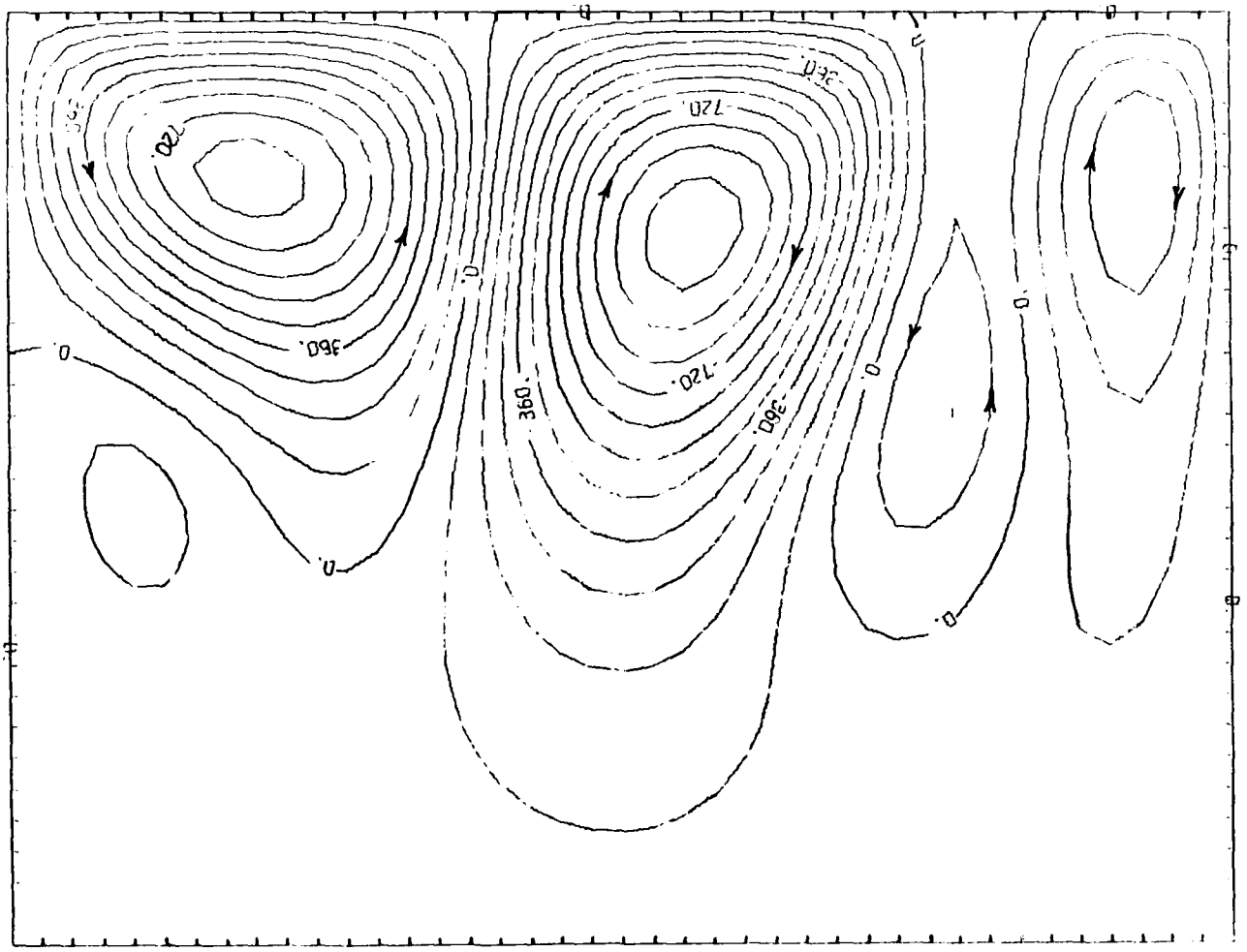

Figure 4-2. Same as Figure 4-1, but after 50 time units have elapsed.

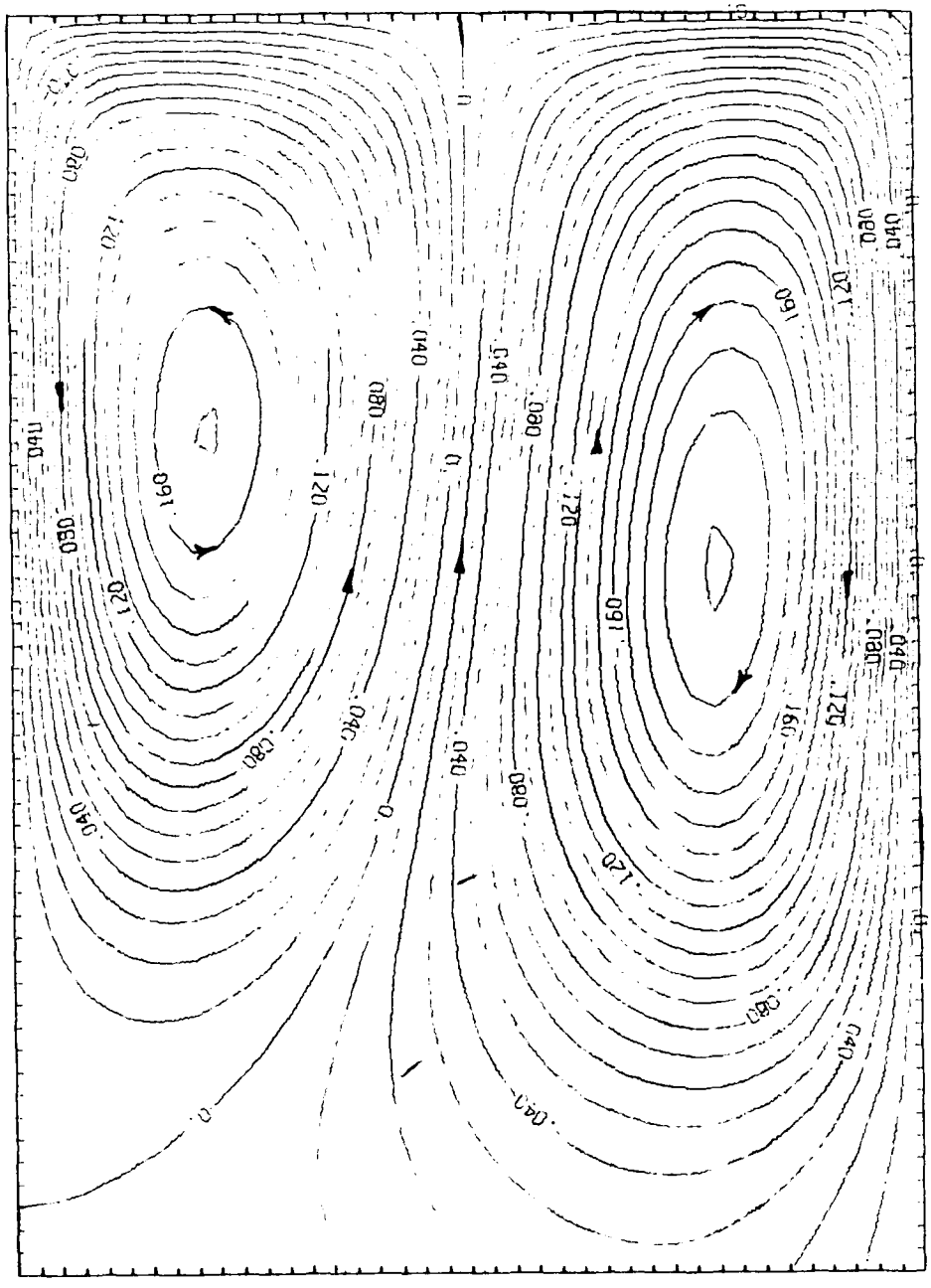

Figure 4-3. Same as Figure 4-1, but after 95 time units have elapsed.

$$Y_{,t} = v = \psi_{,z} \qquad \text{(a)}$$
$$Z_{,t} = w + V_T = -(\psi - V_T y)_{,y}. \qquad \text{(b)} \qquad (4\text{-}9)$$

If the fluid motion is steady in time, then $\partial\psi/\partial t = 0$, and trajectories of oil particles in the cross-plane determined by (4.9)coincide with level curves of the function

$$\Psi(y,z) = \psi(y,z) - V_T y. \qquad (4\text{-}10)$$

It is not hard to see that, if $w + V_T < 0$ for given V_T anywhere on a downwelling plane, then a Stommel retention zone exists for all particles with terminal velocity of rise less than or equal to V_T. These zones are nested regions for which the contours of Ψ are closed. Each of these nested closed contours (if any exist) is enclosed within its largest member, which forms the boundary of the SRZ. The disposition and extent of an SRZ depends critically upon V_T, the LC convective velocity scale V and length scale κ_0^{-1} (since the fluid streamfunction is proportional to $V\kappa_0^{-1}$). If C is the boundary contour of an SRZ for a given value of V_T in a given LC field, than any particle with this value of V_T or smaller placed inside C will, according to this model, remain trapped within C forever. If V_T is reduced, the SRZ is enlarged; if increased the SRZ is reduced.

The level lines of Ψ are plotted in Figure 4-4 for $V_T = 0.84$ cm/s, $V_a = 10$ m/s, $H_{1/3} = 0.7$ m. Note that the SRZ is very extensive, and distribute oil to depths exceeding 20 meters. Retention zones for a number of terminal velocities are given in the Appendix: the examples cover all twenty-seven LC fields that we have computed.

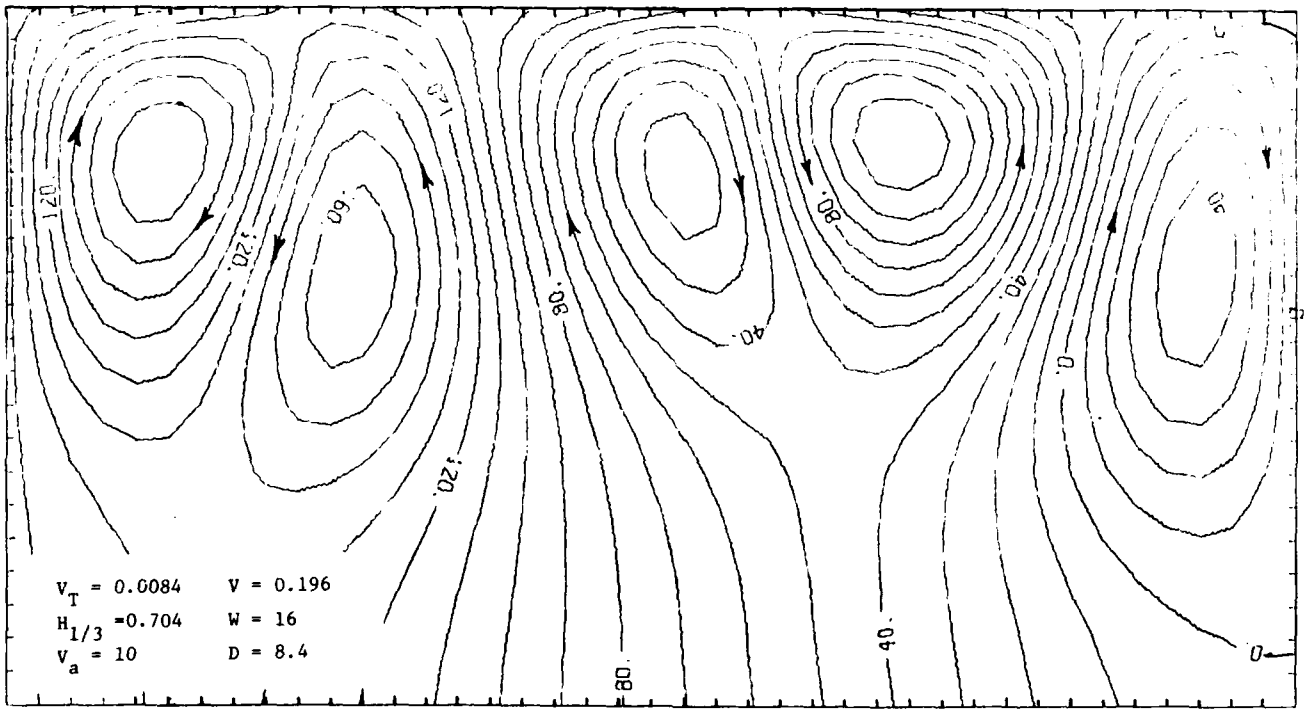

Figure 4-4. Stommel retention zone for particles with terminal velocities V_T or less. Inset legend: V_T = particle terminal velocity in m/s. $H_{1/3}$ = significant wave height in meters. V_a = wind speed in m/s. V = Langmuir circulation velocity scale in m/s. W = width of computational domain shown in meters. D = depth of domain shown in meters.

4.4 The Diffusion Model for Oil Dispersion

We attempt to describe the concentration of oil, that is, the volume fraction of the water volume occupied by oil at any position and time; this is equivalent (Tennekes and Lumley, 1972); Monin and Yaglom, 1971) to asking for the probability that a single oil particle may be found in the subvolume centered on the position of interest. The concentration, C, will be assumed to be controlled by the following diffusion equation

$$C_{,t} + \mathbf{v}\cdot\nabla C + V_T C_{,z} = (D_1 C_{,y})_{,y} + (D_1 C_{,z})_{,z} \tag{4-11}$$

where we take

$$C = C(y,z,t) \tag{4-12}$$

$\mathbf{v}$ is the velocity vector of the mean motion (here taken to be Langmuir circulations), and V_T is the terminal velocity, positive for positively buoyant oil particles. The parameters D_1 and D_2 are diffusivities resulting from turbulent buffeting of the oil and are in general different for the horizontal (D_1) and the vertical (D_2) directions; they may depend upon depth.

The derivation of this equation is discussed in Lumley (1978b) and the validity of its use for oil particles in water is considered in §5.

In calculations that we will do, it will be assumed that the amount of oil in the region of the ocean considered, is fixed. That is, no new oil is being injected, and our job is to determine how the fixed amount of oil is distributed. The total amount of oil in the volume V of the ocean being considered is

$$\hat{V} = \int_V C \, dxdydz \ . \tag{4-13}$$

Its rate of change with time is zero, by hypothesis. The Langmuir circulation cells described in sections (4.1), (4.2) are periodic in the cross-wind horizontal direction y and are independent of x. Consider a volume V of unit distance in the x-direction, and consisting of one period $(0,Y_1)$ of the LC in the spanwise (y) direction, and of infinite depth. Since the spanwise distribution of oil is determined strictly by the LC

cell, C will have the same periodicity, and $C_{,y}$ vanishes of the boundaries of the cell, say at y=0 and $y=Y_1$. Integrating (4-11) over this volume ($0 \geq z > -\infty$, $0 \leq x \leq 1$, $0 \leq y \leq Y_1$) we find

$$\hat{V}_{,t} = \int_0^{Y_1} [D_2(0)C_{,z}(y,0,t) - V_T C(y,0,t)]dy$$

since we must have $w(y,0,t) = 0$ in the Langmuir circulations. Since V does not change with time, the integral must vanish. The integral is the flux of oil into the ocean across the mean free ocean surface, so we take as one boundary condition

$$V_T C - D_2 C_{,z} = 0 \text{ at } z = 0, \tag{4-14}$$

and we also have the additional conditions

$$C_{,y} = 0 \text{ at } y = 0, Y_1 \tag{4-15}$$

$$C \to 0 \text{ as } z \to -\infty. \tag{4-16}$$

These boundary cnditions hold for unsteady as well as steady conditions, although we will concern ourselves only with the time-independent case.

The solution of the problem posed by (4-11), (4-14), (4-15) and (4-16) will be dealt with in §6, Here we make two observations. First, the level of C is not determined; if we find a solution, any multiple of it is also a solution. The magnitude of C is determined by the additional condition (4-13) which is just an initial condition for the unsteady problem whose steady limit we seek.

Second, the role of the Stommel retention zones can now be further clarified. If we make (4-11) dimensionless using LC velocity scale V, and LC length scale κ_0^{-1}, then we may write the steady version of (4-11) in dimensionless form as

$$vC_{,y} + (w + V_T/V)\, C_{,z} = (\varepsilon_1 C_{,y})_y + (\varepsilon_2 C_{,z})_{,z} \tag{4-17}$$

where

$$\varepsilon_1 = \kappa_0 D_1/V,\ \varepsilon_2 = \kappa_0 D_2/V \tag{4-18}$$

and otherwise we use the same symbols for dimensional and dimensionless variables.

We find in §5 that ε_1 and ε_2 are small (of order 10^{-3}). Consequently, it is clear that the reduced equation found by neglecting ε_1 and ε_2 altogether will play an important role. Returning now to dimensional variables, the reduced equation is

$$v\, C_{,y} + (w + V_T)\, C_{,z} = 0, \tag{4-19}$$

thus, as usual in problems of boundary layer character, the leading approximation satisfies an equation of reduced order and we are not able to enforce all boundary conditions.

The general solution to (4-19) is

$$C = C(\Psi) \tag{4-20}$$

where

$$v = \Psi_{,z},\ w + V_T = -\Psi_{,y} \tag{4-21}$$

so that C is constant on lines of constant Ψ. These lines, in turn, are the level curves found in the previous section; a closed Ψ = constant line defines an SRZ.

The restoration of the diffusivities, and the enforcement of the boundary conditions is left to §6.

5. THE MATHEMATICAL MODEL FOR DISPERSION OF OIL IN TURBULENT FLOW

Lumley (1978) examines the conditions under which one may treat the dispersion of small particles in a turbulent fluid by the use of a diffusion equation. In the last part of §4, we introduce the diffusion model; the limits of its validity are examined in detail in the present section. In Lumley's approach, steady state diffusivities are determined, assuming that the droplet drag law is linear. The principle problem is to determine whether the assumption of a linear drag law is justified, and to estimate the terminal velocity corresponding to it. Most droplets of interest are too large to be in the Stokes regime, so that a linear law results only from linearization about a mean velocity. This results in slightly different drag coefficients in the horizontal and vertical directions. Below we will consider various aspects of the question of limitations on particle size which will permit a linear(ized) drag law for particles in a turbulent fluid, and also subject to wave accelerations and a large-scale mean flow.

5.1 Permissible Fluctuating Relative Reynolds Numbers

We may write the instantaneous drag force as $(U_i/U)f(U)$, where U is the magnitude of the total instantaneous relative velocity, and U_i is the vector value of the total instantaneous relative velocity. This presumes that the wake is steady, and that changes in the oncoming flow are sufficiently slow that the boundary layers and wake have time to adjust to the changed conditions. It implies that the drag is always aligned with the flow, although it is a non-linear function of the magnitude. This is discussed at length in Lumley (1978). The function f is given by (to second order)

$$f = (U/a_S)[1 + (3/16)R] \tag{5-1}$$

where a_S is the Stokes value of the time constant, given by V_{TS}/g, where V_{TS} is the Stokes value of the terminal velocity given by equation (5-6). Now, we may expand the expression $(U_i/U)f(U)$ in a Taylor series about the value $U_i = (0,0,V_T)$ keeping terms through second order. The derivatives are given in general by

$$\begin{aligned} I &= (f/U)(\delta_{ij} - U_iU_j/U^2) + f'U_iU_j/U^2 \\ II &= (f'/U - f/U^2)(\delta_{ij}U_k/U + \delta_{ik}U_j/U + \delta_{jk}U_i/U - \\ &\qquad 3U_iU_jU_k/U^3) + f''U_iU_jU_k/U^3 \end{aligned} \tag{5-2}$$

where we have indicated by I and II the first and second derivatives respectively, and by f' and f" the first and second derivatives of f. If we write $f = U/a_S + BU^2$, then in a horizontal direction (say, the 1-direction) we have as a requirement that the second derivative be much smaller than the first derivative, that

$$-u_1 u_3 B \ll f/U \tag{5-3}$$

substituting (5-1), this translates to

$$(3/16)R' \ll 1 + (3/16)R \tag{5-4}$$

where R' is the fluctuating relative Reynolds number. If we take $R' \leq 0.218R$, then (5-4) will be satisfied, with the left side being not above 20% of the right side, if R = 60, the largest Reynolds number which will permit a steady wake. In the vertical direction (the 3-direction), if we take the turbulence approximately isotropic, we obtain

$$(6/16)R' \ll 1 + (6/16)R \tag{5-5}$$

Taking $R' \leq 0.21R$ will again assure that the first neglected term will be no more than 20% of the term retained. With R = 60, this suggests that R' = 12.5 is a safe value.

5.2 Limits on Particle Size

The expressions given in Lumley (1978) pp. 297, 301 must be modified, because the ratio ρ_o/ρ_w is not large relative to unity, as was assumed there. The modified forms are (obtained from Lumley 1957):

$$V_T = -d^2 g(\rho_o/\rho_w - 1)/18\nu \tag{5-6}$$

$$R = -d^3 g(\rho_o/\rho_w - 1)/18\nu^2 \tag{5-7}$$

$$R = (2\rho_0/\rho_w + 1)(d/\eta)^3/38 \tag{5-8}$$

$$R = -(\rho_0/\rho_w - 1)(2\rho_0/\rho_w + 1)(d/\eta)^5(\ell g/u^2)/1352R_\ell^{1/4} \tag{5-9}$$

where the notation is the same as that in Lumley (1978): d is droplet diameter, g is the acceleration of gravity, the subscripts 0 and w refer to oil (droplet) and water respectively, ν is the kinematic viscosity, η is the Kolmogorov microscale, ℓ the integral scale of the turbulence and u is the r.m.s. turbulent fluctuating velocity. Equation (5-6) gives the Stokes terminal velocity, equation (5-7) the relative Reynolds number based on the terminal velocity, equation (5-8) the relative Reynolds number (based on the fluctuating relative velocity) supposing that the droplet is approximately Lagrangian (i.e. - follows the fluctuating velocity) in its behavior, and (5-9) the relative Reynolds number (based on the fluctuating relative velocity) supposing that the behavior of the particle is approximately Eulerian (i.e. - rises through the turbulence being little influenced by it). Since, for a given size oil droplet, we do not know a priori what its behavior is, we must calculate the various relative Reynolds numbers to determine its behavior.

For a typical situation we take a mean wind in the atmosphere of 10 m/s, and a wave height of 2 m. Supposing that the wind stress goes into the turbulence primarily, we have

$$u^2 \approx (\rho_a/\rho_w)v_*^2 \approx (\rho_a/\rho_w)(v_*/U_a)^2U_a^2 \tag{5-10}$$

where the subscripts a and w refer to air and water respectively. v_* is the friction velocity in the air. If we take

$$(v_*/U_a)^2 \approx 10^{-3},\ (\rho_a/\rho_w) \approx 10^{-3} \tag{5-11}$$

then $u^2 \approx 10^{-4}$ m^2/s^2. We take ℓ to be of the order of the wave height. This gives $R_\ell \approx 2\times10^4$, which is a reasonable value, while $\eta = \ell/R_\ell^{3/4} \approx 1.19\times10^{-3}$m. This is also typical.

Computing values of V_T/u for two values of the ratio ρ_0/ρ_w (on left), we obtain for various d (across the top))

	100μm	300μm	1000μm	3000μm
0.70	1.63×10^{-1}	1.47	1.63×10^{1}	1.47×10^{2}
0.95	2.72×10^{-2}	2.45×10^{-1}	2.72	2.45×10^{1}

If the terminal velocity is large relative to the r.m.s. fluctuating velocity, we may regard the droplet as essentially Eulerian, and vice versa. We see that, with ρ_0/ρ_w = 0.7, 100 μm particles and smaller may be considered Lagrangian, while particles of 1000 μm and larger are Eulerian; at ρ_0/ρ_w = 0.95, particles of 300 μm and smaller are Lagrangian, while those 3000 μm and larger are Eulerian.

If we now apply the Eulerian and Langrangian criteria for the relative Reynolds number to be below 12.5, we find as limiting diameters

ρ_0/ρ_w	0.7	0.95
Eulerian	1277 μm	1761 μm
Lagrangian	6930 μm	6521 μm

In fact, the full relationship is instructive, and is graphed below:

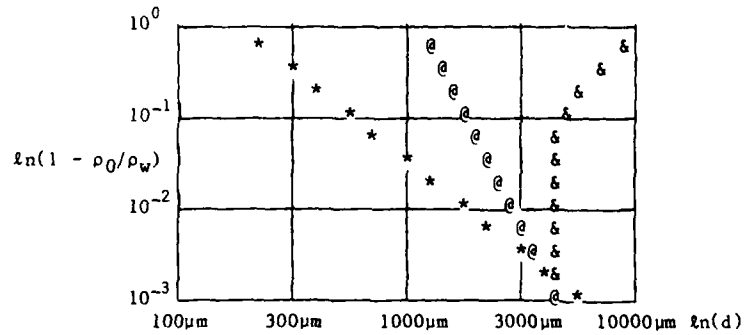

The curve marked *, having a slope of -2, is the dividing line between the Eulerian and Lagrangian cases; Lagrangian cases lie to the left of the line, and Eulerian to the right of the line. The curve designated by @ is the Eulerian criterion; to the left, the fluctuating relative Reynolds number is 12.5. The curve designated & is the Lagrangian criterion; to the left the fluctuating relative Reynolds number is less than 12.5.

It can be seen that the Eulerian and Lagrangian criteria do not cross until ρ_0/ρ_w is of the order of 0.999, and that both cross the Eulerian/Lagrangian dividing line at roughly this point, at a particle diameter of order 4500 μm at this density ratio. Hence, for our densities, the Eulerian criterion is the operative one.

So far as the Reynolds number based on the terminal velocity is concerned, taking the limiting Eulerian diameter, we obtain a value of 340for the case $\rho_0/\rho_w = 0.7$, and a value of 149 for the case $\rho_0/\rho_w = 0.95$. Since these values are well into the non-linear range, the drag will be higher, and the terminal velocity lower, than the Stokes value; hence, the true Reynolds number will be lower. We recall that Van Dyke (1975) gives R = 60 as the approximate limit for steady flow. We must examine the influence of non-linearity on the Reynolds number.

5.3 Reynolds Number Based on Non-Linear Drag

In Van Dyke (1975) we can find an expression for the drag coefficient on a sphere:

$$C_D = (6\pi/R)[1 + (3/8)R + (9/40)R^2 \ell nR + O(R^2)] \qquad (5\text{-}12)$$

where $C_D = D/\rho U^2 a^2$, where D is the drag and a the droplet radius. $R = Ua/\nu$, the Reynolds number. The terminal velocity is given by equating the buoyancy and the drag. If we agree to keep only the first two terms of the drag law, and if we revert to our definition of R based on droplet diameter, we obtain

$$R_S = R[1 + (3/16)R] \qquad (5\text{-}13)$$

where R_S is the Stokes value. If we take R = 60 as the limit for a steady wake, we obtain a value of R_S of 735. Using this value, we obtain limiting diameters of d = 1650 μm for $\rho_0/\rho_w = 0.7$ and d = 3000 μm for $\rho_0/\rho_w = 0.95$.

We may conclude on the basis of this paragraph and 5.2 that particles of roughly 1500 μm and smaller may safely be considered as having steady wakes, and linearization around the terminal velocity is permissable. 1500 μm is also approximately the limit for uniformity of the flow field, since η is approximately of this order.

5.4 Effect of Excessive Particle Size

As we consider larger and larger droplets, a number of possibilities must be considered: for example, in computing the relative velocity, it was assumed that the frequency corresponding to the particle response time was above the spectral cutoff of the turbulence. If this is no longer true, some changes must be made in the various estimates. If we are in the non-linear regime, we can compute the horizontal and vertical time constants for the particle motion, and we find that in the worst case, the diameter at which the time constant would be the same as the spectral

cutoff would correspond, for a density ratio of 0.7, to a diameter of 6190 μm, or, for a density ratio of 0.95, to a diameter of 5200 μm. Since the maximum size of particles we can consider (from a wake-stability point of view) are considerably smaller than these, we may compute the relative velocity supposing that the particle characteristic frequenvy is greater than the spectral cutoff.

Hence, even for these quite large particles of up to 3000 μm, there is no cause for concern that any of our assumptions will be violated. Finally, we may note, however, that even for larger particles, that might violate our assumptions, there will be no ultimate effect on the diffusivity. In the crossing-trajectories formula of *Csanady* (1963) for example, the effect of too large a particle time scale will be to change the equivalent fluid point *diffusivity*, which will be that resulting from a truncated spectrum. However, the integral in question depends primarily on the energy-containing range of wavenumbers, and is relatively little affected by the high wavenumber end of the spectrum - at any reasonable integration time (say, for times greater than two integral scales) the change in the cut-off will have essentially no influence. Hence, the particle diffusivity will be unaffected.

5.5 Influence of Wave Acceleration

The velocity field due to the wave motion is, of course, much larger than the random velocity field due to the turbulence. We must consider how the droplets respond to the wave velocity field, and how this affects their motion.

We need an estimate for the relative velocity between the droplet and the water due to the wave acceleration. This may be obtained from the linearized equation for the droplet motion. We begin with

$$dv_1/dt = (u_1 - v_1)/a_1 \qquad (5\text{-}14)$$

where v is the droplet velocity, u is the fluid velocity at the droplet location, and we are considering a horizontal component, the 1-component. a_1 is the horizontal droplet time constant; the horizontal and vertical time constants are different, as a result of linearization about a

terminal velocity which is in the non-linear regime of the drag law. We consider a horizontal component in order to eliminate the effect of the terminal velocity, which is not germane to this discussion. If we suppose a monochromatic wave of the form

$$\eta = h \exp[i\kappa(x - ct)] \tag{5-15}$$

where η is the instantaneous surface elevation, and h is the maximum value of the surface elevation, then the potential function for the wave motion is given by

$$\phi = i\ c\ h \exp[-\kappa z + i\kappa(x - ct)] \tag{5-16}$$

c is the phase velocity of the wave, and κ its wave number. z is measured positive downward. Substituting the velocity field resulting from (5-16) in the equation (5-14), evaluated at x = 0, we find that the particle velocity v_1 is of the form

$$v_1 = \upsilon \exp[-\kappa z - i\kappa ct] \tag{5-17}$$

where υ is given by

$$\upsilon = -\kappa\ c\ h/(1 - i\kappa c a_1) \tag{5-18}$$

From this we may easily obtain the relative velocity $v_1 - u_1$, and determine the mean square value, to obtain

$$\{(v_1 - u_1)^2\}^{1/2}/\{u_1^2\}^{1/2} = \kappa c a_1/[1 + (\kappa c a_1)^2]^{1/2} \tag{5-19}$$

where we are using $\{\ \}$ to indicate an average.

Now, we must estimate the values of the various quantities appearing in these expressions. The horizontal time constant is given by

$$a_1 g = V_T \tag{5-20}$$

where V_T is the true (as opposed to the Stokes) value. This is given by (using equation (5-13))

$$V_{TS} = V_T[1 + (3/16)R] \tag{5-21}$$

If we consider our largest particle, which will have the largest time constant, we have $V_T = 0.0816V_{TS}$, with R = 60. Using expression (5-6) for the Stokes terminal velocity, we have for $\rho_p/\rho_f = 0.7$, d = 1650 μm, $a_1 = 3.7\times10^{-3}$ sec, while for $\rho_p/\rho_f = 0.95$, d = 3000 μm, $a_1 = 2.04\times10^{-3}$ sec. We must now contrast this with the wave frequency. The phase velocity of the wave is always of the order of the wind speed in the atmosphere U_a, so that the wave frequency κc is of the order of g/U_a. Hence, if the wind speed is of the order of 10 m/s, the wave frequency will be of the order of 1 rad/sec. Hence, the quantity that occurs in equation (5-19)

$$\kappa c a_1 \approx 3\times10^{-3} \tag{5-22}$$

Hence, from equation (5-19), the r.m.s. relative velocity is of the order of 0.1% of the orbital velocity of the wave under the worst conditions.

Thus, even under the most severe circumstances, the droplet will simply follow the orbital motion of the wave. Since the velocity field of a wave is non-dispersive to lowest order, the dispersion of the droplets will be the result entirely of the rotational component of the velocity field, the turbulence. We could formally write the droplet velocity as the sum of the orbital velocity and the turbulent velocity (plus the

terminal velocity and the velocity of the Langmuir circulation), but we will not bother to do this formally, and will simply suppress the orbital velocity in what follows.

5.6 Particle Inertia

We may carry out a calculation similar to that in § 5.5 to see whether the inertia terms in the particle equation are important for the turbulent component. There is a possibility that they could be neglected, since they may be neglected for dust particles in the atmosphere, for example (see Lumley, 1978). The relative velocity may be obtained from the relative Reynolds number, expressions (5-8) and (5-9). The ratio of the relative velocity to the turbulent velocity is given by

$$\{(v_1 - u_1)^2\}^{1/2}/\{u_1^2\}^{1/2} = (\eta/d)R/R_\ell^{1/4} \qquad (5\text{-}23)$$

We have selected for our worst case $R = 12.5$, and η/d is approximately 1 for this case. $R_\ell = 2\times10^4$, as a typical value, and the 1/4 power of this is about 12. Hence, we may expect the left side of (5-23) to be about unity. Thus, the inertia terms may be expected to be quite important so far as the turbulence is concerned, as important as the other terms in the equation.

Fortunately, however, we are helped by a happy circumstance. As is explained in Lumley (1978), the direct influence of the droplet inertia drops out of the expression for the droplet diffusivity in the asymptotic limit, so that the asymptotic diffusivity is dependent only on the correlation of the fluid velocity seen by the droplet. The inertia affects both the mean square droplet fluctuating velocity, reducing it below that of the fluid velocity seen by the droplet, and the integral time scale of the droplet velocity, increasing it above that of the fluid velocity seen by the droplet by the same amount, but the product remains the same. Hence, so long as our diffusion times are long relative to the integral time scales of droplet motion, we may ignore droplet inertia in calculating droplet diffusivities.

We may make a crude estimate of the droplet-attached time scale by first estimating the droplet-attached mean square fluctuating velocity. The expression for the mean square droplet fluctuating velocity (in the horizontal direction) is given by

$$\{v_1^2\} = (\{u_1^2\}/a_1)\int \exp[-\tau/a_1]g_{11}(\tau)d\tau \qquad (5\text{-}24)$$

where the range of integration is the right half-line. We are again using $\{\ \}$ to indicate an average, and g_{11} is the autocorrelation of the fluid velocity seen by the droplet. We know from section 5.2 that the droplet motion may be considered essentially Eulerian, so that $g_{11} = g(V_T\tau)$, where $g(x)$ is the Eulerian transverse spacial correlation. We may pick a simple form for this function:

$$g(x) = (1 - \xi/4)\exp[-\xi/2],\ \xi = x/L_{22} \qquad (5\text{-}25)$$

where L_{22} is the transverse integral scale, one-half the longitudinal scale in an isotropic turbulence. Expression (5-24) can be evaluated to give

$$\{v_1^2\}/\{u_1^2\} = \gamma(1 + 4\gamma)/(1 + 2\gamma)^2 \qquad (5\text{-}26)$$

where $\gamma = L_{22}/V_T a_1 = L_{22}/g a_1^2$, that is, the ratio of the transverse integral scale to the distance the droplet moves (at the terminal velocity) during one time scale. The transverse integral scale is roughly $\ell/4$, or about 0.5 meters in our simple example, if we take ℓ to be the wave height, at 2 meters. We have already estimated $a_1 = 3\times10^{-3}$ sec. Hence, we obtain $\gamma = 5.67\times10^3$. It is clear that any other set of reasonable assumptions will not change the order of magnitude of this quantity. Evaluating expression (5-26), we obtain 0.999. Hence, the mean square fluctuating droplet velocity and the mean square fluctuating fluid

velocity are essentially the same, although the instantaneous velocities are not, due to the phase lag induced by the droplet inertia. Since the droplet attached mean square fluctuating velocity is the same as the mean square fluctuating fluid velocity seen by the droplet, the droplet-attached time scale must be the same as the time scale of the fluid velocity seen by the droplet.

Since the oil droplets are operating in the Eulerian regime, we may estimate the integral time scale of the fluid velocity seen by the droplet as the Eulerian transverse integral scale divided by the droplet mean velocity relative to the fluid, the terminal velocity. We may estimate the Eulerian transverse integral scale as about one-quarter of the wave height. We have been taking as an example a case of waves of two meters height, but here we must use the wave heights corresponding to the various cases in tables 7-2, 7-3, and 7-4. Since the wave slope is constant at .088, the wave heights are respectively (for wave numbers of 1/m, 0.5/m and 0.25/m) 0.088m, 0.176m and 0.352m, giving an Eulerian transverse integral scale of 0.022m, 0.044m, and 0.088m.

The time required to rise up the side of the Stommel retention zone may be estimated from the tables in section 7, using the dimensionless distance S_t and the scaling velocity. Proceeding in this way, we find that the time required to rise up the side and the integral time scale of the fluid velocity seen by the droplet scale the same way with the wave height, and we have a single ratio for each of the cases, giving a ratio of the integral time scale to the convection time of 0.15, 0.2 and 0.26 in the cases A, B and C. Hence, we see that in the worst case the rising droplet spends about four integral time scales rising up the side, so that the diffusion coefficient is in the asymptotic regime long before the droplet reaches the top. Hence, it is legitimate to use the asymptotic form of the diffusivity for our problem, and we may ignore droplet inertia.

5.7 The Crossing-Trajectories effect and the Diffusivities

The construction of the diffusivities within our restrictions is described in Lottey (1979). Briefly, the argument is this: Consider the vertical velocity. For large Reynolds number flows, such as the wave-associated turbulence under consideration, the large scale structure of the velocity field may be considered to be determined by the integral length scale and the r.m.s. velocity. The droplet velocity autocorrelation will be a function of the Eulerian longitudinal integral length scale, the r.m.s. velocity, the droplet terminal velocity and the time lag. These form two dimensionless groupings, one involving the r.m.s. fluctuating velocity, and the other the terminal velocity. If the terminal velocity is small compared to the r.m.s. velocity, the case is essentially Lagrangian, while if the reverse is true, the case is essentially Eulerian. If the correlations in these two limiting cases are assumed to have the same shape, then the function of two variables can be replaced by a function of a single variable - essentially the isocorrelation contours are assumed to have the form of ellipses. There is a constant relating the two axes which is determined by an integral constraint, assuring that the integrals along the two axes give the corresponding (Eulerian and Lagrangian) integral scales. Finally, the integral may be carried out to give the asymptotic dispersion, giving

$$D_2 = (u\ell/3)[1 + (4/9)(V_T/u)^2]^{-1/2} \qquad (5\text{-}27)$$

independent of the form of the correlation. Similar arguments may be made for the horizontal direction, but here a difficulty arises. The Eulerian transverse correlation goes negative due to the requirement that the total mass flux across any plane must be zero. However, the Lagrangian correlation does not go negative; hence, it is not possible to assume that the form of the correlation in the two limiting situations is the same. However, measurements by Snyder & Lumley (1971) indicate that the droplet-attached velocity autocorrelations and the Eulerian transverse correlation are similar down to very small values of the terminal velocity. Hence, proceeding in the same way, we obtain

$$D_1 = D_2/2 \qquad (5\text{-}28)$$

This expression for D_l does not give the right value as $V_T \to 0$, since it gives half the Lagrangian diffusivity. This is due to the fact that the droplet-attached correlation changes rapidly as the Lagrangian case is approached, and no adequate approximation is known. However, down to very small values of V_T/u it is expected that the expression given for D_l will be adequate.

5.8 The Fluid Diffusivity

The quantity appearing in (5-27), $u\ell/3$, is the fluid diffusivity. We need an estimate for this. To obtain such an estimate, we have analyzed measurements taken in Lake Ontario by Donelan, and reported in Kitaigorodskii et al (1981). These measurements were taken under waves from 5 to 15 cm in height, having wavelengths between three and ten meters, with winds (at ten meters height above the mean water surface) between five and fifteen meters per second. These conditions are quite typical of situations of interest here with the exception of the wave height, which we would expect to be larger in the open ocean, with either longer fetches, or greater development time. The measurements have been parameterized as

$$u/u_* = [0.28(h\omega/u_*) + 2.30]\exp[-\kappa z/2] \qquad (5\text{-}29)$$

where the numerical coefficients are independent of sea state. The wavenumber of the exponential decrease is not as certain, the factor ranging from about 0.4 to 0.9; we have selected 0.5 as a compromise value because it results in a considerable simplification, as we shall see shortly.

Unfortunately, the measurements of the dissipation rate ε of turbulent kinetic energy are much less reliable, and little can be learned from them, other than that the length scales predicted are of the order of the wave height. In this connection, we may mention the estimates of ε suggested by Milgram et al (1978), who propose $10g^2/\omega$ for breaking waves. If we calculate from this the logarithmic decrement of the wave in periods, we find that the wave will decrease in amplitude by 1/e in 1/10 of a period. This is clearly much too large, and the values of η they calculate using this value of ε are much too small. Clearly breaking waves will have larger dissipation than non-breaking ones, but one would expect the loss of energy to the breaking to take a number of periods.

Rather than use unreliable experimental results, we have used a theoretical model to obtain the values of ϵ, or equivalently, a length scale. If we suppose that the Reynolds stress induced in the turbulence in the wave by the strain rate of the wave motion is related to the latter by an eddy viscosity, as

$$-\{u_i u_j\} + (q^2/3)\delta_{ij} = \nu_T S_{ij} \tag{5-30}$$

where S_{ij} is the strain rate of the oscillatory motion of the wave, then the rate of production of turbulent energy is given by $\nu_T S_{ij} S_{ij}$, which can be written as u^3/ℓ (Tennekes & Lumley, 1971). Writing ν_T as $u\ell/3$, we obtain (computing the oscillatory motion of the wave)

$$\ell u/3 = \nu_T = u^2/\sqrt{6}hc\kappa^2 \exp[-\kappa z] \tag{5-31}$$

Using the behavior we assumed for u, we obtain in this way a ν_T which is independent of depth of

$$\nu_T = u_*^2[0.28(h\omega/u_*) + 2.30]^2/\sqrt{6}h\omega\kappa \tag{5-32}$$

and we have used this expression in the form for D_1 and D_2.

6. A COMPUTATIONAL METHOD TO IMPLEMENT THE MODEL

Before explaining procedures used to solve the diffusion equation (4-11), we review the features that have already been discovered, and give a descriptive account of the physical processes taking place.

First, we have noted that diffusion, although an essential process, is weak. If ignored, particles move on lines of constant Ψ as indicated in Figure 4-4 . If an oil particle is placed on a Ψ line outside a retention zone, then it will rise along that line until it reaches the surface, $z = 0$. Since all particles reaching the surface reside in a sheet of zero thickness, the subsequent motion of one of these particles cannot be inferred from the figures. Nevertheless, the behaviour of a particle on the surface is clear. According to the diffusion-free approximation, it must stay on the surface and move towards LC convergence lines. Thus, in this simplified view, the entire volume outside of the retention zones is swept free of oil, all of the oil initially there being transported to the surface and then swept into windrows. The final picture would be one where all of the oil is concentrated in a line on the surface - the windrow - and possibly oil trapped below the surface in a SRZ.

With an infinitesimal amount of diffusion acting, any oil trapped in a SRZ would ultimately be uniformly distributed throughout the SRZ. This is one effect of the diffusivity. Since the simplified view gives rise to a singular distribution of surface oil, with infinite concentration gradients, we know that a second effect of small but non-zero diffusivities is to spread the surface oil out into a band of non-zero thickness and non-zero width in the windrow. A third effect is the slow transport of oil across the boundary of the SRZ. Since the diffusivities are weak, oil droplets transferred across the side of an SRZ form a thin layer adjacent to the retention zone boundary; once outside they rise up towards the surface within the thin boundary layer. This is depicted in the sketch of Figure 6-1.

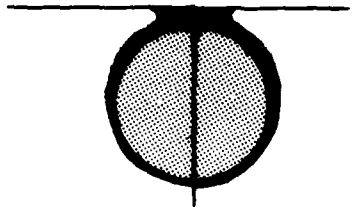

Figure 6-1. -Sketch of SRZ ; its windrow supply source, and boundary layer leakage rising along the sides.

If there were no other effects of diffusion, the boundary leakage would eventually empty the retention zone, and all oil would be collected into surface windrows with vertical and horizontal spreads that are functions of V_T, the Langmuir circulation velocity scale V, and the diffusivities. If, however, the top of the SRZ, defined as the first point below the windrow at which $w = - V_T$, lies within a distance below the surface characteristic of the vertical extent of the windrow, then the vertical concentration gradient in the windrow can produce a vertical flux of oil particles back into the retention zone. Under these circumstances it is possible to arrive at a steady balance between the loss of oil across the sides of the SRZ and the injection of oil from the windrow into the SRZ.

The purpose of this section is to compute the equilibrium balance that ultimately develops. Since the diffusivities are so small, a straightforward calculation (e.g.,by a finite difference algorithm) of the field as a whole is not feasible. A mesh fine enough to resolve the various thin regions would, if applied to the field as a whole, result in excessive storage requirements and computing time. Consequently, the calculation is divided into parts that take advantage of the problem structure.

The boundary layer on the rising side of the zone is calculated analytically; the only parameter that enters the final result is an

effective diffusion time along the rising side and involving the horizontal and vertical diffusivities (reflecting the change of direction of the droplet motion as it rises) as well as the mean droplet speed. The analytical calculation can be done once for all cases. To apply the result, the effective diffusion time must be determined for each Langmuir cell and each set of droplet characteristics.

The region between the top of the Stommel retention zone and the surface must be solved numerically. The dispersion in this region is dependent upon two parameters: the dimensionless distance of the top of the zone from the surface, and the thickness of the droplet boundary layer entering from the side. The calculation is delicate because, even in this reduced region, the gradients are large, and it is necessary to write the program in such a way that the droplets are conserved. From such calculations we determine the relative concentration within the Stommel retention zone and in the windrow for given sea state, Langmuir cell and droplet parameters.

Under other support, measurements of turbulent intensities and scales under various sea states have been analyzed, and computational modeling of the turbulence in the surface mixed layer of the ocean in the presence of waves has been carried out. By a combination of these two, we have arrived at a distribution of turbulent droplet diffusivities as a function of sea state as described in the previous section. These diffusivities enter into the determination of the effective dimensionless distance of the top of the Stommel retention zone from the surface, and of the effective diffusion time for the rising droplets on the edge of the Zone.

6.1 Preliminary Survey

We now put the picture outlined above into mathematical form. Consider the diffusion equation in its dimensionless form (4-17). It is convenient to choose $D_2(0)$ to serve as a scale for the diffusivities, and to write

$$\Delta_1(z) = D_1(z)/D_2(0),\ \Delta_2(z) = D_2(z)/D_2(0),\ \varepsilon = \kappa_0 D_2(0)/V; \tag{6-1}$$

thus $\Delta_2(0) = 1$ and ε is a small parameter. In this notation, the diffusion equation and boundary conditions on $C(y,z)$ for steady conditions are expressed as

$$vC_{,y} + (w + V'_T)C_{,z} = \epsilon\{(\Delta_1 C_{,y})_{,y} + (\Delta_2 C_{,z})_{,z}\} \qquad (a)$$

$$C_{,y}(y,0) = V'_T\, C(y,0) \qquad (b)$$

$$C_{,y}(0,z) = C_{,y}(Y_2,z) = 0 \qquad (c)$$

$$C \to 0 \text{ as } z \to -\infty \qquad (d)$$

where all quantities are dimensionless, $V'_T = V_T/V$; $y = 0$ is assumed to be the location of a downwelling plane, and $y = Y_2$ the dimensionless location of an upwelling plane, so a single cell in the given Langmuir circulation system lies in $0 \leq y \leq Y_2$. Furthermore, an SRZ lies below the LC windrow. Assuming symmetry in y, half of the SRZ lies in the LC cell considered, and its boundary $\Psi = 0$ includes an interval on the z-axis from $z = z_-$, the lower boundary of the SRZ to $z = z_+$, the top of the SRZ. The sketch of Figure 6-2 shows the situation analyzed.

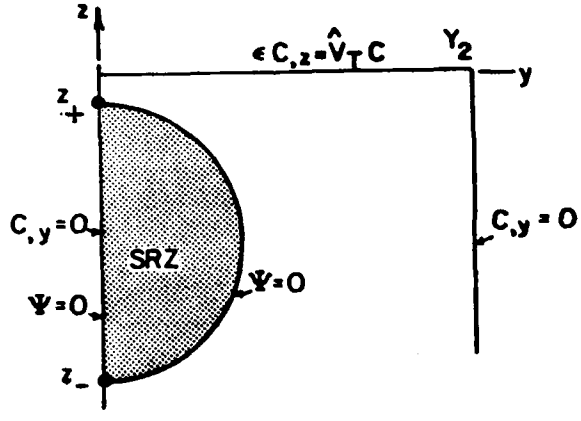

Figure 6-2. Definition sketch for diffusion calculation.

Consider the computing requirements for a finite difference analysis of this problem for $\epsilon = 0.005$, a typical value for conditions to be dealt with; and $Y_2 = 2$, which, upon referring to the Figures in §4, is one of the cases (1) we analyze. If we suppose that we were to compute with a mesh of $\Delta y = \Delta z = 0.1$ and imagine iterating or, equivalently, calculating an initial value problem until a convergence to a steady state is reached, then this mesh is about the largest we can use to avoid unacceptable levels of artificial diffusion. With this mesh, the computational domain $0 \leq y \leq 2$, $0 \leq -z \leq 5$ (this is the maximum penetration of the LC) would be resolved with a 20x50 grid,or 1000 mesh points. To achieve a steady state, we must integrate an initial value problem for a time comparable to the diffusion time in the problem. Based upon the horizontal distance Y_2 (which may be optimistic), since the vertical extent of the first is larger than Y_2, this is a dimensionless time $t = Y_2^2/\epsilon = .8 \times 10^3$. Numerical stability requirements demand that the time step be restricted to the smaller of the advective time scale based upon the spatial mesh or the diffusion time based upon the mesh. The former is operative here, and the time step is on the order of 0.1. Thus, a minimal calculation at field sight requires approximately 10,000 computations at each 1000 mesh points, leading to more than 10^8 arithmetical operations. While this is manageable, large concentration gradients in the windrow region require a substantially finer grid in that critical area, and this we estimate would double the storage required and increase the overall number of operations by a factor exceeding 10^5.

While better numerical methods are probably possible that can reduce the computational effort considerably, it seemed to us that the end result would lead inevitably to very large computational problem. Rather than fight the smallness of ϵ we preferred to choose a method that exploits it. This we have done by dividing the Langmuir cell into the regions described in the introduction to this section. These regions are schematically indicated in Figure 6-3; the decomposition of the problem and the thickness of the various regions, are the subject of this subsection.

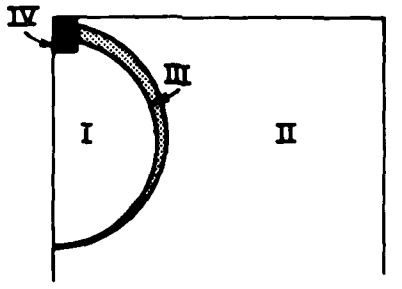

Figure 6-3. Decomposition of the domain.

We begin by noting that in (6-1) v and w are $O(\varepsilon^0)$. Regions I and II are those defined by the limit problem, $\varepsilon = 0$, and consists of the SRZ (I) and the region outside it (II). Since the SRZ has a uniform oil concentration, and since the solution of the steady problem is, as we have already discussed, invariant with respect to an arbitrary multiplication factor, we take $c = 1$ in the SRZ. In region II, being free of oil if $\varepsilon = 0$, $c = 0$. Regions I and II are the "outer" regions (van Dyke, 1975) and are separated by an "inner" transition region III in which oil from inside the SRZ escapes and travels up towards the surface. This transition region has a thickness proportional to $\sqrt{\varepsilon}$, so diffusion tangent to the SRZ boundary is negligible compared to that normal to it, and is therefore ignored. This approximation cannot be made to satisfy the boundary condition at $y = 0$; thus region IV, in which the full equations must be solved, is needed. Region IV, as will be shown, is a layer along the y axis with thickness of order $[\varepsilon|z_+|/V'_T]^{1/2}$.

6.2 Region III. Escape of Oil from the Retention Zone.

To treat the transfer of oil across the curved boundary of the SRZ, we adopt intrinsic coordinates lying along and normal to the droplet pathlines. The droplet velocity and "streamfunction" are $(u, w + V_T)$ and Ψ, respectively, and $\Psi = 0$ is taken to be the boundary of the SRZ. Let s be arclength measured along the SRZ boundary beginning at the bottom

($z = z_-$) and let n be the coordinate normal to the boundary and directed towards the interior of the retention zone with $n = 0$ coinciding with $\Psi = 0$. Let

$$q = [v^2 + (w + V'_T)^2]^{1/2} \tag{6-2}$$

be the speed of particles as they rise: this depends upon s and n, but the difference of q (and Δ_1 or Δ_2 as well) from its value at $n = 0$ to any other point in region III is higher order ($0(\sqrt{\varepsilon})$ and can be neglected. With the choices made

$$\Psi = \int_0^n q(s,n)dn = q\ n \tag{6-3}$$

to the order considered.

If we introduce a boundary layer stretch in (6-1) by setting

$$n = \sqrt{\varepsilon}\ N,\ \Psi = \sqrt{\varepsilon}\ \eta \tag{6-4}$$

(where $\eta = q\ N$), equations (6-1) take the form

$$qC_{,s} = [\Delta_1(n_{,y})^2 + \Delta_2(n_{,z})^2]C_{,NN} \tag{6-5}$$

accurate to $0(\sqrt{\varepsilon})$. This equation is more conveniently expressed in terms of the stretched streamfunction η, using (6-4); it then takes the form

$$qC_{,s} = [\Delta_1(w + V'_T)^2 + \Delta_2 v^2]C_{,\eta\eta}. \tag{6-6}$$

Finally, we note that Δ_1, Δ_2, v, w, q all may be considered to vary only with s in III, and so we make a transformation to a new coordinate

$$\xi = \int_0^s q^{-1}[\Delta_1(w + V'_T)^2 + \Delta_2 v^2]ds \tag{6-7}$$

to arrive at the form of the concentration equation that we deal with in region III:

$$C_{,\xi} = C_{,\eta\eta}. \tag{6-8}$$

This is the heat equation in its simplest form.

The boundary conditions on (6-8) are matching with regions I and II, or

$$\begin{aligned} C &\to 1 \text{ as } \eta \to -\infty \\ C &\to 0 \text{ as } \eta \to \infty \end{aligned} \tag{6-9}$$

and it is assumed that region III starts at $\xi = 0$, the bottom of the SRZ, at which point $C = 1$ for $\eta > 0$ and $C = 0$ for $\eta < 0$.

The solution for region III is

$$C = (1/2)\text{erfc}(-\eta/2\sqrt{\xi}) \tag{6-10}$$

where erfc is the complementary error function (Abramowitz and Stegun, 1964). As indicated earlier the solution (6-10) cannot be made to satisfy the boundary condition (6-1 c), and we are therefore forced to consider region IV.

6.3 Region IV. Oil Transfer from Windrow to Retention Zone.

In order to meet the conditions imposed at $y = 0$, the end of the rising droplet layer, diffusion in the direction along the retention zone boundary must be restored. Since this failure of the boundary layer solution occurs at the top of the SRZ, at z_+ and $y = 0$, directions of s increasing and n increasing are anti-parallel to y increasing and z increasing. Clearly, the additional term is important because gradients in the y-direction become as large as those in the z (i.e., n) direction in the neighborhood of $y = 0$. To make this explicit, a stretching in the y-direction with the same magnification provided in the n-direction is required.

To begin the analysis of this region, suppose we try a stretch ε^{-a}, $a > 0$, so

$$y = Y'\varepsilon^{a} \tag{6-11}$$

We continue to look at the boundary layer, so we retain the $\varepsilon^{-1/2}$ stretch in the n-direction, but re-written in terms of z. In particular, let us put

$$z = z_+ + Z'\sqrt{\varepsilon} \tag{6-12}$$

so that Y = 0, Z = 0 is the top of the retention zone. Substitute (6-11) and (6-12) into (6-1); the dominant terms are

$$\begin{aligned} &\varepsilon^{-a}\, v(\varepsilon^a Y', z_+ + \sqrt{\varepsilon}Z)C_{,Y'} + [w(\varepsilon^a Y', \\ &z_+ + \sqrt{\varepsilon}\, Z)+V'_T]C_{,Z'}/\sqrt{\varepsilon} \\ &= \varepsilon^{1-2a}\Delta_1(z_+ + \sqrt{\varepsilon}\, Z')C_{,Y'Y'} + \Delta_2(z_+ + \sqrt{\varepsilon}\, Z')C_{,Z'Z'}. \end{aligned} \tag{6-13}$$

Now the velocity field may be expanded in a series. Since $v(0, z) \equiv 0$,

$$v(\varepsilon^a Y',\ z_+ + \sqrt{\varepsilon}\, Z') = \varepsilon^a Y' v_{,y}(0, z_+) + O(\varepsilon^{1/2+a}).$$

At the top of the retention zone,

$$w(0,\ z_+) + V'_T = 0$$

hence the function

$$w(\varepsilon^a Y', z_+ + \sqrt{\varepsilon}Z') + V'_T = \sqrt{\varepsilon}Z' w_{,z}(0, z_+)$$

since

$$w_{,y}\ (0,\ z_+) = 0, \text{ and from continuity}$$

$$w_{,z}(0, z_+) = -\, v_{,y}(0, z_+)$$

and we let α be the common value. In terms of the strain rate α, then, (6-13) is

$$-\alpha\, Y'C_{,Y'} + \alpha\, Z'C_{,Z'} = \varepsilon^{1-2a}\Delta_1(z_+)C_{,Y'Y'} + \Delta_2(z_+)C_{,Z'Z'} \tag{6-14}$$

and we choose a = 1/2 to retain the diffusion term we had intended to restore.

Equation (6-14) can be written in a neater form by taking

$$Y' = Y(\Delta_1(z_+)/\alpha)^{1/2},\ Z' = Z(\Delta_2(z_+)/\alpha)^{1/2} \tag{6-15}$$

in which case (6-14) is

$$-Y\ C_{,Y} + Z\ C_{,Z} = C_{,YY} + C_{,ZZ} \tag{6-16}$$

and this is the equation that we solve in region IV.

Retracing the transformations used, we see that final coordinate choice is related to the y and z coordinates as follows

$$y = Y(\varepsilon\Delta_1/\alpha)^{1/2},\ z = z_+ + Z(\varepsilon\Delta_2/\alpha)^{1/2} \tag{6-17}$$

Note that $(\varepsilon\Delta_1/\alpha)^{1/2}$ is the (dimensionless) thickness of a boundary layer formed by the balance between (turblent) diffusion and mean strain rate.

Before we proceed to solve the problem in region IV, we make the following important observation. If region IV does not overlap with the windrow, then all oil entering it from the rising boundary layer will leave through the top of region IV and rise to the surface; thus the SRZ will be swept free of oil unless there is an overlap. Thus, we must require that the top of the SRZ have (dimensionless) depth

$$d = |z_+| = O(\varepsilon\alpha/\Delta_2)^{1/2}$$

if there is to be oil in the SRZ. Since $|z_+| = O(\sqrt{\varepsilon})$ we may replace $\Delta_1(z_+)$ by $\Delta_1(0)$, $\Delta_2(z_+) = \Delta_2(0) = 1$, and we may also relate the strain rate α to V'_T. In particular, since

$$w + V'_T = \alpha\ (z - z_+) = \alpha\ (z + d), \tag{6-18}$$

if z = 0 is included in IV,

$$V'_T = \alpha\ d, \tag{6-19}$$

since w = 0 at z = 0.

Assuming that the overlap exists, we let

$$Z = \gamma \tag{6-20}$$

locate the free surface z = 0, so

$$\gamma = d(\alpha/\epsilon\Delta_2)^{1/2} = d(a/\epsilon)^{1/2} \tag{6-21}$$

on recalling that $\Delta_2(0) = 1$.

The boundary condition at z = 0 now takes the form

$$C_{,Z} = \gamma\ C \text{ at } z = \gamma \tag{6-22}$$

The problem in region IV may now be summarized. We solve (6-16) subject to the boundary condition (6-22); the condition

$$C_{,Y} = 0 \text{ at } Y = 0 \tag{6-23}$$

arising from (6-1); matching with the SRZ, or

$$C \to 1 \text{ as } Z \to -\infty\ ; \tag{6-24}$$

and matching with the rising boundary layer. This latter condition is now derived.

The matching condition is derived (van Dyke, 1975) by rewriting the "outer" (rising boundary layer) solution in inner (Y, Z) variables, expanding for small ϵ and regrouping. The outer solution is given by (6-10). Since

$$\xi = \xi_t + O(\sqrt{\epsilon}),$$

where ξ_t is the value obtained by placing s (6-7) equal to the total arclength around one side of the SRZ, and since, from (6-4)

$$\eta = \Psi/\sqrt{\epsilon}$$

substitution into (6-10) yields

$$C = (1/2)\text{erfc}\ [-\Psi/(\epsilon\xi_t)^{1/2}]. \qquad (6\text{-}25)$$

We know that

$$\Psi(y,z) = -\int_0^y (w + V_T)dy$$

Substituting from (6-17) for y and z and using (6-18) we have

$$C = 1/2\ \text{erfc}[-YZ(\epsilon\Delta_1/4\xi_t)^{1/2}]. \qquad (6\text{-}26)$$

Which is to hold for $Y \gg 1$.

We solve the problem in region IV numerically by a finite difference algorithm, described below. In implementing (6-26), at the right-hand edge of IV, we set Y = 50; this is large enough to ensure that the function (6-26)is essentially zero at the top boundary for all interesting values of γ and ξ_t.

Note that the dimensionless quantity $\epsilon\Delta_1/\xi_t$ depends only on the value of the terminal velocity and the Langmuir cell velocity and length scales. This variable determines the width of the incoming concentration distribution at the right edge of the field under the windrow. We computed the values of this variable for a number of different configurations.

6.4 Computational Procedure

We computed solutions of equation (6-5) in a region extending from Z = -2 to Z = γ, and from Y = 0 to Y = 50, for a number of different values of γ and a number of different Langmuir circulation fields and terminal velocities. Equation (6-5) was written as an unsteady equation (simply including the time derivative), and a simple forward-time centered-space differencing scheme was used. The grid points were centered in the cells, and the equation and boundary conditions were written in a conservative form. Each computation resulted in a value of the ratio of the concentration in the center of the windrow (Y = 0, Z = γ) to that in the Stommel retention zone. A typical iso-concentration plot is shown in Figure 6-4. The iso-concentration contours become too close together in the center of the windrow for the plotting routine to display them.

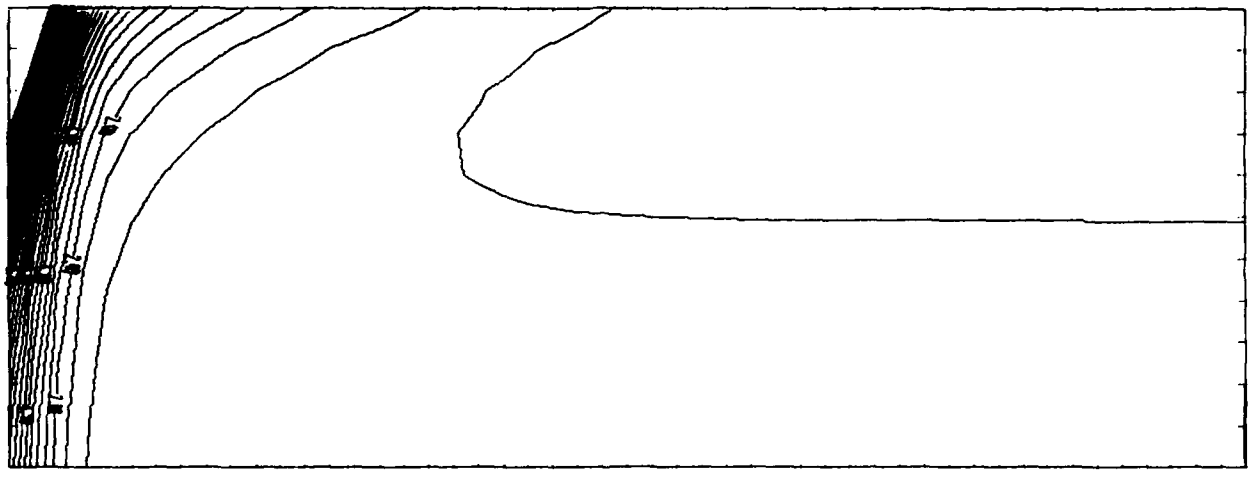

Figure 6-4. Example of a contour of oil concentration in region IV. Upper edge is the water surface; top of the Stommel retention zone is half-way up. Contours become too dense for the plotter to follow in the upper left corner (center of windrow). Contour intervals are 0.125. Vertical scale is expanded by a factor of five.

7. RESULTS OF DISPERSION COMPUTATIONS

The results of the concentration computations that we have made using the method of §6 are summarized in Tables 7-1 to 7-4.

One of the principal measures of oil below the surface in this analysis is the ratio of the maximum surface concentration, which appears in the center of a windrow, to the concentration of oil distributed throughout the Stommel retention zone. This ratio we designate to be C*. As the dispersion increases, C* decreases. Tables 7-1 through 7-4 show the effects of wind speed, sea state, and depth of penetration upon C*. In these Tables, the wind speed is identified by the first letter of the code (A→5 m s^{-1}, B→10 m s^{-1}, C→15 m s^{-1}), the sea state by the first numeral (1→κ_0 = 1 m^{-1}, 2→κ_0 = .5 m^{-1}, 3→κ_0 .25 m^{-1}), aspect ratio of the convective cells (penetration depth/windrow separation) is indicated by the last pair of symbols which refer to the dimensionless development time of the cells (T1→35 units, T2→50 units, T3→95 units).

Table 7-1 displays these results for a wind speed of 5 m/s for particle terminal velocities of .26 cm/s, .65 cm/s and 1.3 cm/s. The value of C* for a given wind speed depends strongly upon V_T, but only weakly upon the sea state or penetration depth of the cells. Cases A1T1 and A3T1 represent situations occuring for the same wind speed and cell aspect ratio but sea states with wave heights differing by a factor of four. As can be seen, the values of C* are not much different. The last three rows compare C* for the same terminal velocity, but different aspect ratios and/or sea states. Again, the values of C* are comparable.

We may conclude from Table 7-1 that C* is a rapidly increasing function of V_T/V, where V is the LC convective velocity scale, and depends only weakly upon the sea state or cell aspect ratio. The fact that C* is not a large number means that for the cases computed, at least, vertical dispersion is effective, and a considerable amount of oil is held in suspension.

Table 7-1 -Concentration Ratio Case A. Wind speed 5 m/s. Case codes as described in text. C* is the ratio of the maximum concentration in the windrow to the concentration in the Stommel retention zone. More extensive data is reported for V_T = .0065 to show that C* depends only weakly on κ_0 (represented by first digit of case code) or upon cell aspect ratio.

Case	V_T m/s	C*
A1T1	.0026	1.6
	.0065	3.3
	.013	11.0
A3T1	.0026	1.6
	.0065	3.8
	.013	11.7
A1T2	.0065	3.6
A1T3	.0065	3.1
A2T1	.0065	3.6

The main results of the dispersion calculations are shown in Tables 7-2 through 7-4, for terminal velocities of 0.5, 1.0, and 0.2 cm/s, and for representative values of cell aspect ratios and/or sea states. These Tables contain all of the relevant data used in the calculations (surface value of diffusivities, $D_2(0)$; ε; ξ_t; γ) as well as C*. In addition, the final two columns of each Table give the fraction of oil held in suspension in the retention zones, and the depth of the deepest retention zone. The oil fraction is the percentage of the total amount of oil present that is located in the retention zone, excluding oil in the region IV overlap with the windrow. These two entries are the key results of the dispersion model.

Tables 7-3 and 7-4 are abbreviated, and show only the

Table 7-2 $-V_T = 5\times10^{-3}$ m/s. Results of dispersion analysis.

Case T1	$D_2(0)$ m^2/s	ε	ξ_t	γ	C*	suspended oil, %	Depth of SRZ m
A1T1 V_a=5 m/s $1/\kappa_0$= 1 m	0.00298	0.030	0.20	0.304	2.12	16	1.8
A3T1 V_a=5 m/s $1/\kappa_0$= 4 m	0.00988	0.025	0.20	0.334	2.29	47	7.2
B1T1 V_a=10m/s $1/\kappa_0$= 1 m	0.00418	0.021	0.18	0.182	1.53	25	2.1
B3T1 V_a=10m/s $1/\kappa_0$= 4 m	0.01198	0.015	0.18	0.215	1.67	65	8.4
C1T1 V_a=15m/s $1/\kappa_0$= 1 m	0.00558	0.019	0.17	0.128	1.33	21	2.4
C3T1 V_a=15m/s $1/\kappa_0$= 4 m	0.01428	0.012	0.17	0.161	1.45	62	9.6
A1T3 V_a=5 m/s $1/\kappa_0$= 1 m	0.00298	0.030	0.80	0.291	2.03	62	5.3
A3T3 V_a=5 m/s $1/\kappa_0$= 4 m	0.00988	0.025	0.80	0.319	2.19	89	21.2
B1T3 V_a=10m/s $1/\kappa_0$= 1 m	0.00418	0.021	0.73	0.174	1.49	70	6.1
B3T3 V_a=10m/s $1/\kappa_0$= 4 m	0.01198	0.015	0.73	0.205	1.61	93	24.4
C1T3 V_a=15m/s $1/\kappa_0$= 1 m	0.00558	0.019	0.71	0.122	1.28	78	6.5
C3T3 V_a=15m/s $1/\kappa_0$= 4 m	0.01428	0.012	0.70	0.153	1.38	96	26

Table 7-3 $-V_T = 1\times10^{-2}$ m/s. Results of dispersion analysis.

Case T1	$D_2(0)$ m^2/s	ϵ	ξ_t	γ	C*	suspended oil, %	Depth of SRZ m
A1T1 V_a= 5m/s $1/\kappa_0$= 1 m	0.00297	0.030	0.17	0.619	4.53	9	1.6
A3T1 V_a=5 m/s $1/\kappa_0$= 4 m	0.00987	0.025	0.17	0.679	5.21	16	6.2
C1T1 V_a=15m/s $1/\kappa_0$= 1 m	0.00557	0.019	0.19	0.257	1.86	24	2.1
C3T1 V_a=15m/s $1/\kappa_0$ 4 m	0.01428	0.012	0.19	0.321	2.19	66	8.4

Table 7-4 $-V_T = 2\times10^{-3}$ m/s. Results of dispersion analysis.

Case T1	$D_2(0)$ m^2/s	ϵ	ξ_t	γ	C*	suspended oil, %	Depth of SRZ m
A1T1 V_a=5 m/s $1/\kappa_0$= 1 m	0.00297	0.030	0.17	0.122	1.28	21	2.2
A3T1 V_a=5 m/s $1/\kappa_0$ 4 m	0.00987	0.025	0.17	0.134	1.32	93	9.0

cases corresponding to the smallest cell aspect ratio computed, since the trends are clear from Table 7-2. Table 7-4 also includes only the lowest sea state; for the small value of V_T used for this table, our numerical results were felt to be too uncertain to report for the higher sea states.

The overall size of a retention zone increases as the sea state increases (since the length of surface waves and consequently the windrow separation and SRZ width increases) and as the aspect ratio increases (since the cell penetration and consequently the SRZ height increases). Since the volume of oil in a retention zone is the oil concentration multiplied by the SRZ volume, the amount of oil trapped in an SRZ increases with sea state and aspect ratio. Notice that a substantial amount of oil is suspended in the retention zones, and these zones are deep, even for light winds, low seas, and relatively small LC penetration depths. Two points may be relevant here. Assuming the fractions of oil shown in these Tables are correct, the actual concentrations of oil (recall that our concentrations are normalized to give unit concentration in the retention zone) in the SRZ will be very small in most cases. Secondly, our analysis assumes that all of the oil is in the form of small, noninteracting particles. This assumption may reflect with reasonable accuracy situations in which dispersants have been used. Under natural conditions, however, the oil to which our work applies is that part which has been torn off of the floating surface oil layer, and one must interpret the present data as the fraction of that oil is held in suspension.

As a point of reference in interpreting the results of this section, note that the diameter, d, of spherical oil droplets in water of (molecular) kinematic viscosity ν, will have a terminal velocity

$$V_T = 1/18\ (g/\nu)(1-\rho o/\rho w)d^2$$

if motion is in the Stokes regime. Thus, a one millimeter diameter droplet of oil with $\rho o/\rho w = 0.99$ corresponds to $V_T = 0.5$ cm/s, and if $\rho o/\rho w = 0.98$, $V_T = 1.0$ cm/s.

8.0 Collection of Floating Oil in Windrows

Floating surface oil will be gathered by Langmuir circulations into long windrows. This prominent feature, a generally reported one for those oil spills for which extensive observations are available (see Atwood et al (1980)), is considered in this section.

The purpose of the section is to estimate the thickness and total volume of oil in a windrow by a method simple enough to be used by an observer at an oil-spill site. Oil is assumed to exist in the surface as a thin, coherent sheet of variable thickness. The spreading pressure due to interfacial tension is assumed to be zero, an assumption that is reasonable if the oil is sufficiently weathered and remains thick enough to be measured by mechanical means. Under these circumstances, the oil layer is influenced by gravity, which acts to spread the oil into a layer of uniform thickness, and friction at the oil-water and oil-air interfaces.

We are interested here in the build-up of oil held against gravity by the horizontal sweeping motions in Langmuir circulations; variations in the direction of the wind are ignored (the stress imparted by the wind is directed along windrows and therefore is at right angles to the direction of interest here). Langmuir circulations are assumed to exist, and to be unaffected by the oil on the surface.

Adopting a conventional "shallow water" model for this problem (see Leibovich 1977c, Appendix A, for example), and assuming that a steady balance between applied stress and gravity spread has been achieved, the oil thickness varies with spanwise distance y (measured from the LC convergence line), and $\tau_w(y)$ the stress applied to the oil layer by Langmuir circulations according to the rule

$$\rho_0 g \lambda h \partial h/\partial y = \tau_w(y) \tag{8-1}$$

where

$$\lambda = (\rho_w - \rho_0)/\rho_w \tag{8-2}$$

and g is the acceleration of gravity.

The shear stress on the oil layer may be related to the velocity (v) of the water below it by use of a dimensionless friction coefficient, c_f, with

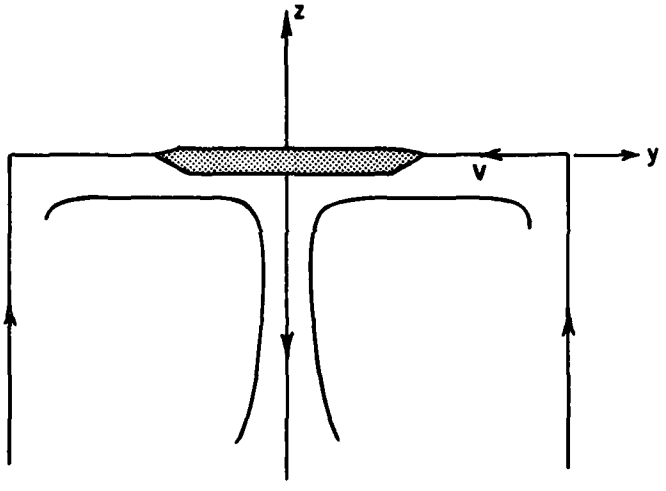

Figure 8-1. Definition sketch for the analysis of oil collection in windrows.

$$\tau_w = (1/2)\rho_w c_f v^2 \tag{8-3}$$

Experiments on oil containment barriers (Lindenmuth et al 1970) indicate that c_f depends upon oil type and is in the range 0.002 to 0.009. Hoult and Cross (1971) adopted the (constant) value $c_f = 0.008$, and we make the same assumption here.

Referring to the sketch in figure (8-1), suppose v is the surface sweeping velocity in the LC, and LW is the observed width of a band of oil collected in a windrow. Then h = 0 at $y \equiv LW/2$, and the maximum oil thickness, $h=h_{max}$ occurs at y= 0. Integrating (7-1), we obtain the oil thickness at any station y as

$$h(y) = \left[\frac{2}{\rho_0 \lambda g} \int_y^{LW/2} \tau_w \, dy\right]^{1/2}. \tag{8-4}$$

The total volume of oil collected per unit length of windrow is

$$V_0 = 2\int_0^{LW/2} h(y)dy. \tag{8-5}$$

Suppose LLC is the distance between windrow centers. Examination of LC simulations shows that v rises from zero at y = 0 to a maximum, say v_{max}, at about 1/3 the distance between convergence and upwelling planes, or about LLC/6, and that it falls back to zero at the upwelling plane, which we may put at y = LLC/2. Our estimate of oil collection into windrows can only be a crude one at best, and it seems that the replacement of v by a piecewise linear form is consistant with the accuracy of the models. Consequently, set

$$v(y) = \begin{cases} 6v_{max}\, y/LLC, & 0 \le y \le LLC/6 \\ (3v_{max}/2)(1-2y/LLC), & LLC/6 \le y \le LLC/2 \end{cases} \tag{8-6}$$

Furthermore, v_{max} will be a fraction of the LC convective velocity scale V. If we let α represent the fraction, $v_{max} = \alpha V$, then our model is

complete. Inputs are LW and LLC, ρ_o, ρ_w, α and V. A survey of a number of LC simulations suggests that $\alpha = 0.25$ is a reasonable estimate that should be typical. The results of the model are being displayed in dimensionless form in Figures 8-2 and 8-3. Here we have replaced V in favor of V_a through (3-18).

Two dimensional cases are shown in Table 8-1 to give the reader an idea of the numbers involved; (3-18) has again been used to replace V by V_a.

Table 8-1 -Maximum oil thickness and volume of oil collected per unit length of windrow for a wind speed of $10 ms^{-1}$, width oil band in windrow is assumed to be 2 m, distance between windrows is assumed to be 5 m.

Wind Speed	$\rho o/\rho w$	h_{max}(mm)	VO(cc/cm)
5 m/s	.98	3.3	53
10 m/s	.98	6.5	106
10 m/s	.99	9.2	150
15 m/s	.98	9.8	160

As with the other theoretical models in this report, it is important to compare predictions with observations in the field; tuning of the model by appropriate adjustments of constants is prudent.

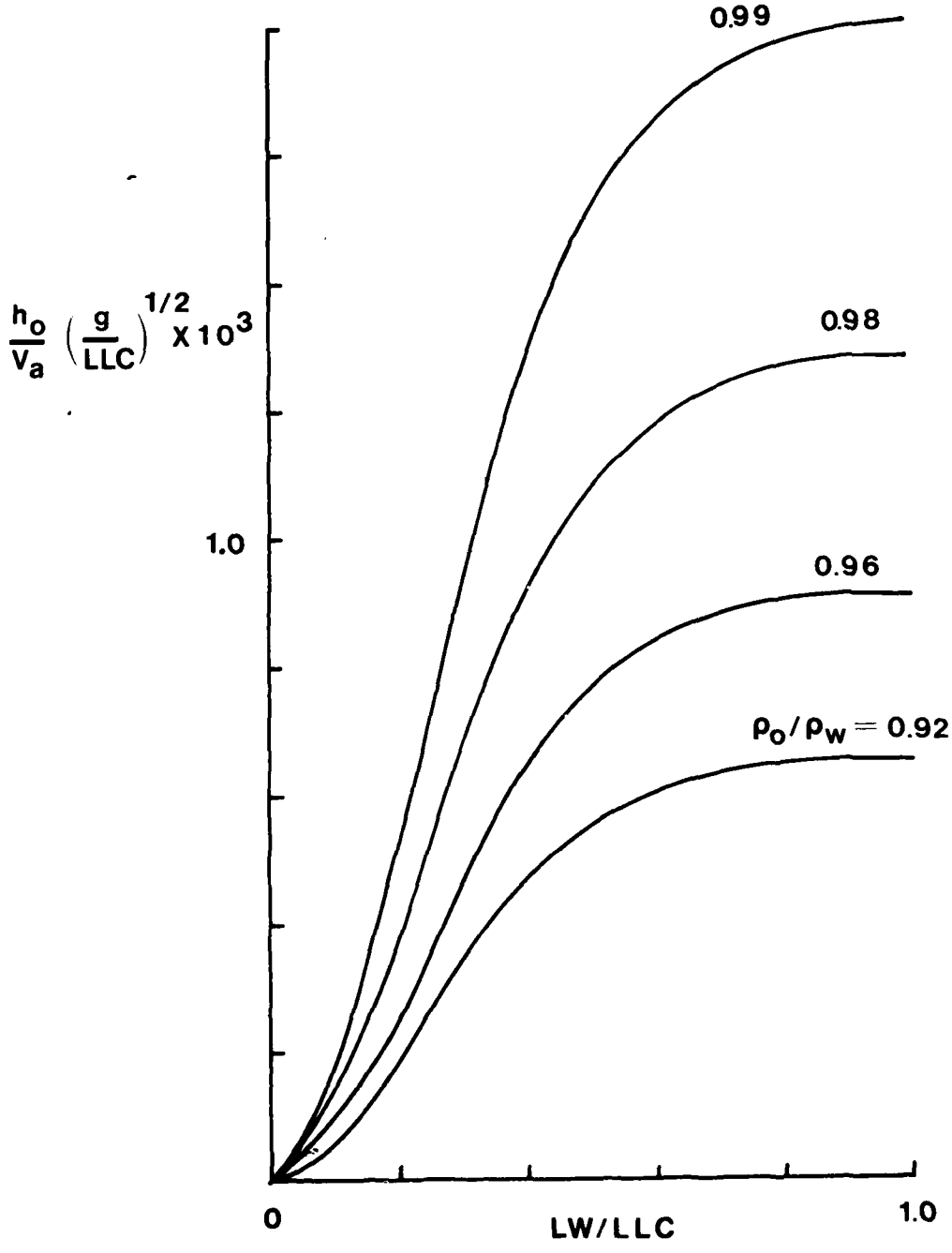

Figure 8.2 Maximum thickness h_0 of oil collected in windrows. V_a is wind speed; LLC is distance separating windrows: LW is the width of oil band in a windrow; g is acceleration of gravity; ρ_0 is the oil density; ρ_w is the water density.

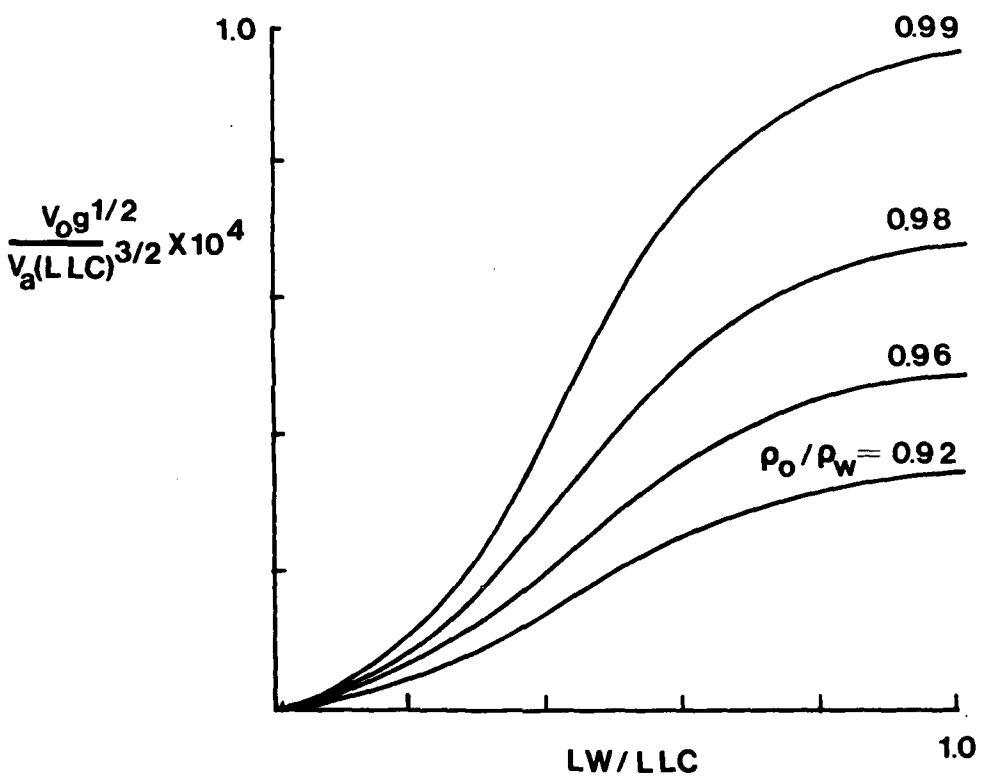

Figure 8-3. V_o is the volume of oil in windrow per unit length of row. See Figure 8-2 for other variables on graph.

9. CONCLUSIONS AND RECOMMENDATIONS

Our investigation indicates that oil is readily mixed in the water column to significant depths, provided the oil exists in the form of small noninteracting particles. Oil is expected to be in this form when dispersants are successfully used; in this case, the conclusions arrived at here are encouraging. Under natural circumstances, a fraction of the oil will be torn into small pieces if the seas are sufficiently severe, and this body of oil will be subject to the dispersion processes we have analyzed here. The determination of the extent of this prerequisite fragmentation in specified environmental conditions in the ocean remains an important open question.

In order to make progress, we have been forced to make a number of simplifying assumptions. Some of these assumptions no doubt can be weakened or removed. The problem as a whole, however, is of such complexity that uncertainities inevitably will remain. It is our feeling that the present results, which may not be quantitatively accurate, incorporate the essential physics and should therefore give correct qualitative trends, and be correct so far as orders of magnitudes are concerned. Theoretical estimates such as ours can be improved as data is made available; experiments designed to generate the required data may be feasible, and certainly would be desirable.

The same remarks can be made for our simple model of the collection of floating oil into windrows. Since these oil bands are readily visible, and the surface water motions are monitored more easily than subsurface motions, it should be relatively easy to "tune" this model. It has been programmed on a hand held calculator, and is therefore easily taken to the field; if it is verified, it should be well suited for rapid estimation of floating oil volumes and thicknesses.

REFERENCES

Abramowitz, M. and Stegun, I. A. (eds.) 1964. Handbook of Mathematical Functions. Washington, D.C., National Bureau of Standards.

Adams, N. K. 1936. The Pollution of the Sea and Shore by Oil. Special Report to the Council of the Royal Society of London.

Andrews, D. G. and McIntyre, 1978. An exact theory of nonlinear waves on a Langrangian-mean flow. J. Fluid Mech., 89:609-646.

Assaf, G., Gerard, R. and Gordon, A. L. 1971. Some mechanisms of oceanic mixing revealed in aerial photographs, J. Geophys. Res., 76: 6550-6572.

Atwood, D. K., Benjamin, J. A. and Farrington, J. 1980. The mission of the September 1979 RESEARCHER/PIERCE IXTOC-I cruise and the physical situation encountered, pp. 1-18 in Preliminary Results from the September 1979 RESEARCHER/PIERCE IXTOC-I cruise, D. K. Atwood (ed.) U.S. Dept. Commerce, NOAA.

Battelle Memorial Institute 1969. Review of the Santa Barbara Channel Oil Pollution Incident. Report to Dept. of Interior, FWPCA and to Dept. of Transportation, U.S.C.G.

Bretschneider, C. L. 1966. Chapter 3 in Estuary and Coastline Hydrodynamics, A. T. Ippen (ed.) McGraw-Hill.

Canevari, G. P. 1978. Some Observations on the Mechanism and Chemistry Aspects of Chemical Dispersion, in Chemical Dispersants for the Control of Oil Spills, McCarthy et al (eds.), ASTM, Philadelphia.

Csanady, G. T. 1963. Turbulent diffusion of heavy particles in the atmosphere. J. Atmos. Sci., 20: 201-208.

Craik, A. D. D. and Leibovich, S. 1976. A rational model for Langmuir circulations, J. Fluid Mech. 73: 401-426.

Craik, A. D. D., 1977. The generation of Langmuir circulations by an instability mechanism, J. Fluid Mech., 81: 209-223.

Cross, R. H. and Hoult, D. P. 1971. Collection of Oil Slicks. J. Waterways, Harbors, and Coastal Eng. Div., ASCE (May 1971) 313-322.

Faller, A. J. and Woodcock, A. H. 1964. The spacing of windrows of Sargassum in the ocean. J. Marine Res., 22: 22-29.

Faller, A. J. 1969. The generation of Langmuir circulations by the eddy pressure of surface waves. Limn. Ocean., 14: 504-513.

Faller, A. J. and Caponi, E. A. 1978. Laboratory studies of wind driven Langmuir circulations, J. Geophys. Res. 83: 3617-3633.

Faller, 1978. Experiments with controlled Langmuir circulations, Science, 201: 618-620.

Faller, A. J. 1981. The origin and development of laboratory models and analogues of the ocean circulation. In Evolution of Physical Oceanography, Chapter 16: 477, B. A. Warren and C. Wunsch (eds.). MIT Press; Cambridge, MA.

Forrester, W. P. 1971. Distribution of suspended oil particles following the grounding of the tanker ARROW, J. Marine Res., 29: 151-170.

Galt, J. 1980. Personal Communication. NOAA, Seattle, Washington.

Galt, J. 1978. Investigations of physical processes, The AMOCO CADIZ Oil Spill, NOAA/EPA Special Report, W. Hess (ed.), Chapter 2.

Garrett, C. J. R. 1976. Generation of Langmuir circulations by surface waves - a feedback mechanism. J. Marine Res., 34: 117-130.

Gordon, A. L. 1970. Vertical momentum flux accomplished by Langmuir circulations. J. Geophys. Res., 75: 4177-4179.

Hess, W. 1978. The AMOCO CADIZ Oil Spill. NOAA/EPA Special Report.

Hooper, C. 1981. Personal Communication. NOAA, Boulder, CO.

Ichiye, T. 1967. Upper ocean boundary-layer flow determined by dye diffusion. Physics of Fluids, Supplement: 5270-5277.

Katz, B., Gerard, R. and Costin, M. 1965. Responses of dye tracers to sea surface conditions. J. Geophys. Res., 70: 5505-5513.

Kenyon, K. E. 1969. Stokes drift for random gravity waves. J. Geophys. Res., 74: 6991-6994.

Kitaigorodskii, S. A., Donelan, M., Lumley, J. L., Terray, E., and Zeman, O. 1981. Towards modeling wind-induced three-dimensional turbulence in the upper ocean mixed layer. Submitted for publication.

Langmuir, I. 1938. Surface water motion induced by wind. Science, 87:119-123.

Leibovich, S. 1975. A natural limit to the containment and removal of oil spills at sea. Ocean Engineering, 3: 29-36.

Leibovich, S. 1977a. On the evolution of the system of wind drift currents and Langmuir circulations in the ocean. Part 1. Theory and the averaged current. J. Fluid Mech., 79: 715-743.

Leibovich, S. and Radhakrishnan, K. 1977. On the evolution of the system of wind drift currents and Langmuir circulations in the ocean. Part 2. Structure of the Langmuir vortices, J. Fluid Mech., 80: 481-507.

Leibovich, S. 1977b. Convective instability of stably stratified water in the ocean. J. Fluid Mech., 82: 561-585.

Leibovich, S. 1977c. Hydrodynamic Problems in Oil-Spill Control and Removal. J. of Petroleum Tech., March 1977, 311-324.

Leibovich, S. 1980. On wave-mean flow interaction theories of Langmuir circulation. J. Fluid Mech. 99: 715-724.

Leibovich, S. and Paolucci, S. 1980a. The Langmuir circulation instability as a mixing mechanism in the upper ocean. J. Phys. Oceanography, 10: 186-207.

Leibovich, S. 1980. Mixing of the upper ocean by Langmuir circulations. Ocean Modeling, 29: 1-5.

Leibovich, S. and Paolucci, S. 1980b. Energy stability of the Eulerian-mean motion in the upper ocean to three-dimensional disturbances. Phys. of Fluids 23: 1286-1290.

Leibovich, S. and Paolucci, S. 1981. The instability of the ocean to Langmuir circulations. J. Fluid Mech. 102: 141-167

Lindenmuth, W. T., Miller, E. R. and Hsu, C. C. 1970. Studies in Oil Retention Boom Hydrodynamics. Report No. 714102/A/008, AD 719 294, U.S. Coast Guard.

Longuet-Higgins, M. S. 1952. On the statistical distribution of the heights of sea waves. J. Marine Res., 11: 245-266.

Longuet-Higgins, M. S. 1953. Mass transport in water waves. Phil. Trans. A. [illegible] 535-581.

Longuet-Higgins, M. S. 1969. On wave breaking and the equilibrium spectrum of wind-generated waves. Proc. Roy. Soc., A, 310: 151-159.

Lottey, J. M. 1979. The Turbulent Transport of Atmospheric Aerosols. Ithaca, NY: Cornell University.

Lumley, J. L. 1957. Some Problems Connected with the Motion of Small Particles in Turbulent Fluid, ONR Contract Report NONR 248(38), The Johns Hopkins University.

Lumley, J. L. 1976. Two-phase and non-Newtonian flows. In Topics in Applied Physics, ed. P. Bradshaw, ch. 7, pp.289-324. Springer-Verlag.

Lumley, J. L. 1978. Turbulent transport of passive contaminants and particles: fundamentals and advanced methods of numerical modeling, in Lecture Series 1978-7, Pollutant Dispersal, Von Karman Institute for Fluid Dynamics, Rhode-St-Genese, Belgium.

Maratos, A. 1971. Study of the near shore surface characteristics of windrows and Langmuir circulation in Monterey Bay. M.Sc. thesis, U.S. Naval Postgraduate School, Monterey, CA.

McCarthy, L. T., Lindblom, G. P., Walter, H. F., (eds.) 1978. Chemical Dispersants for the Control of Oil Spills, Am. Soc. Testing & Materials, Philadelphia.

Milgram, J. a., Donnelly, R. G., Van Houten, R. J. and Camperman, J. M.1978. Effects of Oil Slick Properties on the Dispersion of Floating Oil into the Sea. Final Report to the U.S. Coast Guard Office of Research & Development, Report No. CG-D-64-78.

Monin, A. S. and Yaglom A. M. 1971. Statistical Fluid Mechanics, Vol. I (J. L. Lumley, ed.) Cambridge, MA: MIT Press.

Neuman, G. and Pierson, Jr., W. J. 1966. Principals of Physical Oceanography, Englewood Cliffs NJ: Prentice Hall.

Paolucci, S. 1979. Langmuir circulations as a convective instability mechanism and its effect on the ocean mixed layer. Ph.D. thesis, Cornell University, 218 pp.

Phillips, O. M. 1977. Dynamics of the Upper Ocean, 2nd Edition, Cambridge, UK; Cambridge University Press.

Raj, P. K. 1977. Theoretical Study to Determine the Sea State Limit for the Survival of Oil Slicks on the Ocean, Arthur D. Little Rept. No. 79299.

Robinson, J. 1980. Personal Communication. NOAA, Boulder, CO.

Scott, J. T., Meyer, G. E., Stewart, R. and Walther, E. G. 1969. Science, 87: 119-123.

Snyder, W. H., and Lumley, J. L. 1971. Some measurements of particle velocity autocorrelation functions in a turbulent flow. J. Fluid Mech. 48: 41-71.

Stewart, R. W. 1967. Mechanics of the air-sea interface. Phys. of Fluids, Supplement 10, S: 47-55.

Stommel, H. 1949. Trajectories of small bodies sinking slowly through convection cells. J. Marine Res., 8: 24-29.

Stommel, H. 1951. Streaks on natural water surfaces. Weather, 6: 72-74.

Tennekes, H. and Lumley, J. L. 1972. A First Course in Turbulence. Cambridge, MA; MIT Press.

Thomson, J. 1862. On the calm lines often seen on a rippled sea. Phil. Mag., 24, Series 4: 247-248.

Van Dyke, M. 1975. Perturbation Methods in Fluid Mechanics, Stanford, CA: Parabolic Press.

Williams, K. G. 1965. Turbulent water flow patterns resulting from wind stress on the ocean. NRL Memorandum Rept. 1653.

Williams, R 1979. Personal Communication. Exxon Production. Research Company, Houston, TX.

Yudine, M. I. 1959. Advances in Geophysics, 6: 185.

AD-A117 844 FLOW ANALYSIS ASSOCIATES ITHACA NY F/G 13/2
A THEORETICAL APPRAISAL OF THE JOINT EFFECTS OF TURBULENCE AND --ETC(U)
SEP 81 S LEIBOVICH, J L LUMLEY DTC823-80-C-20019
UNCLASSIFIED FAA-8101 USCG-D-26-82 NL

2 of 2
AD A117844

END
DATE FILMED
8 82
DTIC

APPENDIX

STOMMEL RETENTION ZONES

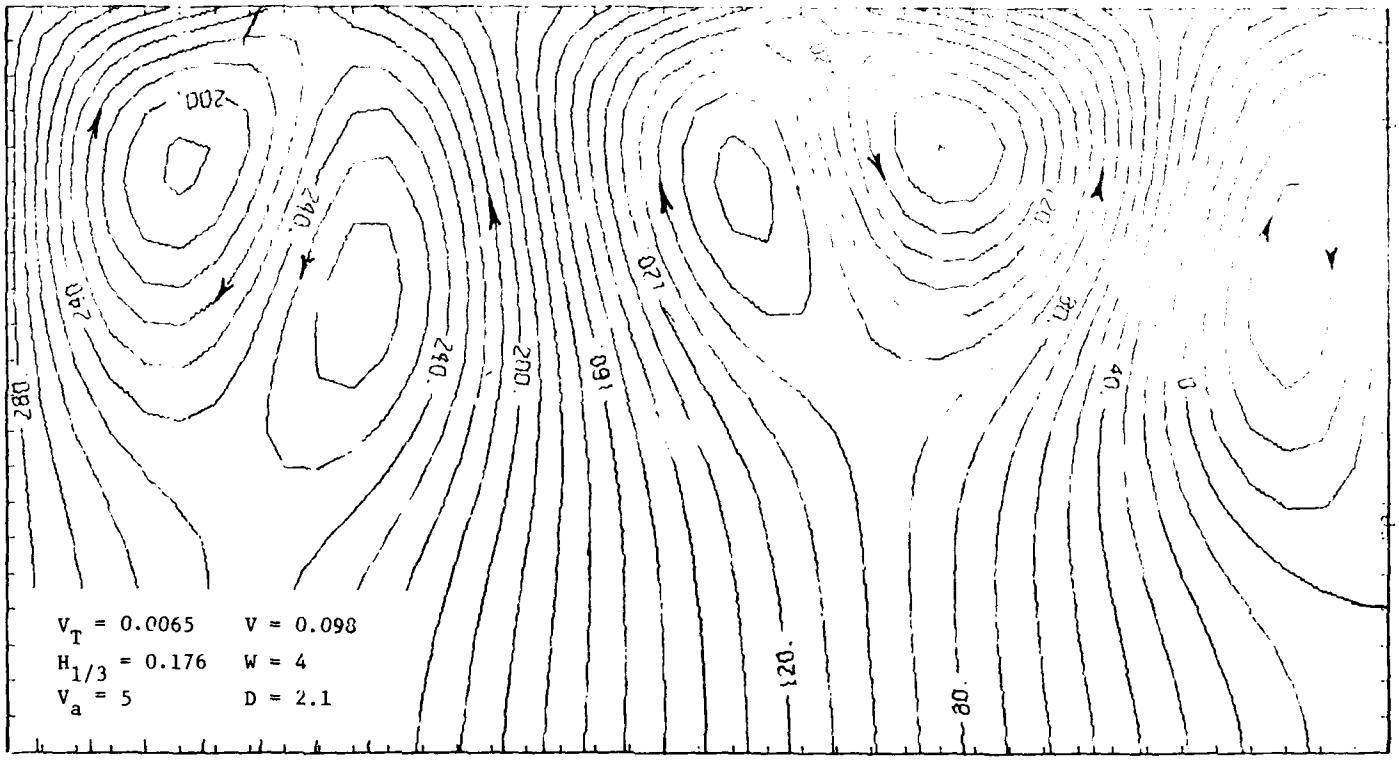

Figure A-1. See Figure 4-4 for caption.

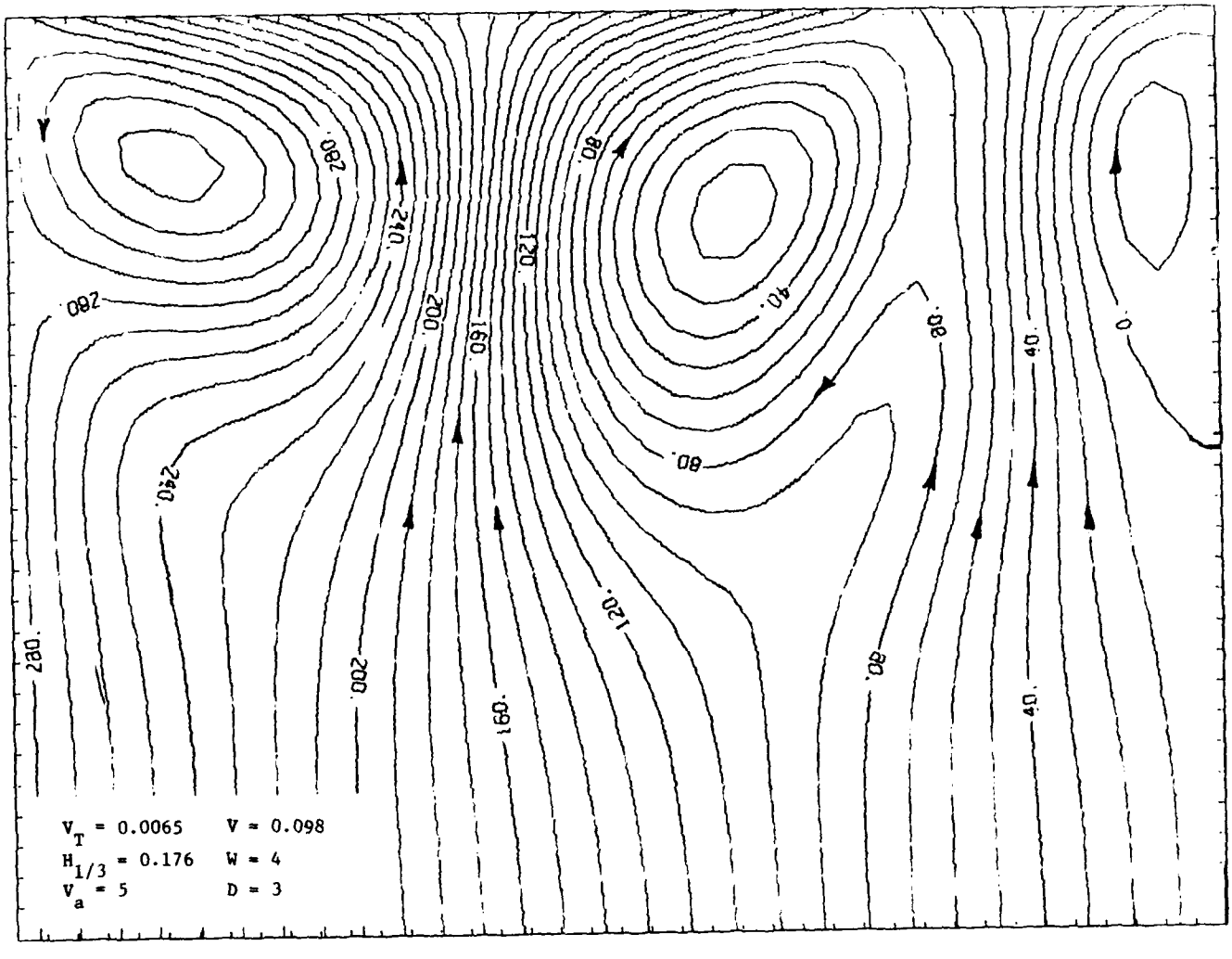

Figure A-2. See Figure 4-4 for caption.

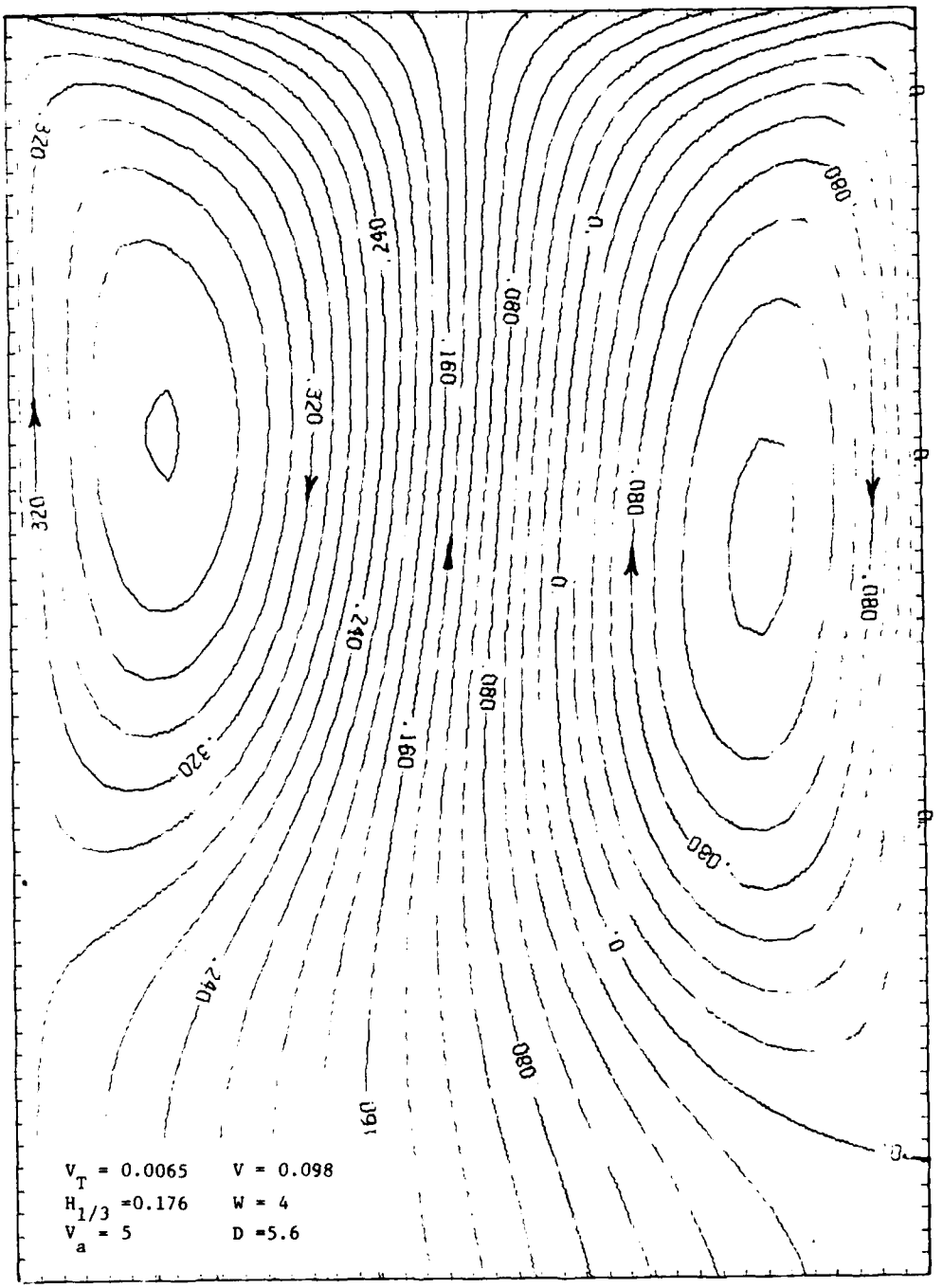

Figure A-3. See Figure 4-4 for caption

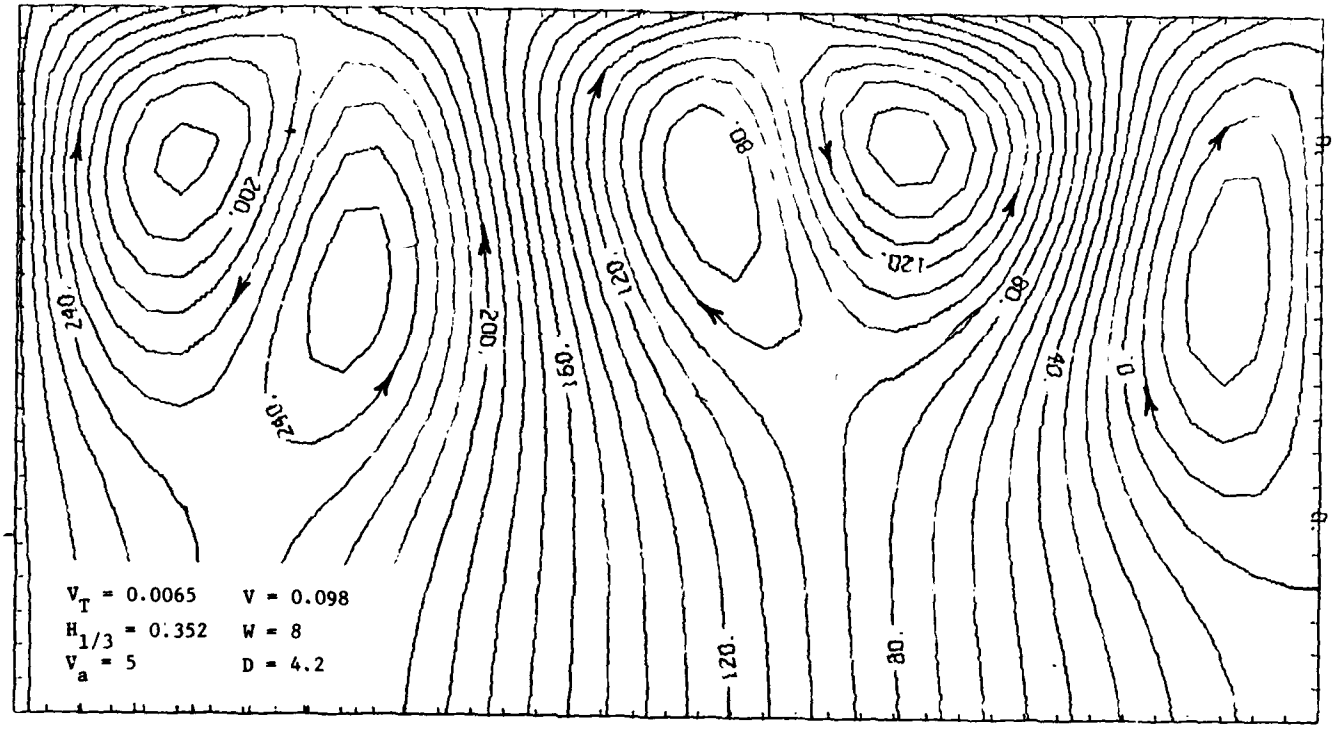

Figure A-4. See Figure 4-4 for caption.

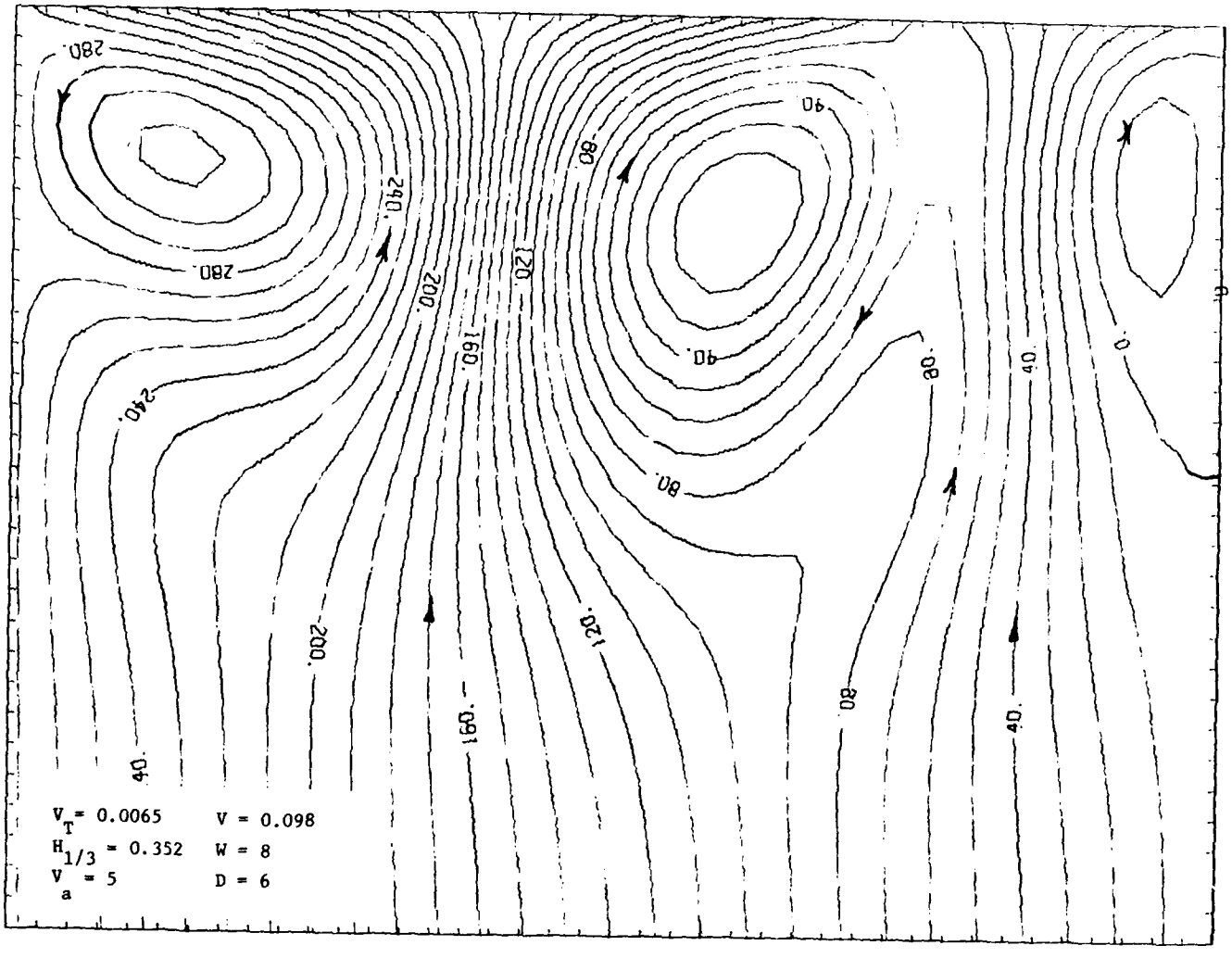

Figure A-5. See Figure 4-4 for caption.

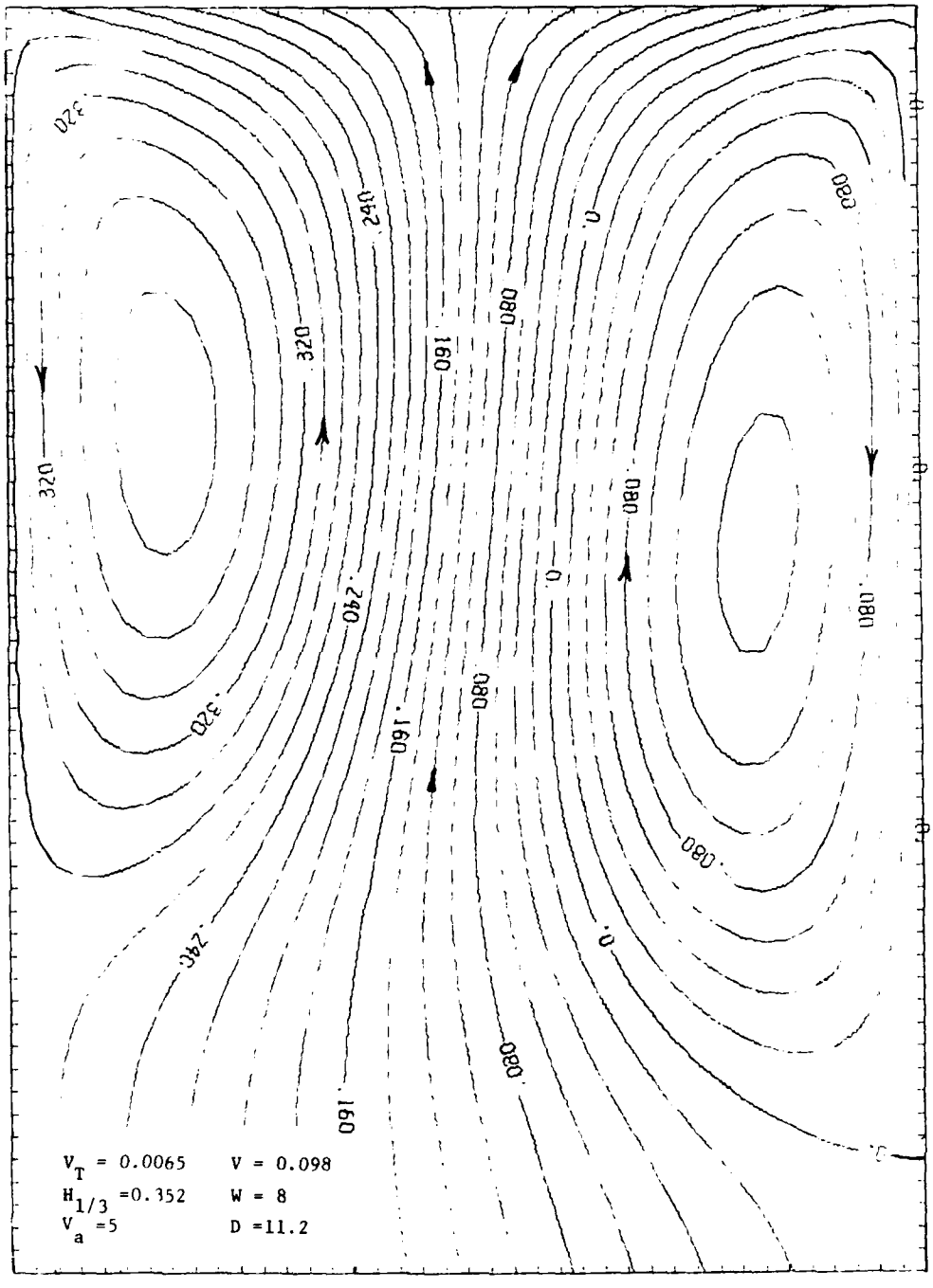

Figure A-6. See Figure 4-4 for caption.

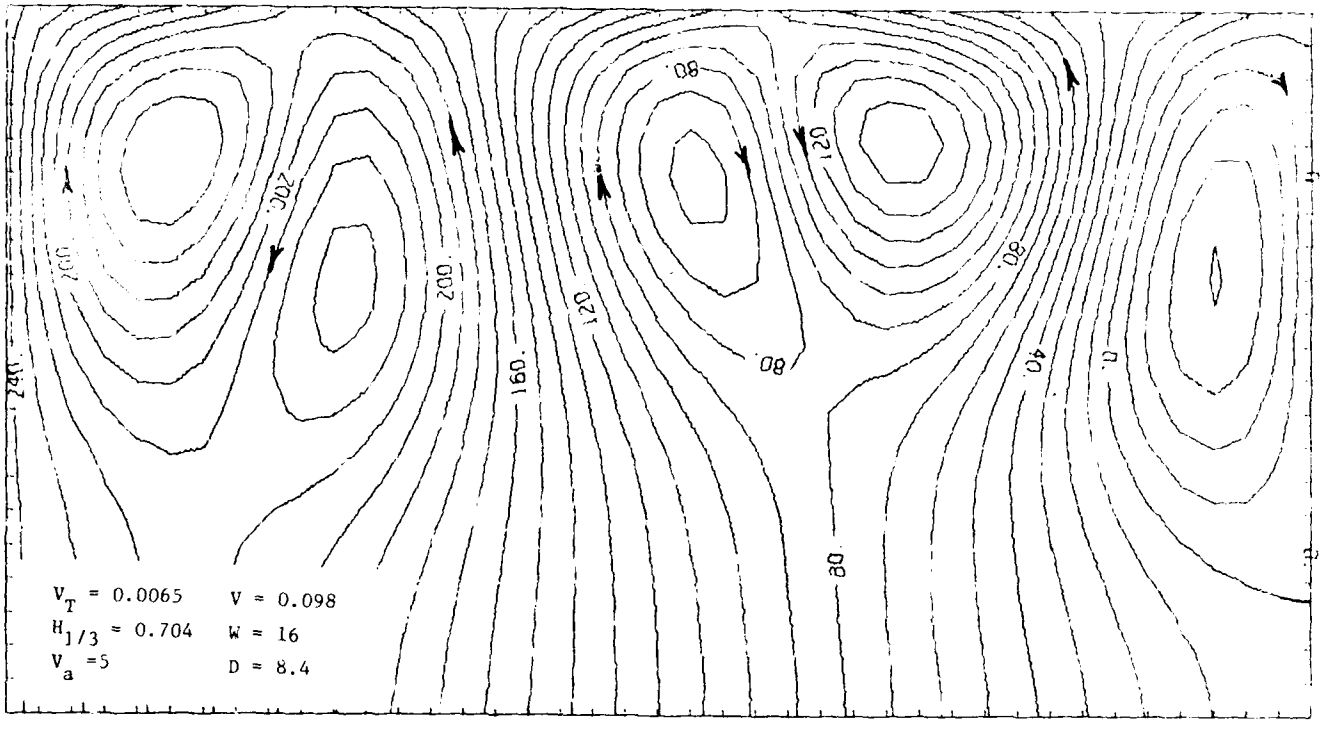

Figure A-7. See Figure 4-4 for caption.

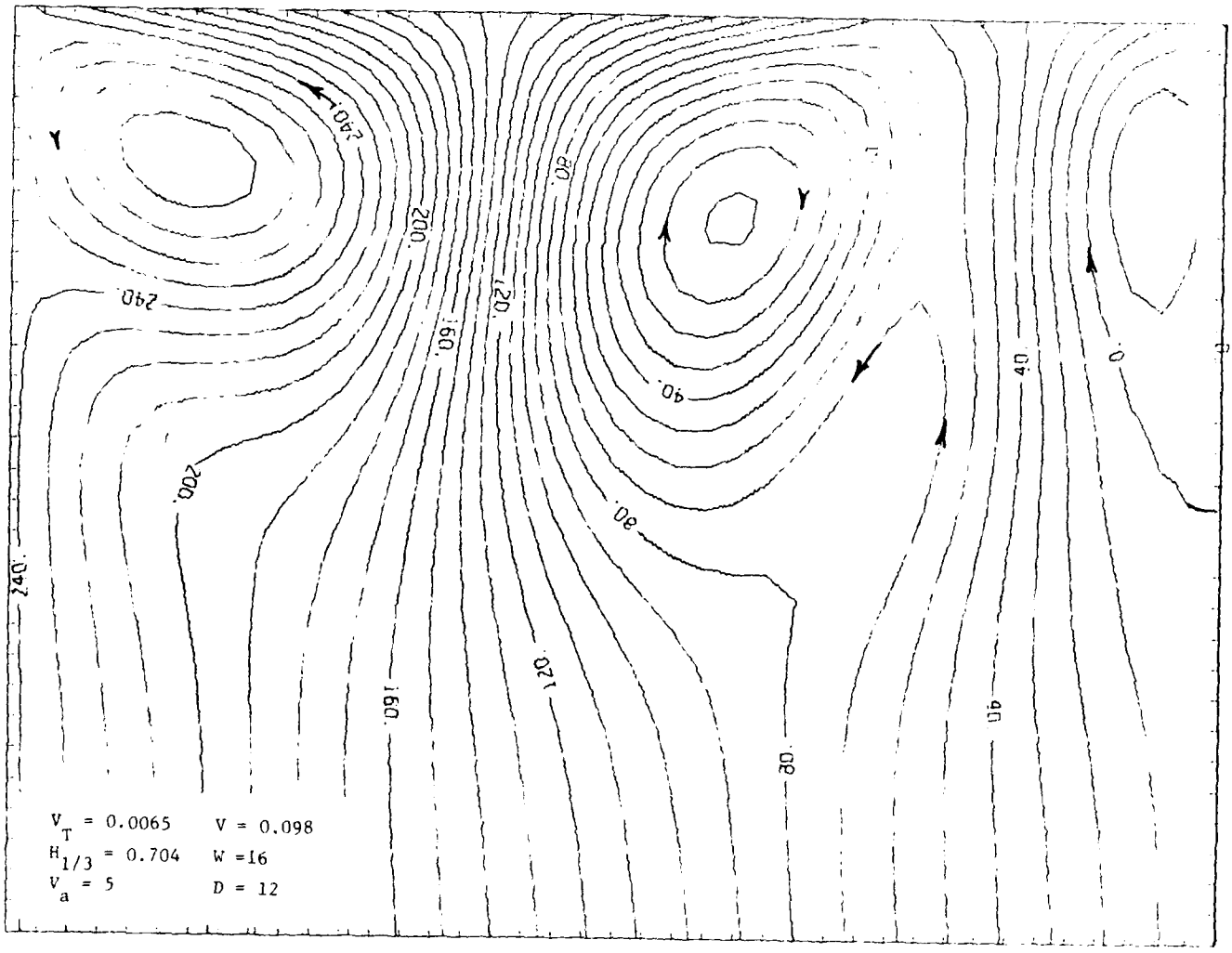

Figure A-8. See Figure 4-4 for caption.

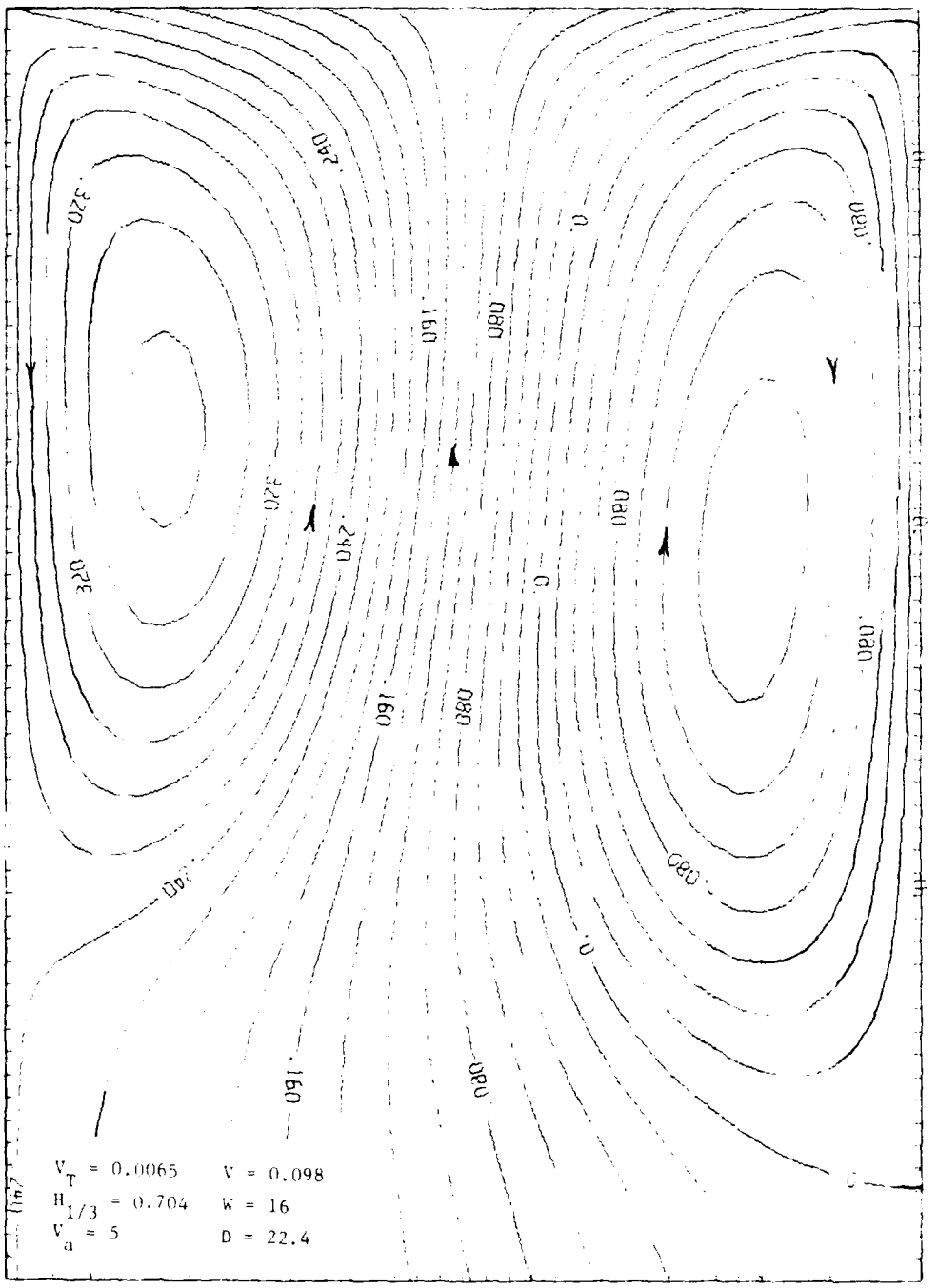

Figure A-9. See Figure 4-4 for caption.

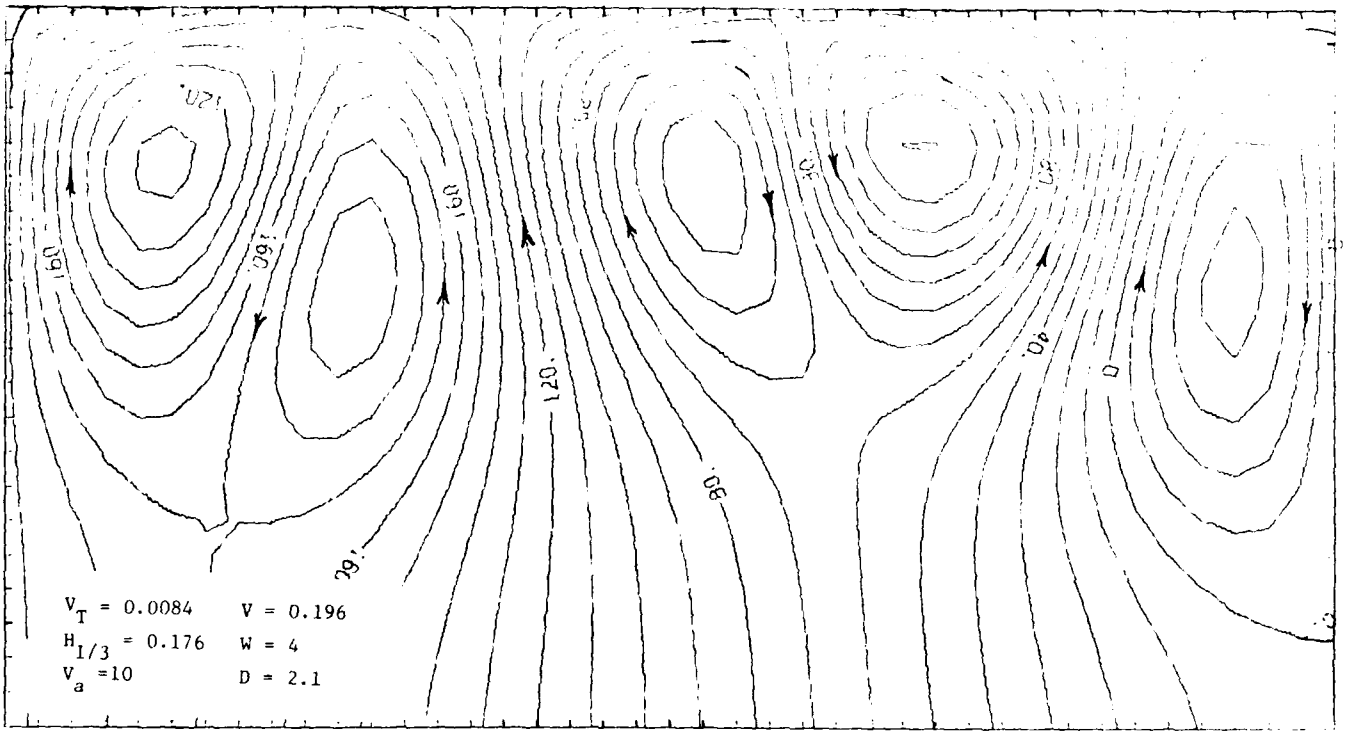

Figure A-10. See Figure 4-4 for caption.

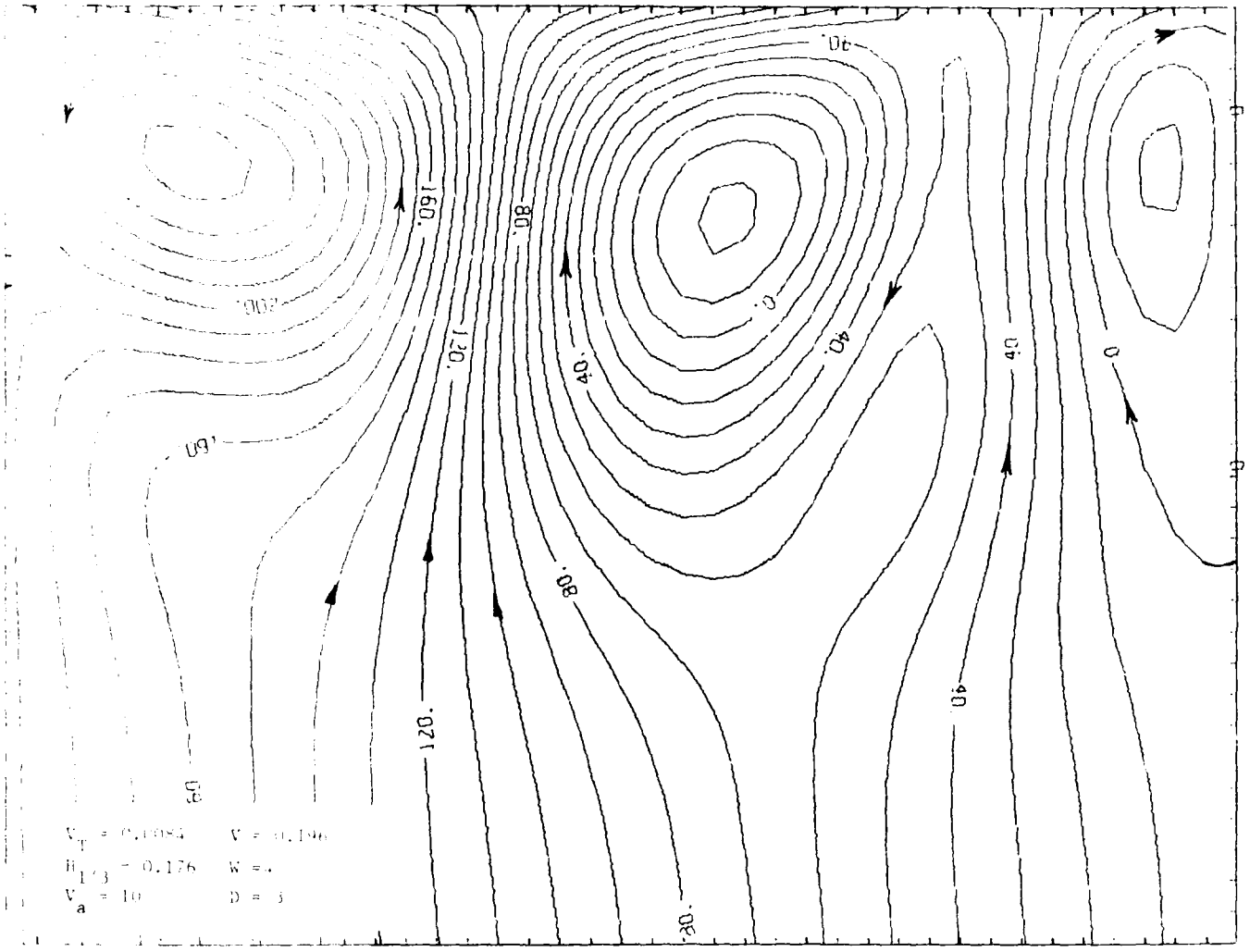

Figure A-11. See Figure 4-4 for caption.

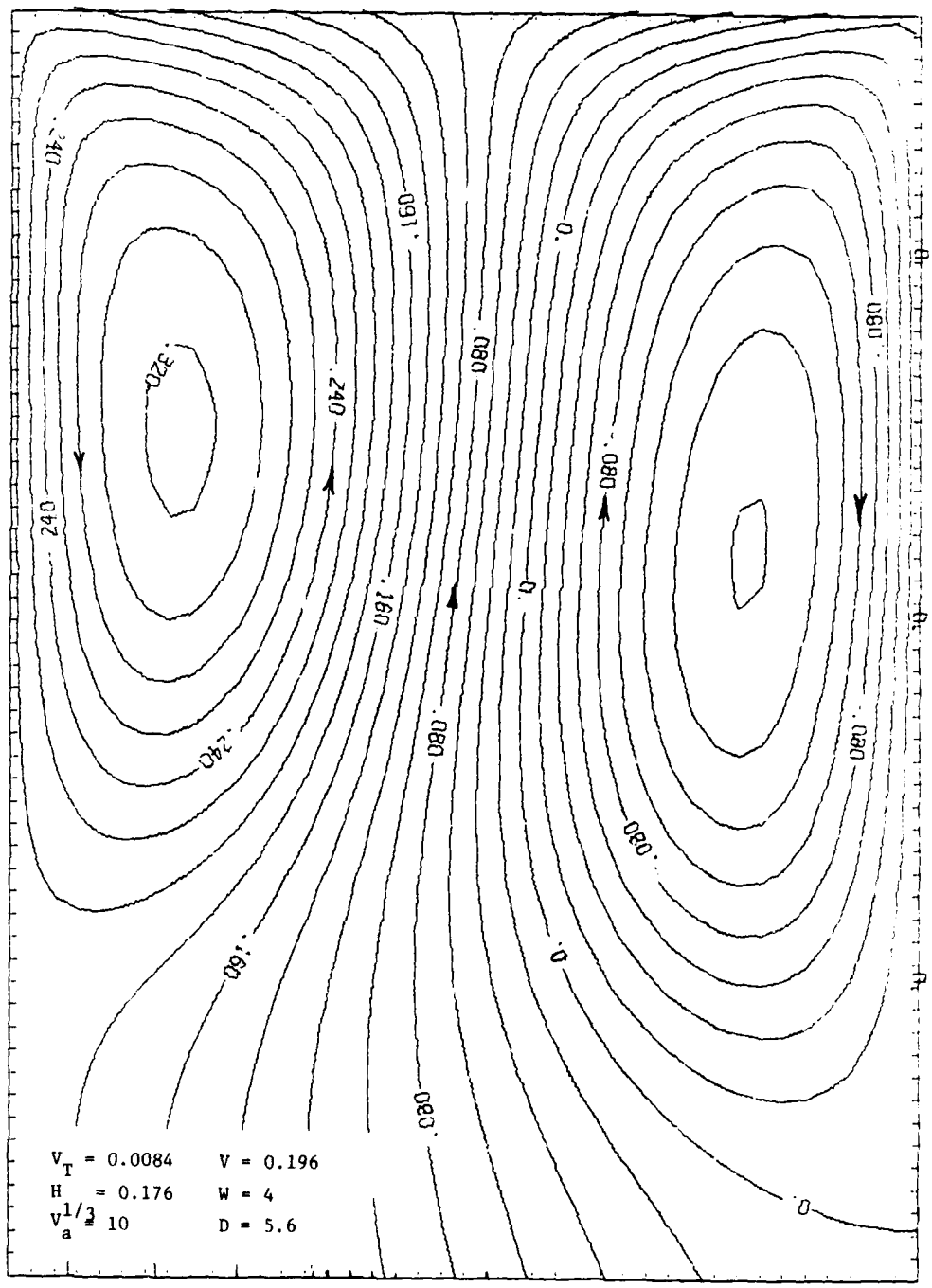

Figure A-12. See Figure 4-4 for caption.

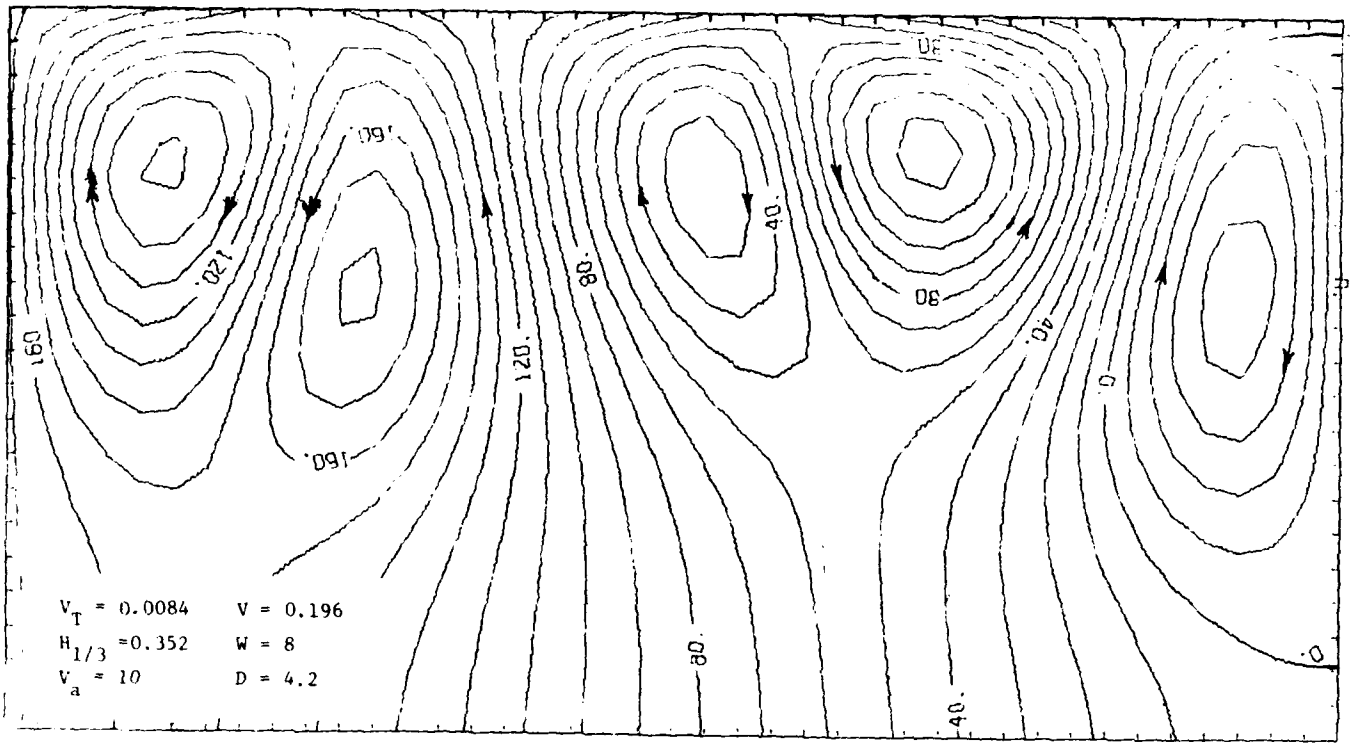

Figure A-13. See Figure 4-4 for caption.

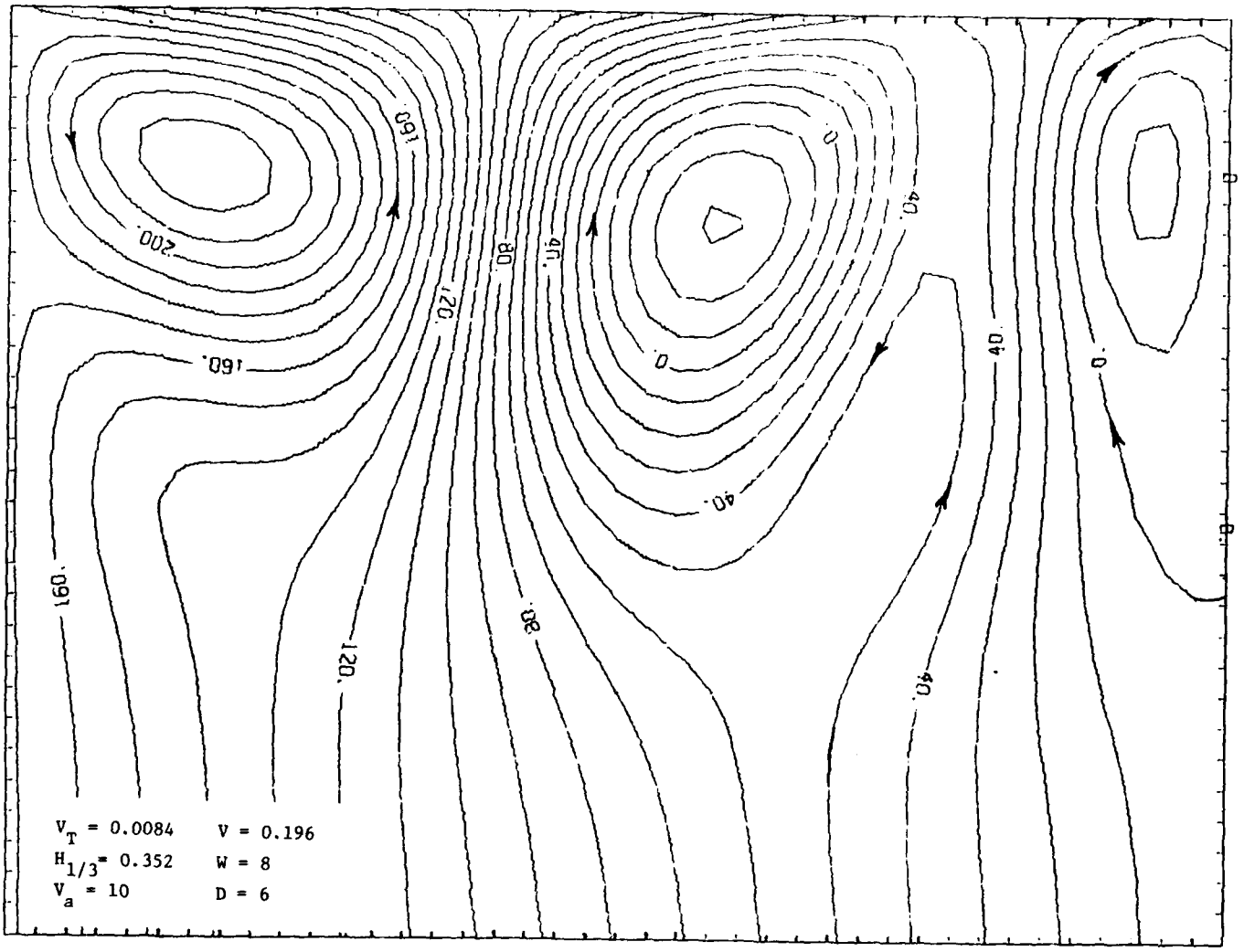

Figure A-14. See Figure 4-4 for caption.

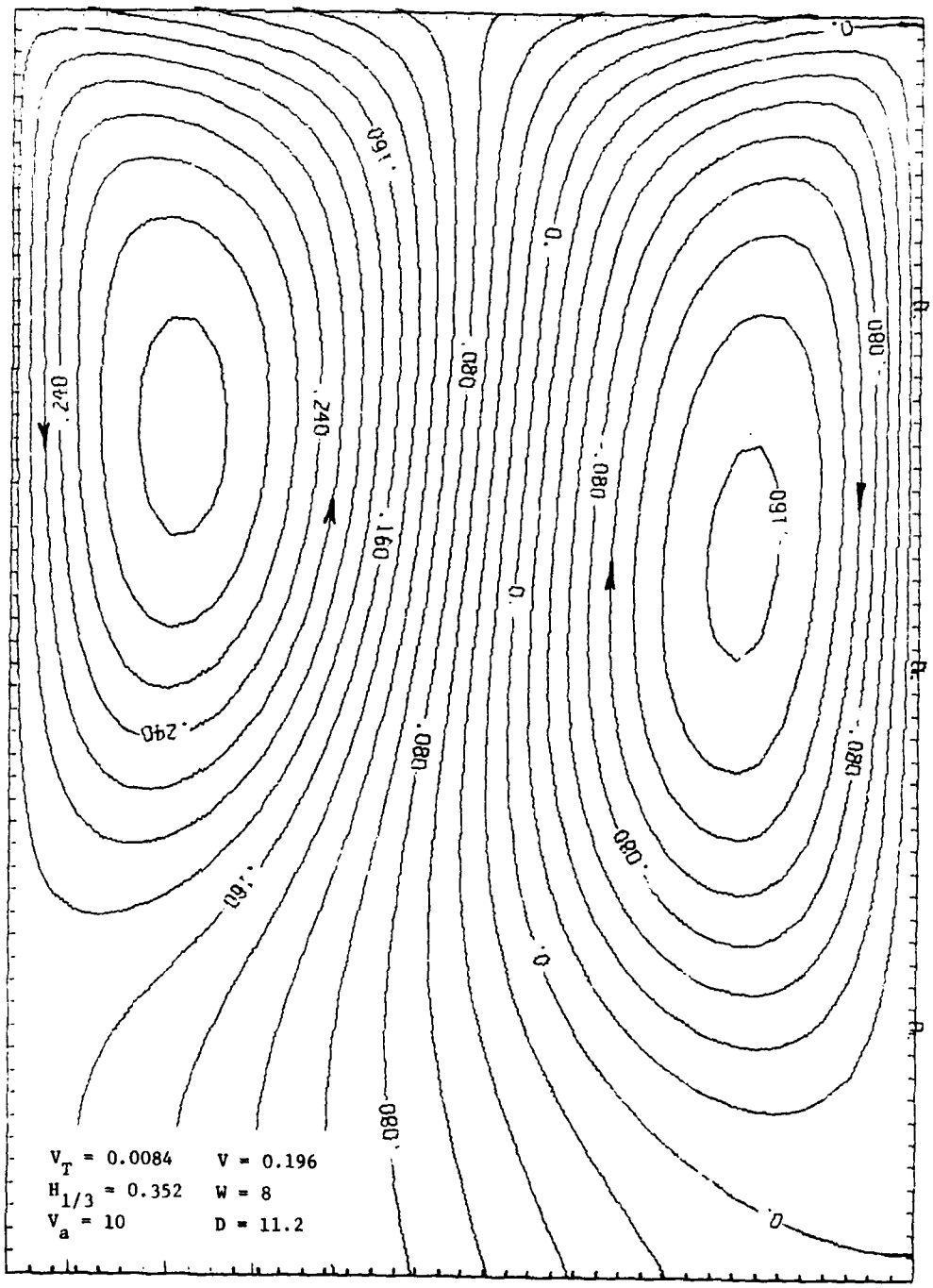

Figure A-15. See Figure 4-4 for caption.

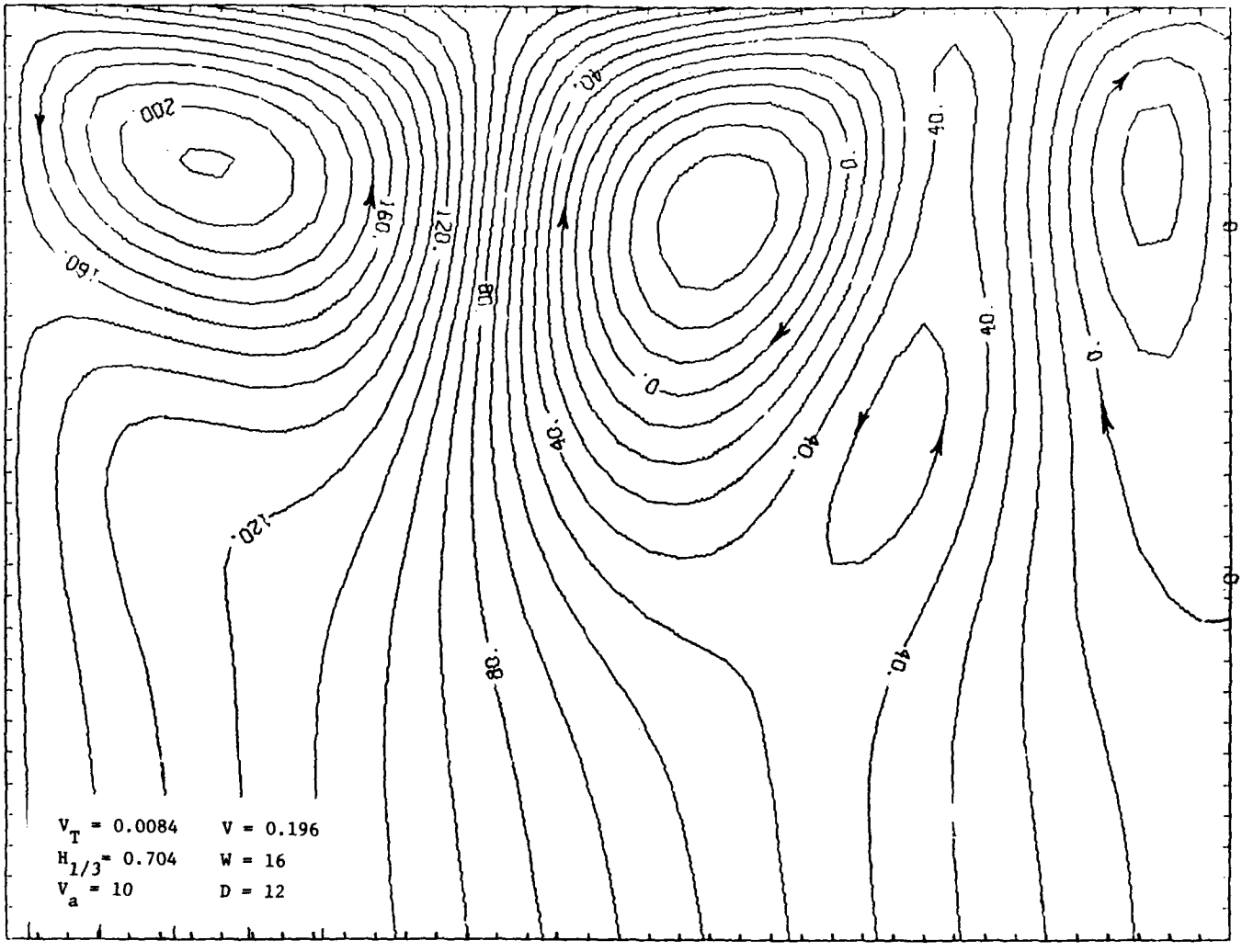

Figure A-16. See Figure 4-4 for caption.

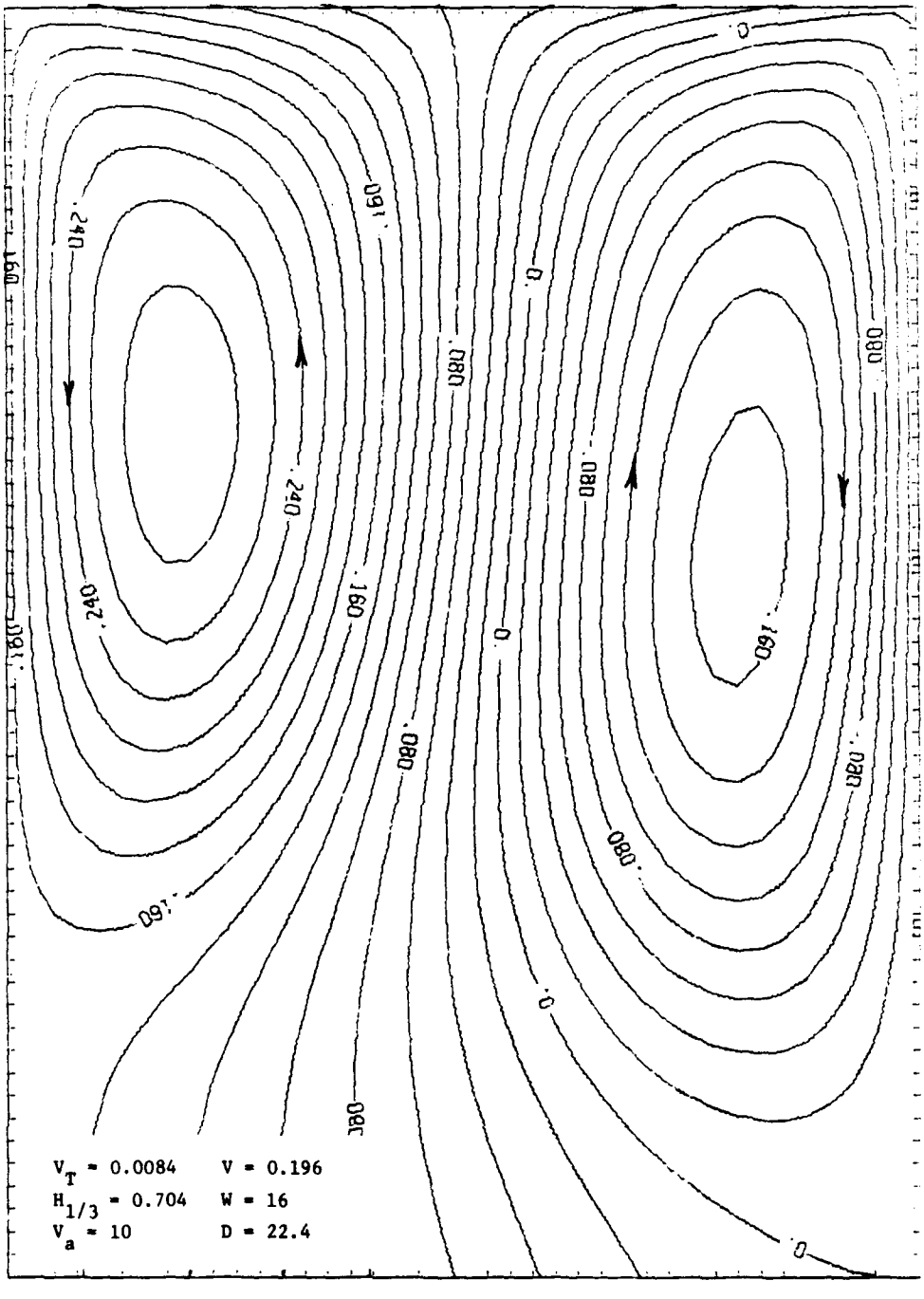

Figure A-17. See Figure 4-4 for caption.

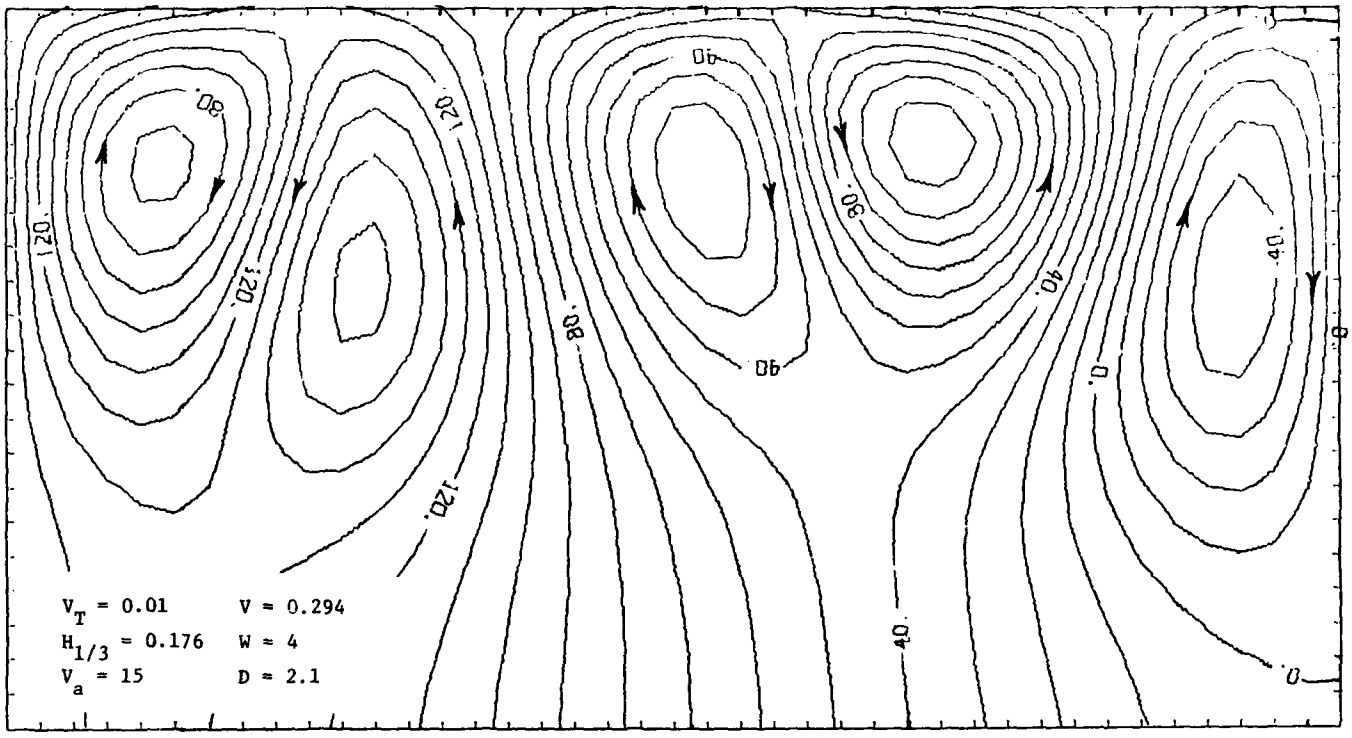

Figure A-18. See Figure 4-4 for caption.

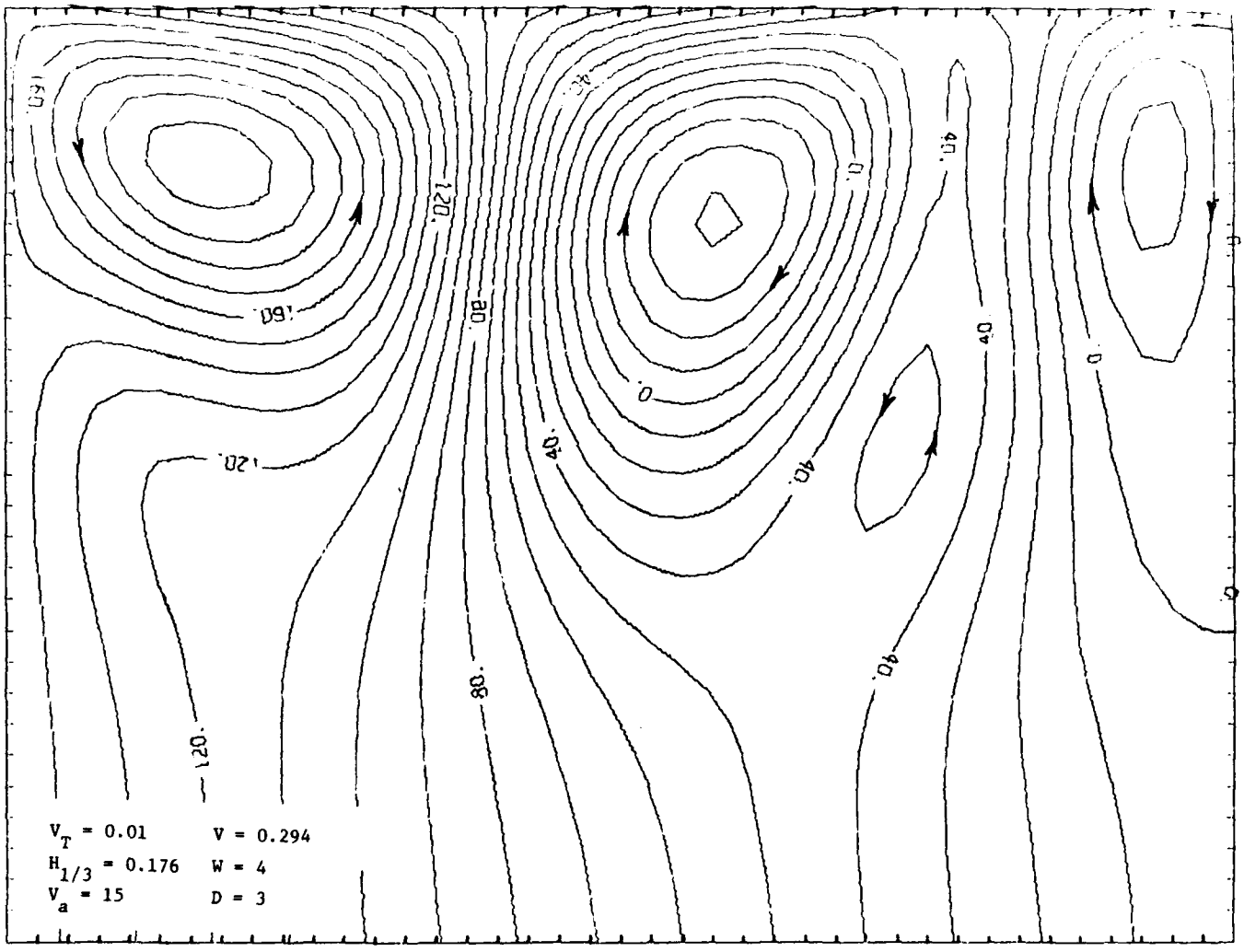

Figure A-19. See Figure 4-4 for caption.

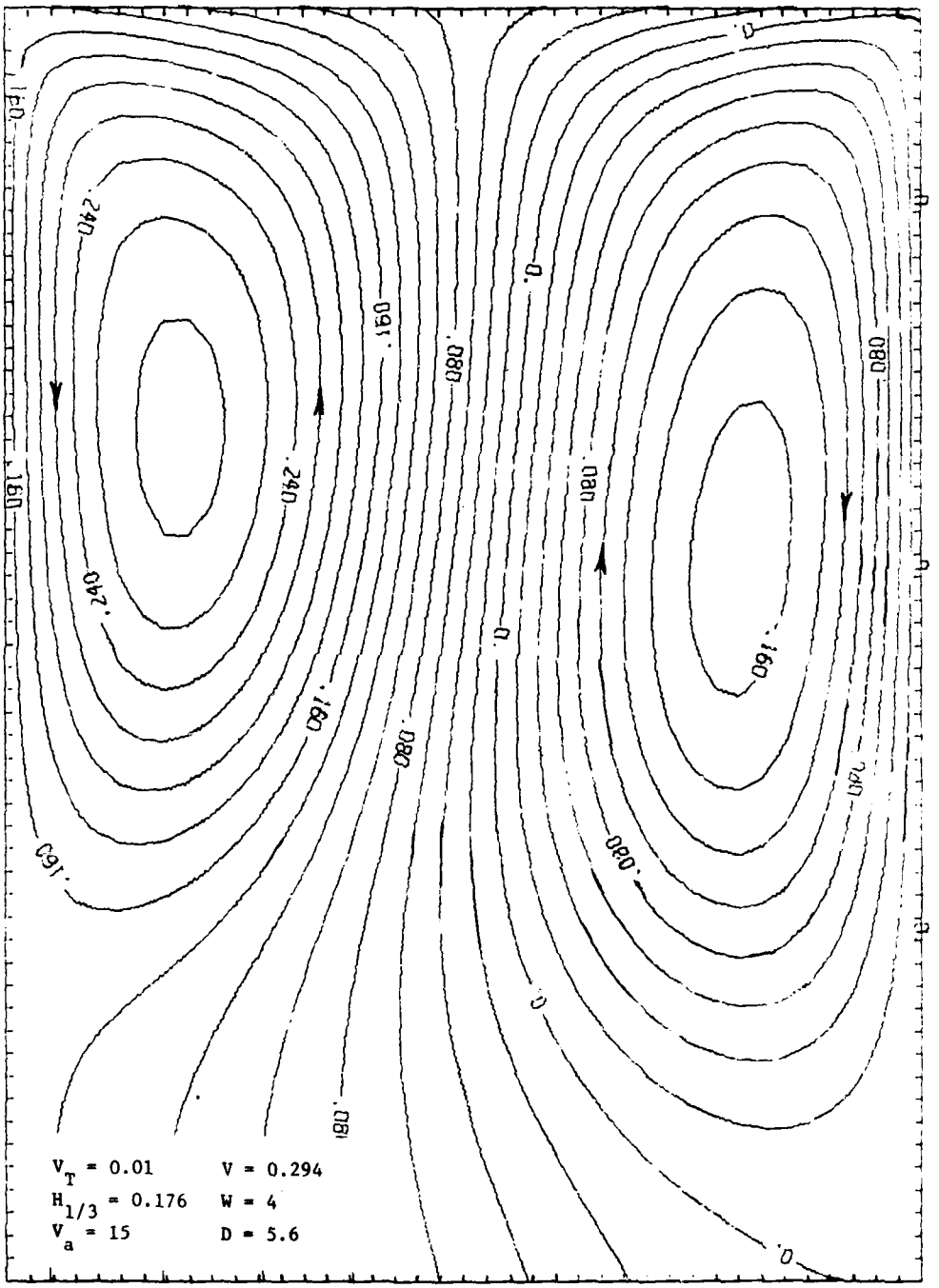

Figure A-20. See Figure 4-4 for caption.

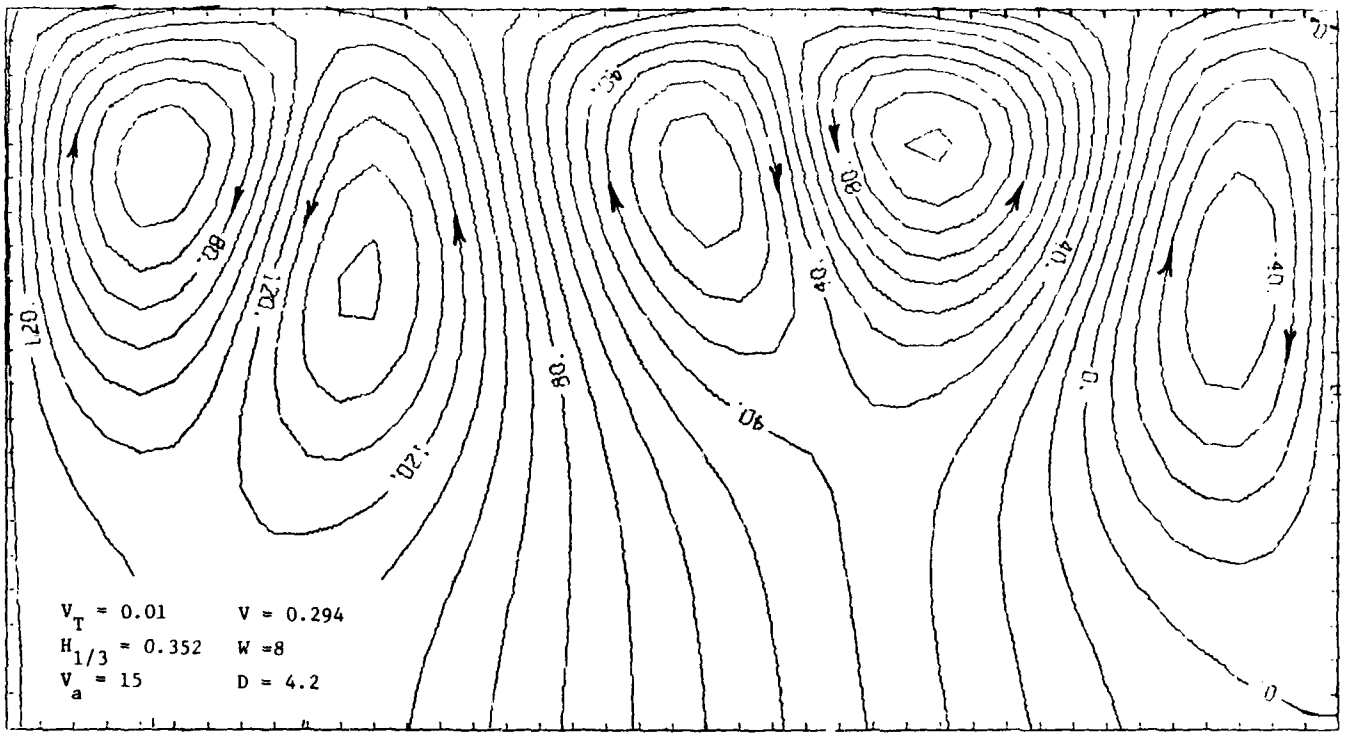

Figure A-21. See Figure 4-4 for caption.

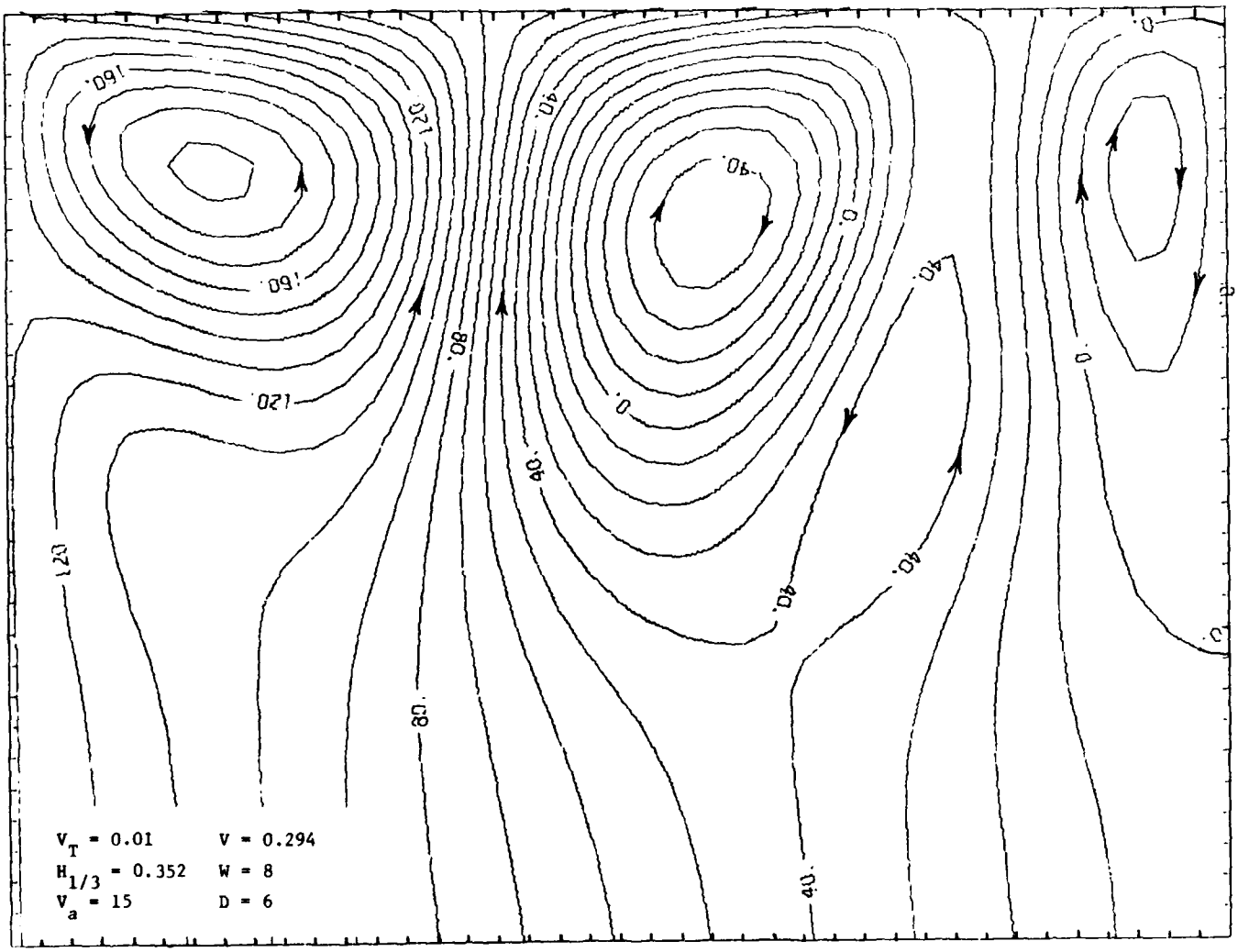

Figure A-22. See Figure 4-4 for caption.

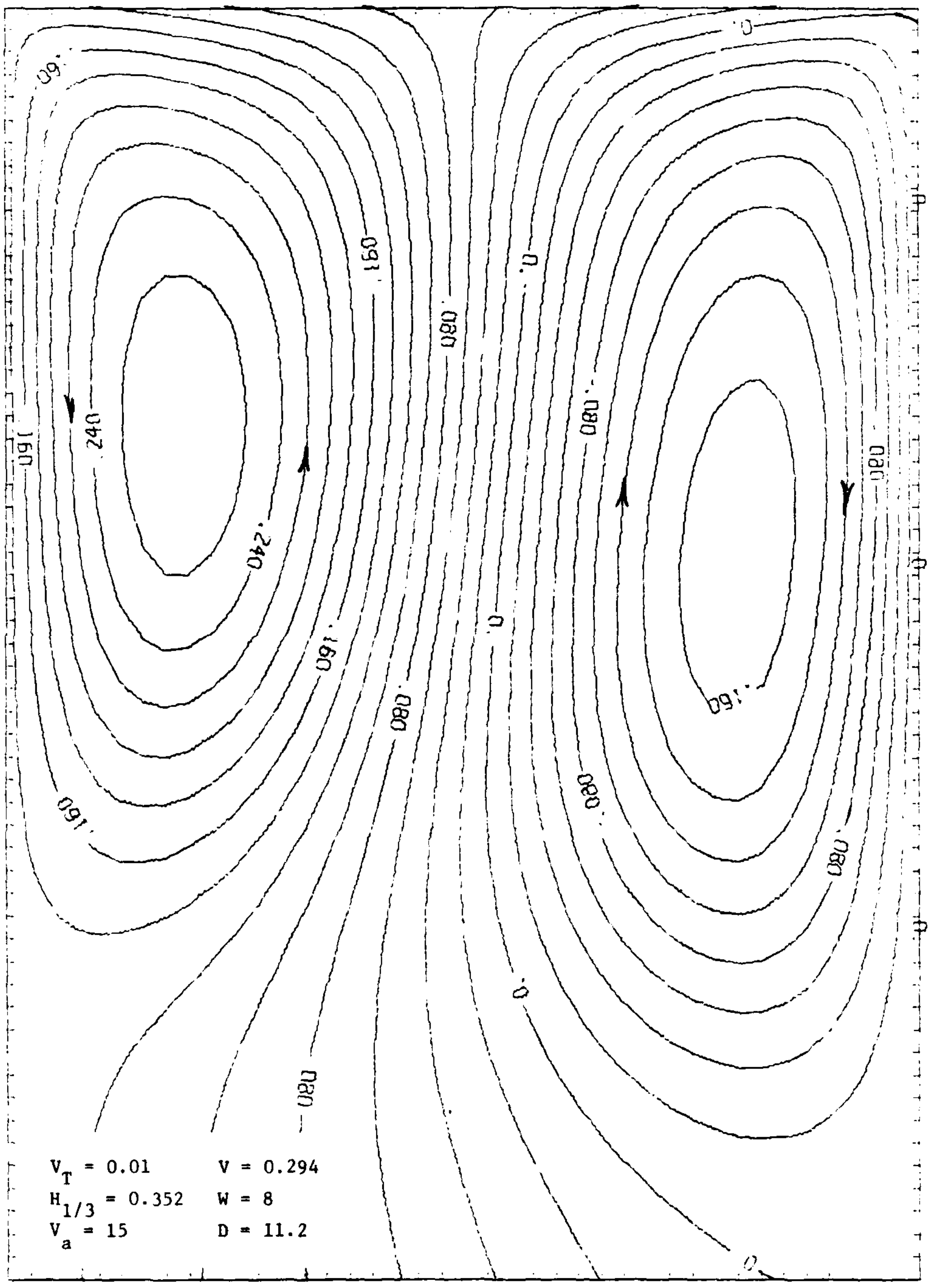

Figure A-23. See Figure 4-4 for caption.

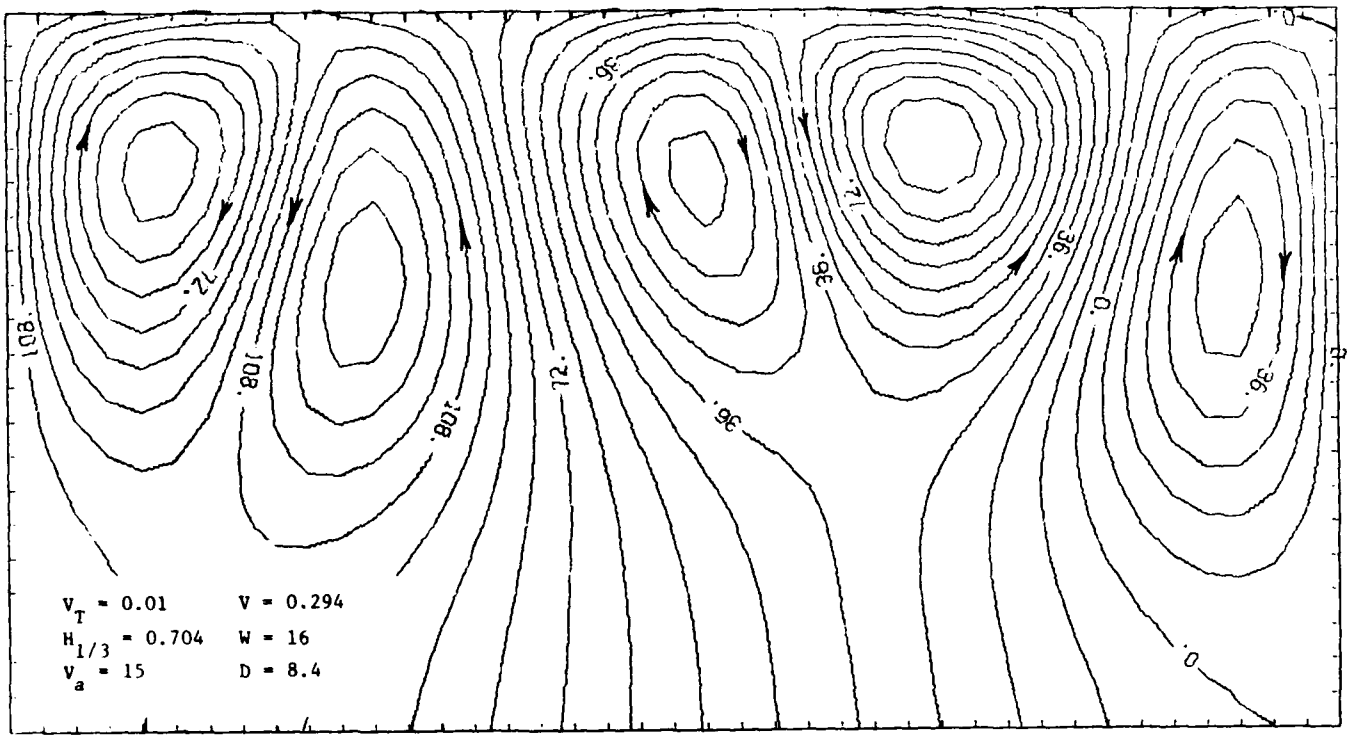

Figure A-24. See Figure 4-4 for caption.

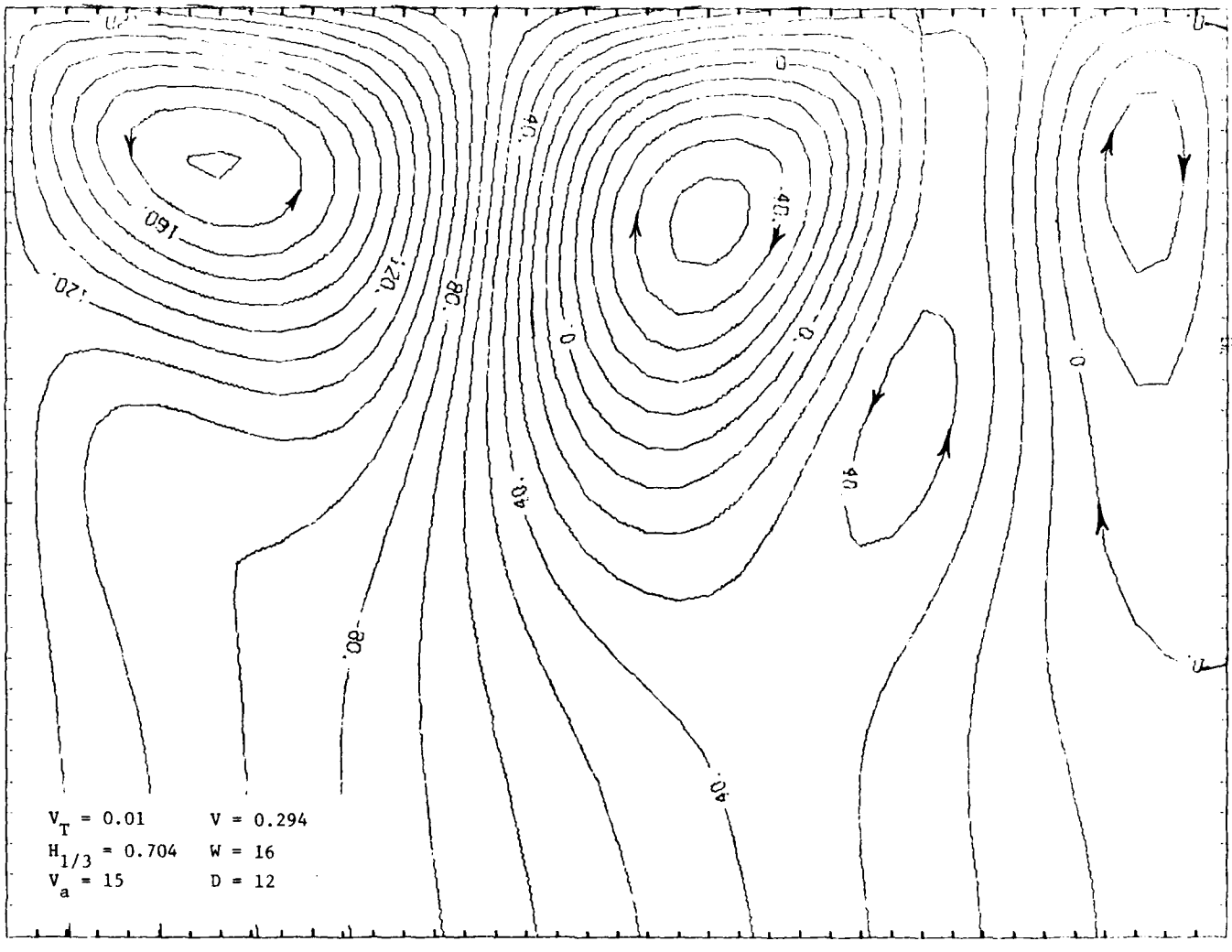

Figure A-25. See Figure 4-4 for caption.

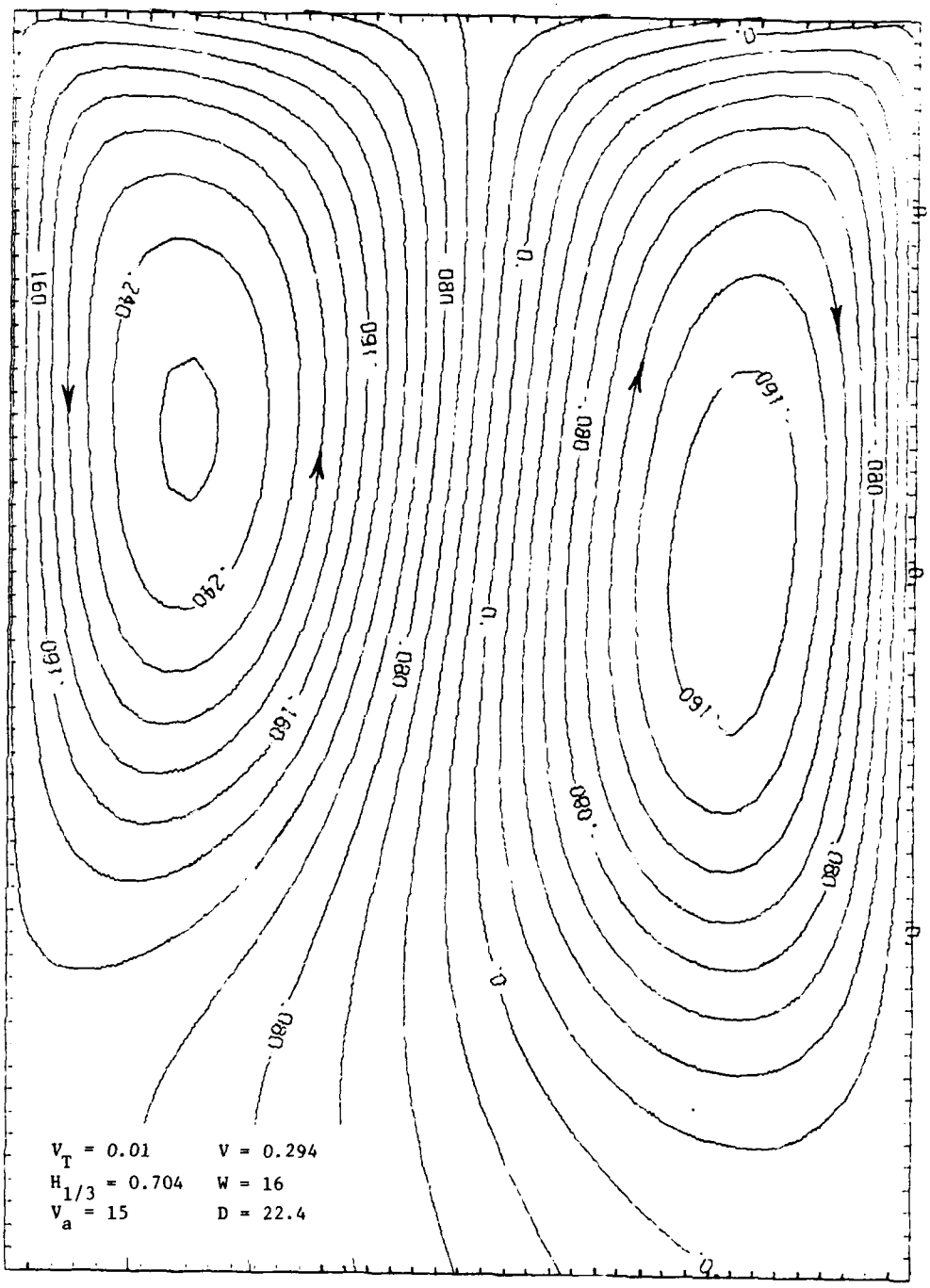

Figure A-26. See Figure 4-4 for caption.

END

DATE
FILMED

8-82

DTIC